Using Synthetic Fibres in Concrete to Control Drying Shrinkage Cracking in Concrete Slabs-on-Grade

by
Daniel Erasmus van der Westhuizen

Thesis presented in fulfilment of the requirements for the degree of Master of Science in the Department of Civil Engineering at the University of Stellenbosch

Supervisor: Prof. William Peter Boshoff

December 2013

Declaration

By submitting this thesis/dissertation electronically, I declare that the entirety of the work contained therein is my own, original work, that I am the sole author thereof (save to the extent explicitly otherwise stated), that reproduction and publication thereof by Stellenbosch University will not infringe any third party rights and that I have not previously in its entirety or in part submitted it for obtaining any qualification.

Date: December 2013

Summary

Macro synthetic fibre reinforced concrete (SynFRC) is a relatively new concrete for the purpose of being used in structural elements which only require minimum reinforcement and are supported continuously by sub-layers. One structural element that is of particular interest is slabs-on-grade which is supported by a subgrade/sub-base and requires minimum reinforcement to control the shrinkage strains which may result in cracking.

The aim of this project is to investigate the potential use of macro SynFRC in the application of controlling drying shrinkage cracking (DSC) in concrete slabs-on-grade. The focus is on the use of concrete slabs-on-grade that is intended for industrial floors.

The SynFRC material parameters of interest were characterised first with the aid of various experimental tests. These are: flexural tests, compression tests, friction tests between the SynFRC and wooden surfaces used for full scale testing, and the shrinkage of the concrete.

Next the post-cracking tensile behaviour of the SynFRC was determined by way of an inverse analysis. These tensile responses were subsequently used to perform a series of different finite element analyses. These analyses were performed on specific slabs-on-grade to determine the effects of the added tensile behaviour of the SynFRC on the DSC.

The results obtained concerned: the spacing of cracks, the maximum and average crack width, and the difference in crack width between the normal concrete (NC) and the SynFRC. These changes take place in accordance to the concrete age. From the analyses it was determined that the addition of fibres gives the concrete a ductility that allows the concrete to crack more than NC, yet does not allow the cracks to propagate. This applies to low fibre contents of less than 0.4% by volume and a slab thickness of 200mm, as well as to fibre contents that have $R_{e,3}$ values of 0.51 and higher. Moreover, it results in improvements seen when adding fibres if the friction is sticky, meaning when the maximum friction between the slab and the subgrade is reached with a very small amount of movement. With a stickier friction though smaller crack widths occur within both the NC and the SynFRC.

Opsomming

Makro sintetiese vesel versterkte beton (SynFRC) is 'n relatiewe nuwe beton. Dit het ten doel om gebruik te word in strukturele elemente wat minimale versterking benodig en wat deurlopend deur sublae ondersteun word. Een spesifieke strukturele element van belang is grondvloere wat deur 'n sublaag ondersteun word en wat minimale ondersteuning benodig om die krimping vervorming te beheer wat moontlike krake kan veroorsaak.

Die doel van die projek was om die potensiële gebruik van makro sintetiese vesels te ondersoek tydens die beheer van die uitdroog krimp kraking van 'n beton grondvloer. Die fokus was op die gebruik van betonvloere vir fabrieksdoeleindes.

Die eienskappe van SynFRC materiale is vooraf vasgestel vir die doel van verskeie eksperimentele toetse. Hierdie toetse sluit in buigbaarheidstoetse, druktoetse, krimping van beton en toets van wrywing tussen die SynFRC en hout oppervlaktes wat gebruik is vir volskaalse toets.

Die trek gedrag van SynFRC na kraking is vasgestel deur inverse analise. Hierdie trek gedrag is dan gebruik om 'n reeks eindige element analises uit te voer. Hierdie analises is uitgevoer op spesifieke grondvloere om die effek te bepaal van verhoogde trek gedrag van SynFRC op die uitdroog krimp kraking.

Volgens die uitslae sodoende verkry was die kraakspasiëring, die maksimum en gemiddelde kraakwydte en die verskil in die kraakwydte tussen normale beton en die SynFRC as ‘n funksie van beton oudedom. Vanuit die analises het dit duidelik geblyk dat die byvoeging van vesels die beton se smeebaarheid verhoog het en dit het tot gevolg gehad dat die beton meer krake vorm, maar dat die krake nie vergroot nie. Dit is waargeneem by 'n lae vesel inhoud van minder as 0.4% per volume en 'n betonblad met 'n dikte van 200mm. Dit is ook waargeneem by 'n hoër vesel volume wat $R_{e,3}$ waardes van 0.51 en hoër het. Kleiner kraakwydte is waargeneem waar vesel volume verhoog is indien die wrywing hoër is, bedoelende dat die maksimum wrywing tussen die betonblad en die sublaag bereik is met baie min beweging. Daar het wel kleiner kraakwydtes in beide die normale beton en die SynFRC voorgekom waar daar hoër wrywing was.

Acknowledgements

I would like to thank the following people for their support and time to help me complete this research project:

- Prof. William Peter Boshoff, my supervisor, for his guidance, knowledge and time during this study. He helped me develop the skills to implement my own ideas under his expert opinions.

- The laboratory staff from the Stellenbosch University for their hard work and time to help me complete my testing within time.

- My parents and my girlfriend, for their love and support, for helping me to get through the hard times and for always believing in me.

Table of Content

List of Figures

List of Tables

List of Abbreviations

2D	Two dimensional
AASHTO	American Association of State Highway and Transportation Officials
ASTM	American Society of Testing and Materials
BS	British Standards
CMOD	Crack mouth opening displacement
COV	Coefficient of variance
DSC	Drying shrinkage cracking
FEA	Finite element analysis
FEAs	Finite element analyses
FEM	Finite element model
FIB	Fédération Internationale du Béton
FRC	Fibre reinforced concrete
FRCs	Fibre reinforced concretes
LL	Liquid limit
LVDT	Linear variable displacement transducer
LVDTs	Linear variable displacement transducers
MOR	Modulus of rupture
NC	Normal concrete
OPC	Ordinary Portland cement
PI	Plasticity index
PL	Plastic limit
PPC	Pretoria Portland cement

PSC	Plastic shrinkage cracking
RC	Reinforced concrete
RD	Relative humidity
RILEM	Reunion Internationale des Laboratoires et Experts des Materiaux
SABS	South African Bureau of Standards
SANS	South African National Standards
SF	Safety factor
SynFRC	Synthetic fibre reinforced concrete

Chapter 1 Introduction

1.1 Background

Concrete is a brittle material which performs well in compression but is weak in tension. Steel reinforcement is used within concrete structures to resist tensile forces once the concrete has cracked. Another method is to pre-stress or post-stress the reinforcement to keep the concrete in compression under loading. The tensile failure strain of the concrete is considerably lower than the yield strain of the reinforcement and as a result the reinforcement will not yield once concrete starts to crack. This method of reinforcing works well where a structural element is required to resist tensile forces or bending moments.

Some structural elements, like slabs-on-grade and linings, where the concrete element is continuously supported by a substrate, are usually reinforced with the minimum amount of steel. Such reinforcement may yield under service conditions, but may be used to control cracks.

For the last 40 years many different types of fibres were introduced to concrete (Brandt, 2008). The interest in these fibres was initiated by the need to replace the asbestos in many fibre reinforced cementitious products. Steel fibres have been commercially available since the 1970's and are currently widely accepted as an alternative reinforcement for structural elements that only require minimum steel reinforcement (Concrete Society Working Group, 2007). These structural elements include slabs-on-grade, sprayed concrete for ground support, composite floors on steel decking and precast concrete tunnel linings (Oslejs, 2008).

Much more recently macro synthetic fibres have been developed and introduced to the market. The dimensions of these fibres are similar to those of steel fibres and are commonly used in dosages up to a maximum of 1.35% by concrete volume (Concrete Society Working Group, 2007). These fibres provide the concrete with some post-cracking tensile capacity, which may assist with some load bearing (Johnston, 2001). At normal dosages, as indicated above, the fibres will not provide added tensile strength to the concrete, hence the reason for using these fibres in applications where minimum reinforcement is required (Labib & Eden, 2004).

For this research project the macro synthetic fibres were investigated for use in slabs-on-grade to control the drying shrinkage cracking (DSC) which occurs due to the friction restraint beneath the slab and the shrinkage in slab elements. These fibres have been used in some slab-on-grade projects (Roesler, et al., 2006; Labib & Eden, 2004), but little research has been conducted to prove whether this macro synthetic fibre reinforced concrete (SynFRC) can control DSC within slabs-on-grade.

1.2 Objectives

The reason for this study was to determine whether SynFRC could control DSC that occur within slabs-on-grade. The general method of reinforcing for this phenomenon is with a steel wire mesh, but this is expensive and prolongs the construction process. Another general method is using unreinforced slabs with small spacings between joints. Adding fibres will result in fewer joints (larger crack spacing) which results in quicker construction. The ultimate objective of this research was to determine whether the SynFRC can control DSC, decrease the crack widths significantly and determine the number of cracks between joints.

1.3 Scope & Methodology

This research project involved the testing of SynFRC to characterise material properties such as the flexural behaviour, compression strength, friction response and shrinkage behaviour. The flexural behaviour was then transformed into a tension post cracking response for the SynFRC to be used in Finite Element Analyses (FEAs).

FEAs were performed on slabs-on-grade to determine what effect various factors have on the process of DSC as well as to determine the difference in cracking between normal concrete (NC) and SynFRC. These factors included the slab's size, the friction type, the fibre type, the fibre dosages and the ambient relative humidity.

Experimental tests were conducted on full scale slabs-on-grade to determine the difference in cracking and crack widths between NC, reinforced concrete (RC) and SynFRC slabs. Analyses were performed on these tests to determine why the slabs did not crack.

1.4 Outline

This thesis consists of eight chapters with the present chapter focussing on an introduction of the research. Chapter 2 provides a background study on DSC looking at different types of shrinkage, prediction models of shrinkage, influencing factors of DSC in concrete slabs-on-grade, consequences of DSC and how to control DSC. Chapter 3 provides a background study on concrete slabs-on-grade focussing on the conventional slab-on-grade, sub-layers, joints and the design of slabs-on-grade. Chapter 4 provides a background study on SynFRC focussing on fibre classification, fibre properties and mechanisms such as crack control in FRC and the mechanical properties of fibres controlling cracking. Chapter 5 describes the experimental work conducted to determine the characterisation of material properties for the SynFRC, whilst Chapter 6 presents the analyses performed using the material properties obtained in Chapter 5. Chapter 7 covers the full scale experimental tests conducted on slabs-on-grade. Lastly conclusions and future recommendations are made in Chapter 8.

Chapter 2 Background Study on Drying Shrinkage Cracking

Drying shrinkage cracking (DSC) is a common occurrence in concrete slabs-on-grade (Gu, et al., 2011) due to the large exposed surface to volume ratio (Illston & Domone, 2001). The rate of pore water evaporation is equivalent to the exposed surface area. This leads to drying shrinkage, but does not necessarily mean that cracking will occur. DSC only occurs when both drying shrinkage and a form of a restraint are present (Raoufi, et al., 2011). In the case of concrete slabs-on-grade the restraint is mainly where slabs are connected to columns or walls, or due to the friction between the concrete slab and the sub-layers (Lee, 2001). This chapter focuses the mechanics and behaviour of DSC.

2.1 Different Types of Shrinkage

Volume changes occur in concrete in both fresh and hardened states. This section focuses on normal strength concrete where the water/cement ratio is more than 0.4 (Owens, 2009). In the case of normal strength concrete the water content required for full hydration, is usually exceeded, due to large water-cement ratios. Therefore there will always be pore water that can evaporate from the hardened concrete. When pore water evaporates, the concrete dries out and shrinkage occurs. This is called drying shrinkage (Illston & Domone, 2001).

Drying shrinkage is the main focus of this thesis, but this is not the only type of shrinkage. In the following sections all types of shrinkage occurring in concrete are discussed.

2.1.1 Autogenous Shrinkage

Autogenous shrinkage takes place in both the fresh and hardened states of concrete (Illston & Domone, 2001). It is the result of the hydration process between the cement and water, where the product of the hydration process is less dense than the two materials in their original form, resulting in a form of shrinkage that initiates early in the setting of the concrete and continues to occur with drying shrinkage (Tazawa, et al., 1995). Autogenous shrinkage has a more substantial effect compared to drying shrinkage on high strength concrete (Igarashi, et al., 2000), because most of the water is used in the hydration process, leaving less pore water available for evaporation. In the case of normal concrete the autogenous shrinkage is insignificant compared to drying shrinkage (Owens, 2009). Therefore only drying shrinkage is considered.

2.1.2 Plastic Shrinkage

Plastic shrinkage occurs before the concrete has set; normally a few hours after casting the concrete (Boshoff & Combrinck, 2013). Plastic shrinkage is the evaporation of water from within the mix before the concrete has set. This is a type of drying shrinkage, but it is assumed that drying shrinkage only starts to take effect after the final setting of the concrete. Plastic and drying shrinkage can cause cracking to occur in the presence of a restraint, but there is a difference in the cracking patterns (Figure 2.1). The yellow parallel and evenly spaced lines represent DSC whilst the red thin and scattered lines represent plastic shrinkage cracking (PSC).

Figure 2.1 Differences between the cracking of plastic and drying shrinkage (Beushausen, 2011)

2.1.3 Drying Shrinkage

The last and most important type of shrinkage considered, is drying shrinkage. The main mechanism causing drying shrinkage is moisture movement (Illston & Domone, 2001), which occurs due to evaporation (Almusallam, 2001). Drying shrinkage transpires as soon as curing stops and the concrete has reached its final setting time and will continue throughout its entire lifetime. Most of the drying shrinkage takes place at an early age of the concrete decreasing as the water content of the concrete decreases (Zhang, et al., 2009).

Drying shrinkage is partly reversible if it is rewetted. A portion of the shrinkage can, however, not be recovered, although with continuous cycles of wetting and drying almost all the shrinkage can be recovered (Figure 2.2). Concrete also swells if it is continuously submerged, but this swelling strain is relatively small compared to the drying shrinkage strain. The stronger the cement paste, the more the effect of the swelling and shrinkage is diminished (Illston & Domone, 2001).

There are four main mechanisms responsible for drying shrinkage and swelling, namely capillary tension, surface tension or surface energy, disjoining pressure and the movement of interlayer water. Capillary tension builds up between the particles within the cement paste due to the loss of water

through evaporation. This causes the particles to move closer together, hence the occurrence of shrinkage (Powers, 1965).

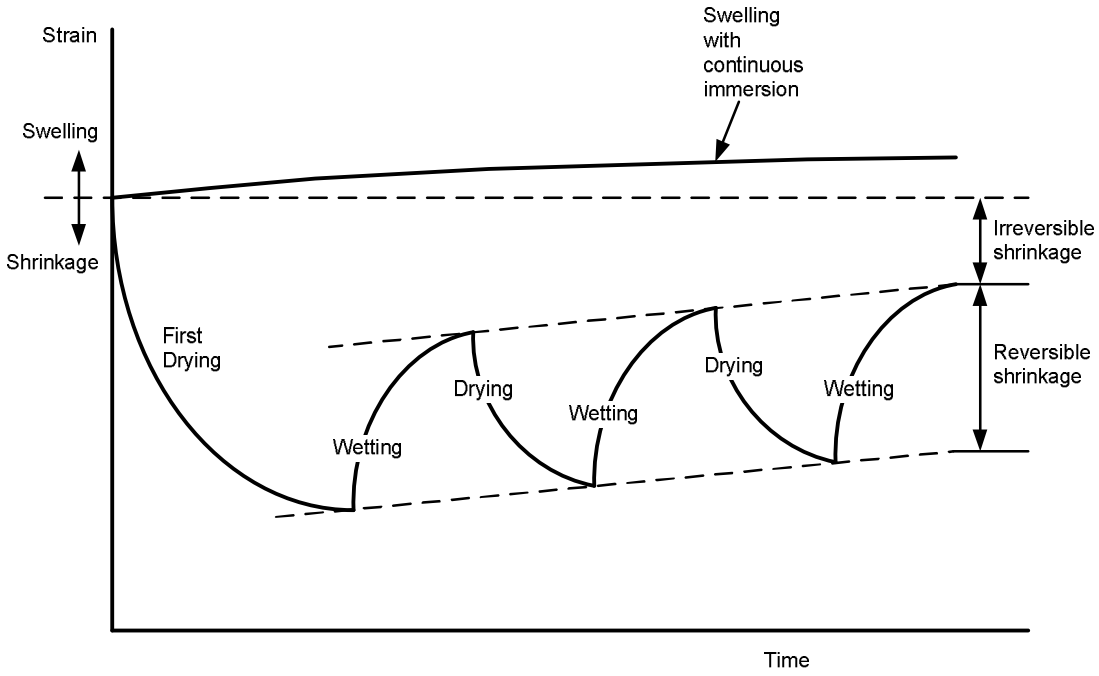

Figure 2.2 Strain response of cement paste or concrete to alternate cycles of drying and wetting (Illston & Domone, 2001)

The solid and liquid materials surfaces are in a state of tension due to the net attraction forces of the molecules within the cement paste (this leads to shrinkage). Work (energy) is required to increase the surface area and this is called the surface energy. Concrete can also swell if subjected to continuous submersion. The absorption of water molecules on the surface of particles reduces surface energy, which reduces internal compressive stresses and this leads to a volume increase called swelling (Wittman, 1968).

Figure 2.3 shows a pore (between two layers) which is narrowing from a wide section that contains free water. The layers are unable to move apart due to Van der Waal's bond forces between the two layers. The presence of absorbed water on each layer causes pressure in the narrower section where the absorbed water layer is less than double the thickness of this layer. This is called disjoining pressure, which results in a swelling balanced by the inter-particle tension. When the concrete dries, the absorption layer decreases in thickness reducing the disjoining pressure which in turn leads to shrinkage (Ishai, 1965).

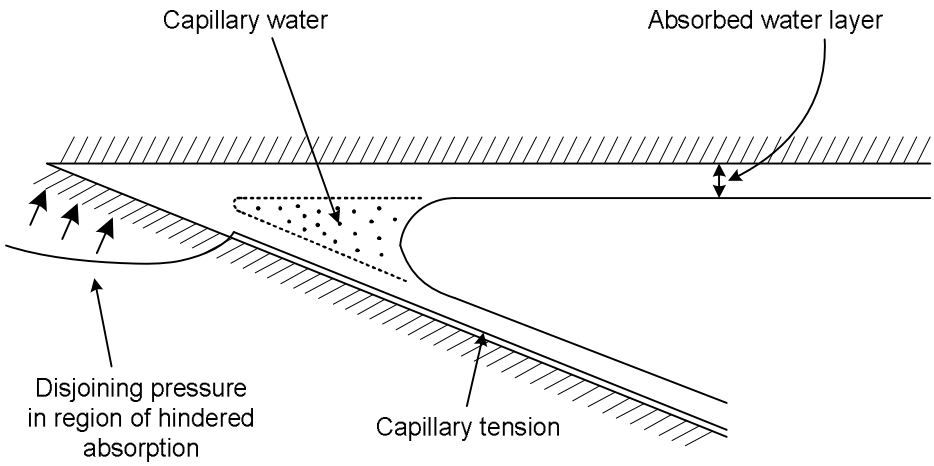

Figure 2.3 Water forces in a gel pore in hardened cement paste (Bazant, 1972)

Drying of the concrete causes a moisture gradient between the concrete surface and the centre of the specimen, hence the movement of interlayer water from the internal part to the surface of the concrete (Feldman & Sereda, 1970). This movement of interlayer water leads to a decrease of concrete volume called shrinkage. Opinions differ regarding the relative importance of the above mechanisms on the percentage of the total shrinkage that occurs within concrete (Table 2.1).

Table 2.1 Summary of suggested shrinkage mechanisms (Soroka, 1979)

Source	Relative Humidity (%)										
	0	10	20	30	40	50	60	70	80	90	100
Powers (1965)	disjoining pressure										
							capillary tension				
Ishai (1965)	surface energy						capillary tension				
Feldman and Sereda (1970)	interlayer water				capillary tension and surface energy						
Witman (1968)	surface energy					disjoining pressure					

A number of mix constituents and proportions affect the behaviour of shrinkage strain. The amount of shrinkage that occurs in concrete is less than that of the cement paste because of the restraining effect of the aggregate in the concrete. Therefore the aggregate content affects shrinkage as shown in Figure 2.4. This is due to the aggregate being dimensionally stable on account of changes in moisture within the concrete. It can be seen that the amount of shrinkage that occurs in normal concrete is usually about 10 to 30 per cent of that of cement paste on its own (Pickett, 1956). Normal density aggregates are stiffer than lightweight aggregates and therefore more shrinkage occurs in concretes that contain lightweight aggregates.

The cement content and the water/cement ratio are also mix constituents that affect the amount of shrinkage that occurs in concrete. If the water/cement ratio is kept constant and the cement content is increased, the water content will increase. If the cement content is kept constant and the water/cement ratio is increased, the water content will increase leading to increased porosity and the amount of water stored in the cement paste. With more water available in the mix, shrinkage could be more pronounced (Figure 2.5).

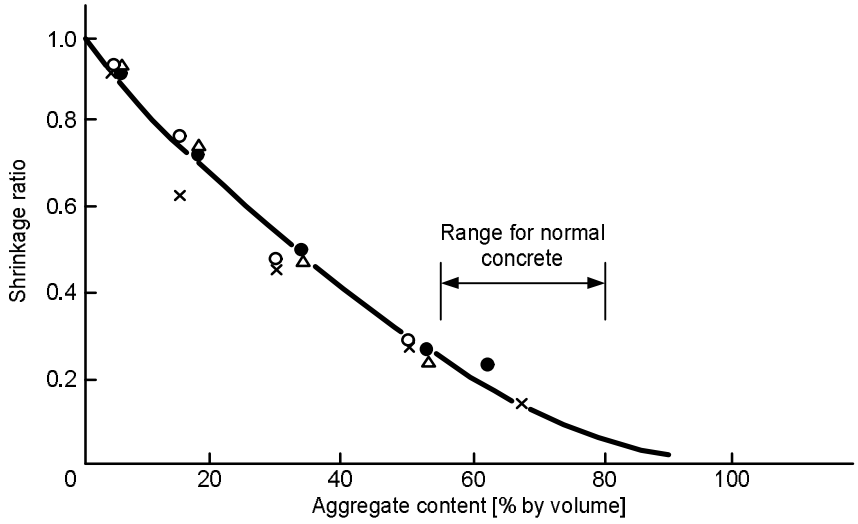

Figure 2.4 Influence of aggregate concrete in concrete on the ratio of shrinkage of concrete to that of the neat cement paste (Pickett, 1956)

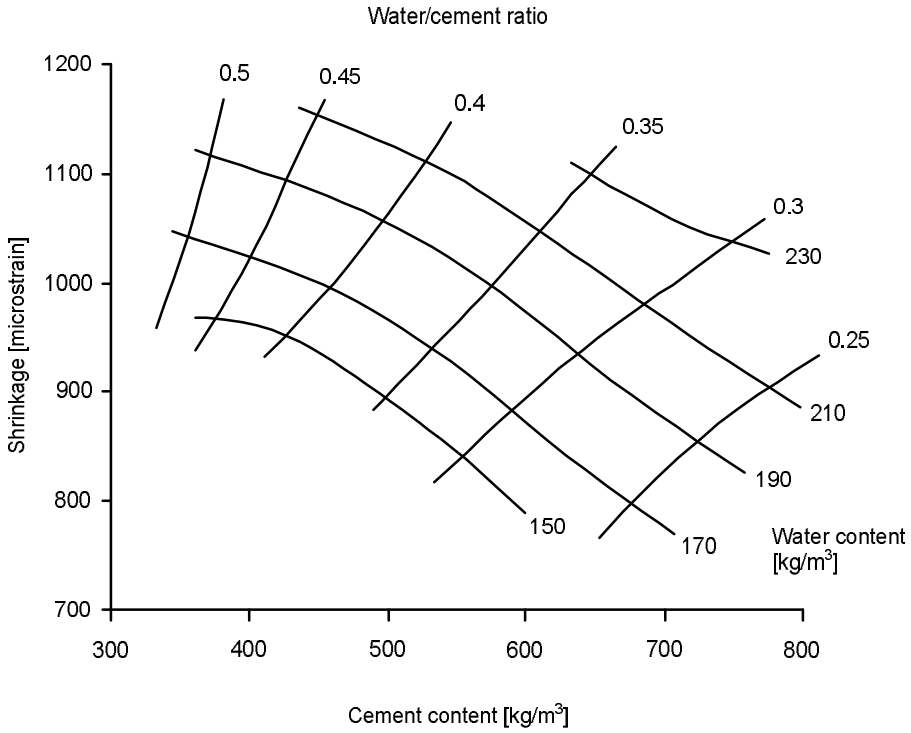

Figure 2.5 Typical effects of cement content, water content and water cement ratio on shrinkage of concrete – moist curing for 28 days followed by drying for 450 days (Shoya, 1979)

The geometry of the concrete specimen also has a significant effect on the behaviour of shrinkage. The size and shape of the specimen influence the rate of moisture loss and also the restraint provided by the core of the concrete specimen. If the core contains a high moisture content, the result would be tension stresses on the surface of the specimen and compressive stresses in the core. This could result in surface cracks (Troxell, et al., 1958). This is a problem particularly in the case of large pours such as dam walls and slabs-on-grade.

2.1.4 Carbonation Shrinkage

Carbonation shrinkage is a chemical mechanism (Illston & Domone, 2001). It is the reaction of the carbon dioxide in the atmosphere and the calcium hydroxide in concrete (a by-product of the hydration process) that results in reducing the volume of the concrete (Jerga, 2004). This type of shrinkage occurs over a long period of time and can exceed the drying shrinkage in special circumstances (Younsi, et al., 2013).

This type of shrinkage requires an environment with a high concentration of carbon dioxide in the atmosphere at intermediate humidities (Owens, 2009). Since water is a requirement for this chemical reaction, the carbon dioxide cannot penetrate the water-filled (Saetta, et al., 1993).

2.2 Prediction Models for Shrinkage Behaviour

The prediction of shrinkage is not the simplest of tasks to perform, mainly because there are many different variables that affect shrinkage (Owens, 2009; Illston & Domone, 2001). The most important factors are environmental factors (such as relative humidity, temperature and wind speed) and the geometrical factors (such as exposed surface area, volume and shape).

Different methods of predicting the shrinkage in concrete have been developed. These methods consider some of the above variables to predict the shrinkage strain that occurs (Eguchi & Teranishi, 2005; Pan, et al., 2013). A few of these methods are discussed in the following paragraphs.

2.2.1 SABS 0100-1:2000

This is the simplest method of the four methods considered (Gaylard, et al., 2013). The method uses a graph (originating from empirical data) to get shrinkage strain values at ages of 6 months or 30 years and takes into account the geometry and relative humidity, see Figure 2.6. This method only considers three effective section thicknesses and interpolation can be used for values between 150, 300 and 600mm (South African Bureau of Standards, 2000).

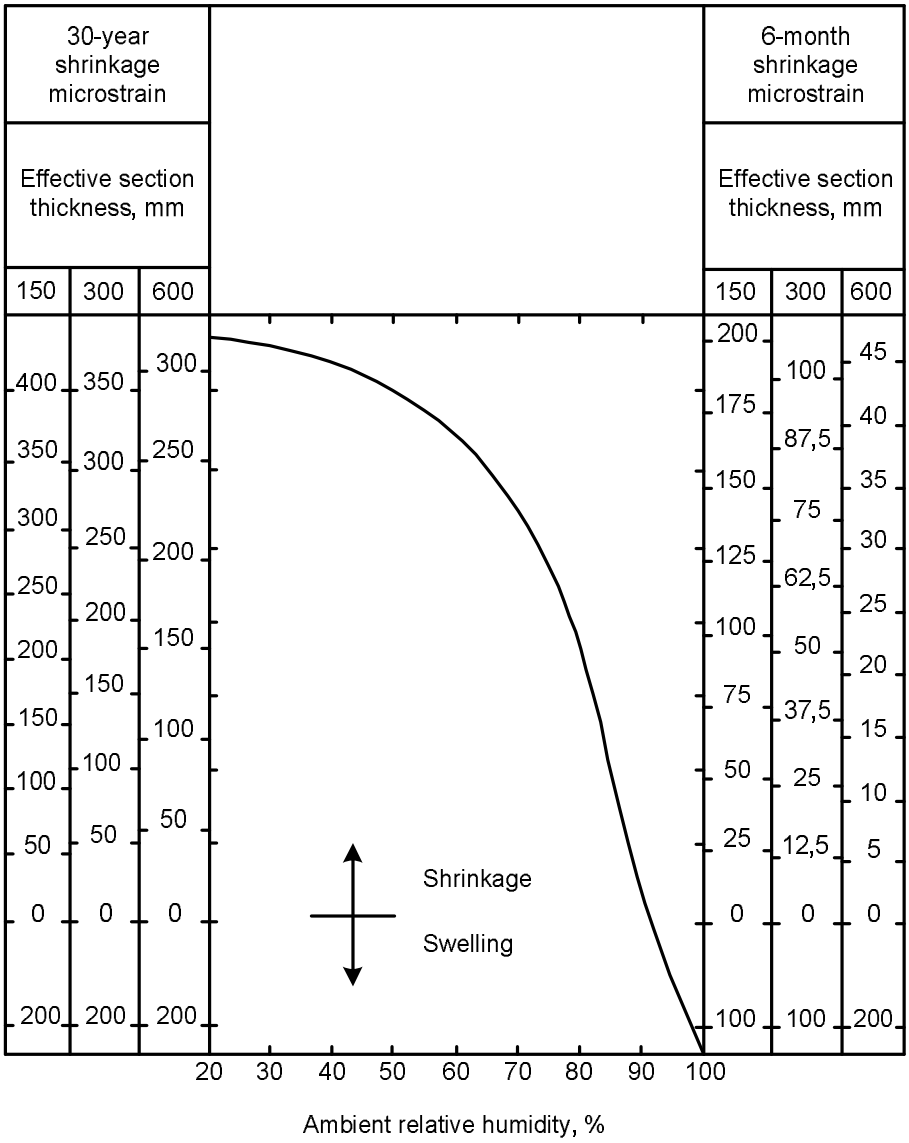

Figure 2.6 Shrinkage of normal-density concrete according to SABS 0100-1:2000 (South African Bureau of Standards, 2000)

2.2.2 BS EN 1992:2004

This model distinguishes between autogenous shrinkage and drying shrinkage components and the total shrinkage is then determined by the sum of the two. Each of these can be determined at any given age. The variables required are the relative humidity, effective section thickness, concrete strength and cement type. This method is an analytical method, not a graphical method as is the case of the SABS 0100-1:2000 method (European Commitee for Standardization, 2004).

2.2.3 RILEM Model B3

This is a sophisticated shrinkage model that is derived from the work of Bazant and his co-workers (Bazant & Baweja, 2000). This model takes into account factors such as the water/cement ratio, cement type, cement content and aggregate/cement ratio. Due to the complexity of the model it is not recommended for use in conventional design and is thus recommended only for structures that are deflection sensitive. This method will therefore not be considered for this study, despite being a trusted method, giving good results for shrinkage behaviour (Gaylard, et al., 2013). This method is not used in this study since slabs-on-grade elements are not deflection sensitive.

2.2.4 FIB 2010 Model Code

The FIB Model Code method takes many variables into account. This method is also simple to use and gives accurate results (FIB Special Activity Group 5, 2010).

This method also divides the total shrinkage into two parts, namely autogenous and drying shrinkage. The variables required for this method are the relative humidity, cement type and strength, concrete strength and the effective section thickness. The total shrinkage is calculated by the following equation:

$$\boldsymbol{\varepsilon_{cs}(t,t_s) = \varepsilon_{cas}(t) + \varepsilon_{cds}(t,t_s)} \tag{2.1}$$

where $\varepsilon_{cs}(t,t_s)$ = total shrinkage strain of concrete at a specific age

$\varepsilon_{cas}(t)$ = total autogenous shrinkage strain of concrete at a specific age

$\varepsilon_{cds}(t,t_s)$ = total drying shrinkage strain of concrete at a specific age

For the determination of the autogenous shrinkage the concrete strength, cement type and strength are required. The ultimate autogenous shrinkage is calculated from the following equation, by using the alpha factor from Table 2.2 and using the mean concrete strength:

$$\boldsymbol{\varepsilon_{cas0}(f_{cm}) = -\alpha_{as}\left(\frac{f_{cm}/10}{6+f_{cm}/10}\right)^{2.5}\cdot 10^{-6}} \tag{2.2}$$

where $\varepsilon_{cas0}(f_{cm})$ = ultimate autogenous shrinkage strain for concrete with a specific strength

α_{as} = coefficient, dependent on the type of cement (see Table 2.2)

f_{cm} = mean cube compressive strength at the age of 28 days in [MPa]

Table 2.2 Alpha factors used to predict shrinkage for FIB 2010 Model Code (FIB Special Activity Group 5, 2010)

Strength class of cement	α_{as}	α_{ds1}	α_{ds2}
32.5 N	800	3	0.013
32.5 R, 42.5 N	700	4	0.012
42.5 R, 52.5 N, 52.5 R	600	6	0.012

A beta factor is then calculated using the following equation which is a function of the concrete age:

$$\boldsymbol{\beta_{as}(t) = 1 - exp\left(-0.2 \cdot \sqrt{t}\right)} \tag{2.3}$$

where $\beta_{as}(t)$ = coefficient, to determine autogenous shrinkage at a specific age

t = concrete age in days

The autogenous shrinkage is then calculated for a specific concrete age using:

$$\boldsymbol{\varepsilon_{cas}(t) = \varepsilon_{cas0}(f_{cm}) \cdot \beta_{as}(t)} \tag{2.4}$$

The drying shrinkage is determined by using the concrete strength, cement type, cement strength, relative humidity and the effective section thickness. The ultimate drying shrinkage is calculated from the following equation, with the alpha factors from Table 2.2 and using the concrete mean cube compressive strength:

$$\boldsymbol{\varepsilon_{cds0}(f_{cm}) = [(220 + 110 \cdot \alpha_{ds1}) \cdot exp(-\alpha_{ds2} \cdot f_{cm})] \cdot 10^{-6}} \tag{2.5}$$

where $\varepsilon_{cds0}(f_{cm})$ = ultimate drying shrinkage strain for concrete with a specific strength

α_{ds1} = coefficient, dependent on the type of cement (see Table 2.2)

α_{ds2} = coefficient, dependent on the type of cement (see Table 2.2)

Then two beta factors are calculated, the first being influenced by the relative humidity using the following equation:

$$\boldsymbol{\beta_{RH}(RH) = \begin{cases} -1.55 \cdot \left[1 - \left(\frac{RH}{100}\right)^3\right] & for\ 40 \leq RH < 99\% \cdot \beta_{s1} \\ 0.25 & for\ RH \geq 99\% \cdot \beta_{s1} \end{cases}} \tag{2.6}$$

with

$$\boldsymbol{\beta_{s1}(f_{cm}) = \left(\frac{35}{f_{cm}}\right)^{0.1} \leq 1.0} \tag{2.7}$$

where $\beta_{RH}(RH)$ = coefficient to determine drying shrinkage for a specific RH

RH = ambient relative humidity in [%]

$\beta_{s1}(f_{cm})$ = coefficient to determine drying shrinkage for a specific concrete strength

The other beta factor changes with time and takes into account the effective section thickness:

$$\boldsymbol{\beta_{ds}(t-t_s)} = \left(\frac{(t-t_s)}{0.035 \cdot h^2 + (t-t_s)}\right)^{0.5} \tag{2.8}$$

where $\beta_{ds}(t\text{-}t_s)$ = coefficient, to determine drying shrinkage for a specific concrete age

t_s = concrete age at the beginning of drying in [days]

$h = 2A_c/u$ is the notional size of member in [mm], with A_c as the cross-section in [mm²] and u as the perimeter of the member in contact with the atmosphere in [mm]

The drying shrinkage at a specific concrete age is then calculated using:

$$\boldsymbol{\varepsilon_{cds}(t, t_s)} = \boldsymbol{\varepsilon_{cds0}(f_{cm}) \cdot \beta_{RH}(RH) \cdot \beta_{ds}(t-t_s)} \tag{2.9}$$

2.3 Influencing Factors of DSC in Concrete Slabs-on-Grade

Drying shrinkage is a common occurrence in concrete and is not a problem if the concrete is free to move. DSC can only occur if a type of restraint is present while drying shrinkage occurs (Banthia, et al., 1993). There are also a few other factors that influence the DSC behaviour. In the case of slabs-on-grade the type of restraint, joint type, slab thickness and environmental conditions are some of these factors and are discussed in the following sections.

2.3.1 Different Types of Restraints

Restraints are causes of DSC and determine if and where cracking can occur. Restraints can be avoided or weakened to prevent cracking from occurring (Marais & Perrie, 1993). Columns, walls and the friction between the slab and sub-layers are relevant restraints concerning concrete slabs-on-grade.

Column and wall restraints can be avoided with the addition of joints around these areas, but the friction beneath the slab cannot be removed (Maitra, et al., 2009). Joints are usually added at a certain spacing to avoid DSC and plastic layers are added between the slab and sub-layers to reduce the friction beneath the slab (Marais & Perrie, 1993). Joints will be discussed in the next section.

There are many different types of sub-layers beneath slabs-on-grade. Some of the most common types with their friction coefficients are shown in Figure 2.7. The friction coefficient is only a factor indicating the severity of the friction. Friction behaviour is shown in Figure 2.8.

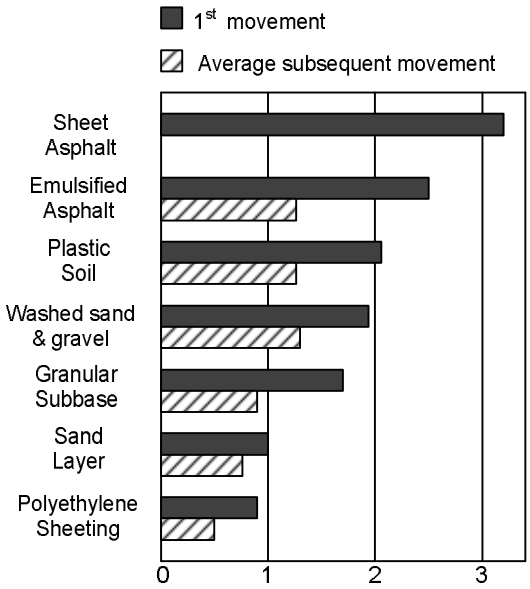

Figure 2.7 Coefficient of different slip media (Marais & Perrie, 1993)

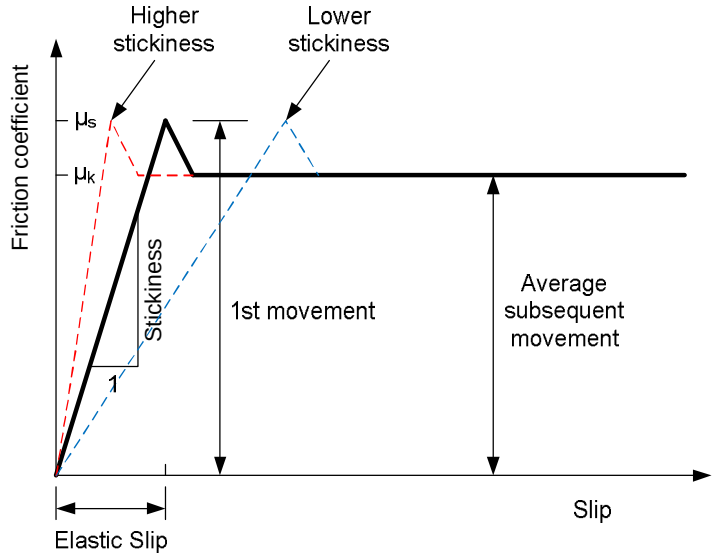

Figure 2.8 Coefficient of friction subjected to a constant movement

When a body is subjected to an increasing slip the coefficient of friction will increase until it reaches the coefficient of first movement. All the displacement up to this point is elastic, meaning if the force applied to the object is released before this point, then the object will return to its original position. This is called the elastic slip. Also shown in Figure 2.8 is the stickiness of the friction. The smaller the elastic slip the stickier the friction. After this point the displacement of the object is permanent (Bellemare, et al., 2008). The first movement coefficient is also known as the static coefficient of friction or μ_s, and the coefficient at average subsequent movement is known as the kinetic coefficient of friction or μ_k. The friction restraint is an important consideration in the prevention of DSC when designing a slab-on-grade (Marais & Perrie, 1993).

2.3.2 Joint Types

There are a few general types of joints, namely contraction joints, sawn-tied joints, construction joints and isolation joints (Marais & Perrie, 1993). The focus of this thesis is shrinkage which is a form of contraction. Therefore the focus will be on contraction joints that are also known as movement joints. The contraction joints are usually sawn, hence the name saw-cut joints.

These joints can only be formed between panels which are cast continuously. They are formed either by sawing or by forming grooves at a typical depth of a quarter of the slab thickness (Concrete Society Working Group, 2003). Contraction joints could be created with dowels to supply load transfer over the joints. These joints are explained in Chapter 3. The main influence of joints on DSC is the spacing of these joints; the closer the joints the better the prevention of DSC in slabs-on-grade. A common rule of thumb is a spacing of no more than 4.5 meters (Marais & Perrie, 1993). This is, however, empirically based.

2.3.3 Slab Thickness

The influence of slab thickness on DSC is that different slab thicknesses have different shrinkage strains and different strengths. With the increase of thickness the tensile force required to crack the concrete is higher and the shrinkage strain that occurs in the slab is smaller (Al-Saleh & Al-Zaid, 2006). Thus DSC can be reduced by increasing slab thickness, but this is a costly method and not recommended. The effect of smaller shrinkage strains with an increase of slab thickness can be seen in Figure 2.9.

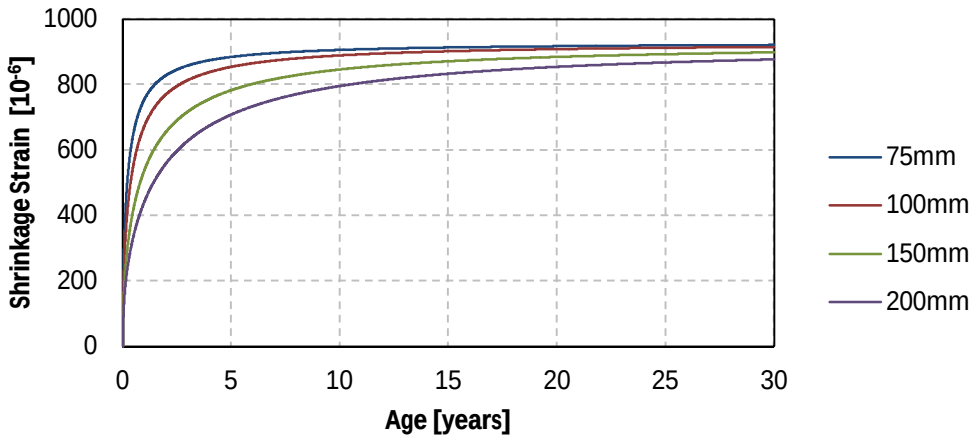

Figure 2.9 The effects of slab thickness on shrinkage strain over the concrete age calculated with FIB Model Code 2010 prediction model

2.4 Consequences of DSC

Concrete is a material that has a tendency to crack due to its low tensile capacity. Some cracks though acceptable, are unsightly. The general public, though, regards cracking in structures as failure. Yet concrete structures are designed to crack.

DSC is a common occurrence in concrete slabs-on-grade and can lead to structural problems. In some cases DSC can form from the top to the bottom of the slab. This can create pathways for water to enter the sub-layers, weakening and causing weak areas where the slab controls all the loading. This results in failure.

The cracking of the concrete allows harmful substances to reach the reinforcement and that may lead to corrosion. The aesthetic value, serviceability, durability and overall workability of the concrete are reduced as a consequence of shrinkage cracking (Wongtanakitcharoen, 2005).

2.5 Controlling DSC

There are a few standard methods of controlling DSC (Marais & Perrie, 1993) which are discussed in the following sections. An alternative method of using synthetic fibre reinforced concrete to enhance the tensile behaviour of concrete (Oslejs, 2008) is also discussed.

2.5.1 Joint Spacing and Reducing Friction

This is the traditional method of controlling DSC and most commonly used (Marais & Perrie, 1993). This method uses joints to create concentrated weaknesses in the slab, which allow the slab to crack at these joints and allow the slab to move horizontally (Bissonnette, et al., 2007). This prevents any unsightly cracks from forming in the slab. The joints can be sealed to prevent any water or dust from entering the cracks at the joints (Concrete Society Working Group, 2003).

Another way of allowing horizontal movement is to reduce the friction between the slab and the sub-layers by adding sheets of polyethylene (Marais & Perrie, 1993). This increases the crack opening at joints, but prevents any DSC to occur between joints.

2.5.2 Reinforcing Concrete with Mesh

It is known that steel enhances the tensile behaviour of concrete and that reinforcing concrete with steel can control cracking (Ytterberg, 1993). As soon as the concrete cracks, the tensile force is restricted by the reinforcing steel. This keeps cracks closed or prevents cracks from increasing in size.

To use a steel wire mesh is one of the methods of reinforcing a slab-on-grade against DSC (Marais & Perrie, 1993). The mesh is prefabricated and a reference number is used to classify the mesh size in accordance with SABS 1024:2006, see Tables 2.3 and 2.4. These meshes are fabricated in sheets of 6m x 2.4m and in rolls of 60m x 2.4m.

Table 2.3 Welded steel fabric: dimensions and mass for square pattern (South African National Standards, 2006)

Fabric reference no.	Nominal pitch of wires (mm)		Nominal wire size (mm)		Cross-sectional area per m width (mm^2)		Nominal mass (kg/m^2)
	Longitudinal	Cross	Longitudinal	Cross	Longitudinal	Cross	
617	200	200	10.0	10.0	393	393	6.17
500	200	200	9.0	9.0	318	318	5.00
395	200	200	8.0	8.0	251	251	3.95
311	200	200	7.1	7.1	197	197	3.11
245	200	200	6.3	6.3	156	156	2.45
193	200	200	5.6	5.6	123	123	1.93
100	200	200	4.0	4.0	63	63	1.00

Table 2.4 Welded steel fabric: dimensions and mass for rectangular pattern (South African National Standards, 2006)

Fabric reference no.	Nominal pitch of wires (mm)		Nominal wire size (mm)		Cross-sectional area per m width (mm^2)		Nominal mass (kg/m^2)
	Longitudinal	Cross	Longitudinal	Cross	Longitudinal	Cross	
772	100	200	10.0	7.1	786	197	7.72
655	100	200	9.0	7.1	636	197	6.55
517	100	200	8.0	6.3	503	156	5.17
433	100	200	7.1	6.3	396	156	4.33
341	100	200	6.3	5.6	312	123	3.41
289	100	200	5.6	5.6	246	123	2.89
278	100	300	6.3	4.0	312	42	2.78
226	100	300	5.6	4.0	246	42	2.26
133	100	300	4.0	4.0	126	42	1.33

This method of controlling DSC still needs contraction joints, but the spacing between these joints can be increased (Concrete Society Working Group, 2003). The mesh may not cross these joints in order to ensure localised cracking and in turn prevent DSC from occurring between joints.

2.5.3 Using SynFRC

Since biblical times, fibres have been used to reinforce structures, i.e. about 3500 years ago (Concrete Society Working Group, 2007). This was when clay-bricks were being reinforced with straw, vegetable fibres and horse hair. In more recent times fibres have been used to reinforce concrete structures, with much research done in the field of steel fibre reinforced concrete.

Steel fibres can increase the tensile strength of concrete (Brandt, 2008) and are considered as a good material for structural use in the industrial industry (Oslejs, 2008). Synthetic fibres are relatively new type of fibre reinforcing concrete, with much research done on slabs-on-grade (Labib & Eden, 2004). Synthetic fibre reinforced concrete (SynFRC) is especially useful to control shrinkage cracking (Pelisser, et al., 2010; Choi, et al., 2011).

The micro SynFRC (which has a diameter of about 32µm, and length ranging between 6 and 12mm) is used to control plastic shrinkage cracking (Maritz, 2012) and the macro SynFRC (with a relative diameter of about 1mm, and lengths ranging between 30 and 50mm) form for drying shrinkage (Choi, et al., 2011). SynFRC does not prevent cracking from occurring; instead it increases the number of cracks and in this way decreases crack widths. Thus, SynFRC controls DSC by controlling the cracking that occurs by bridging the cracks. This method of controlling DSC is discussed in Chapter 4.

2.6 Concluding Summary

An investigation of shrinkage was conducted, with the main focus on drying shrinkage and autogenous shrinkage. Methods for predicting shrinkage strains were discussed, where the FIB 2010 Model Code was selected to predict shrinkage strains due to its simplicity to use and its accuracy.

Controlling DSC was investigated, focussing on the influencing factors of DSC on slabs-on-grade. These factors include the types of restraints, joint types, slab thickness and the environment type.

The traditional way of controlling DSC is to reinforce the slab with a steel mesh and to add joints to the slab to allow horizontal movement in a controlled manner. A relatively new form of controlling DSC is by the use of SynFRC, which is the main focus of this study.

Chapter 3 Concrete Slabs-on-Grade

Concrete slab-on-grade is one of the elements in a structure that does not receive the necessary attention it requires, especially in the case of warehouses where it is a key part of the structure. The demand of goods has significantly increased rack heights and this puts strict limitations on the tolerances on the flatness and uniformity of concrete slabs-on-grade (Concrete Society Working Group, 2003). Slabs-on-grades need more attention and are further investigated in this chapter.

3.1 Conventional Slab-on-Grade

The conventional slab-on-grade is a concrete slab cast on a smooth and uniform sub-layer and contains joints to reduce the amount of restraint in the slab to prevent DSC (Marais & Perrie, 1993). In some cases a steel mesh is added and/or plastic layers are added between the slab and the sub-layer to prevent DSC (Concrete Society Working Group, 2003). This is the conventional method for constructing slabs-on-grade, but with the demands on limiting construction expenses and the rise in price of steel reinforcing, new alternative methods should be investigated. One of these methods is to use fibres to add a post-cracking tensile capacity to the concrete. Some projects where steel fibres were used for this application are discussed by Oslejs (2008). The purpose of this study is to determine if it is possible to use synthetic fibre reinforced concrete (SynFRC) to control DSC. For the purpose of comparison the conventional method is discussed in the following sections.

3.2 Sub-Layers

Concrete slabs-on-grade can either be constructed on a subgrade or a sub-base, with a subgrade being the natural ground which is graded or compacted and a sub-base being a relatively thin layer of granular or cemented material placed on top of the subgrade. If the subgrade is uniform and consists of a soil with good properties it is not necessary to add a sub-base (Marais & Perrie, 1993). To determine if a sub-base is necessary the subgrade soil should be classified to identify possible problem soils. Two common classification systems are: the ASTM D2487 (ASTM International, 2000) and the AASHTO M145 (AASHTO, 2000).

3.2.1 Soil Strength

Soil strength is classified by the soil's supporting capacity and its resistance to movement or consolidation, which are important factors for the performance of slabs-on-grade. This is especially important if the slab needs to support heavy loads. The moisture content and degree of compaction of the soil are factors which affect the soils strength (Marais & Perrie, 1993). Compaction is the most economical method of improving the structural properties of soil.

Other important soil characteristics include the bearing capacity, which is the pressure required to allow a shear failure within a soil. Compressibility of a soil can determine the long-term settlement of a soil under a load. Lastly, the soil-reaction modulus is commonly used in design procedures for concrete slabs-on-grade. The soil-reaction modulus is also known as the Westergaard's modulus of subgrade reaction, and presented by the symbol 'k' in design procedures (Concrete Society Working Group, 2003).

3.2.2 Plastic Index

A moist soil that has a high ductility and stays uniform without breaking, it is called a plastic soil. This is mostly the case in soils that have a fine grain, like clay minerals. If a moist soil is non-ductile and it breaks when it is deformed, it is called a non-plastic soil. The degree of plasticity of a soil is classified as the plasticity index (PI), with the PI being the difference between the liquid limit (LL) and the plastic limit (PL). The LL is the moisture content of a soil when it changes from a plastic to a liquid state and the PL is the moisture content when a soil changes from a semi-solid to a plastic state. (Marais & Perrie, 1993)

3.2.3 Uniformity

To provide a uniform subgrade for a slab-on-grade it is important to prevent any non-uniformity from occurring in the sub layers or sub-base. Expansive soils, hard and soft spots (Figure 3.1), and poorly compacted backfilling can cause non-uniformity in the subgrade.

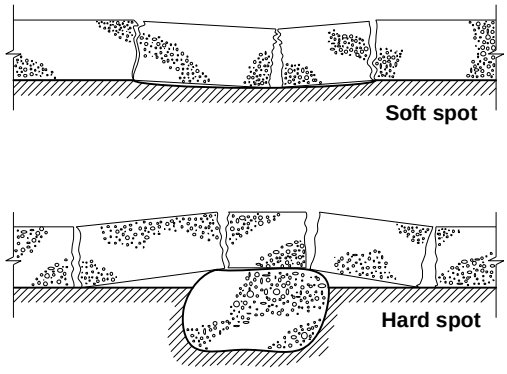

Figure 3.1 Damage caused to slabs due to hard and soft spots (Marais & Perrie, 1993)

3.2.4 Sub-base

A sub-base is not mandatory for casting a concrete slab-on-grade, but if a uniform subgrade cannot be achieved, a sub-base could provide the required uniformity. The sub-base also provides a stable working platform for construction. In Table 3.1 the bearing values for different soil types are shown and the effects of sub-base thickness on the bearing values are shown in Table 3.2.

Table 3.1 Relationship between soil type and bearing values (Marais & Perrie, 1993)

Type of soil	Subgrade strength	California bearing ratio [%]	Design k value [kPa/mm]
Silts and clays of high compressibility at natural density	Low	2 or less	15
Silts and clays of high compressibility			
Silts and clays of low compressibility	Average	3	30
Sandy silts and clays, gravelly silts and clays			
Poorly graded sands			
Gravelly soils, well-graded sands, and sand-gravel mixtures relatively free of plastic fines	High	10	55

Table 3.2 Effects of sub-base thickness on bearing values (Marais & Perrie, 1993)

Subgrade k value	Subbase k value			
	Subbase thickness [mm]			
	100	150	225	300
	kPa/mm			
20	23	26	32	38
40	45	49	57	66
60	64	66	76	90
80	87	90	100	117

3.3 Joints

Joints are the most common method to control DSC in concrete slabs-on-grade. It has the added benefit of controlling curling, also known as warping (Bissonnette, et al., 2007; Al-Nasra, 1997). If provided with joints the slab is divided into sections which are allowed to move separately from one another. Load transfer in joints can be provided with aggregate interlocking, keyways, mechanical devices and cement–stabilized sub-bases (Marais & Perrie, 1993). Mechanical devices used for load

transfer across joints include dowel bars and tie bars. Different types of joints have different purposes and the different types are discussed in the following sections.

3.3.1 Contraction Joints

The purpose of contraction joints is to allow horizontal movement to the slab sections, which prevents DSC from occurring between joints, but allows localised cracks to occur at the joints. This is the most common type of joint and they are easily constructed. Contraction joints are also known as movement joints and are constructed after the slab has been cast. These joints are formed either by sawing or by forming grooves (Concrete Society Working Group, 2003). These joints may include dowels to supply a form of load transfer. See Figure 3.2 for the typical details for a contraction joint (Marais & Perrie, 1993).

The spacing required for contraction joints depends on the shrinkage properties of the specific slab. It also depends on the type of friction as well as whether the slab contains reinforcement. Column layout should be taken into account when joint spacing is determined. To minimize curling and prevent random cracking, the joint spacing should be the lesser of the following: 30 times the slab thickness or 4.5 m, if the slab is un-reinforced (Marais & Perrie, 1993).

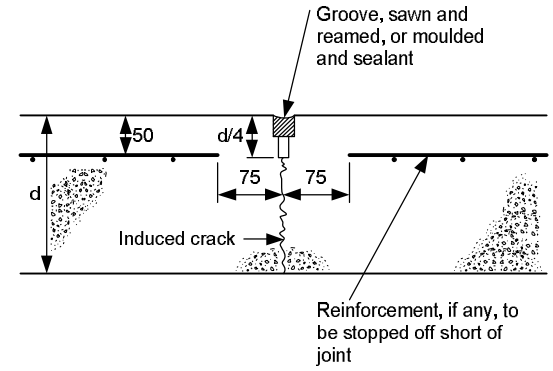

(a) UNDOWELLED JOINT

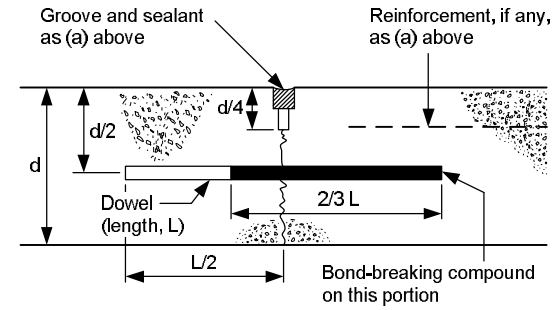

(b) DOWELLED JOINT

Figure 3.2 Details of typical contraction joints (Marais & Perrie, 1993)

3.3.2 Sawn-Tied Joints

The purpose of a sawn-tied joint is to increase the joint spacing with the addition of reinforcement. With the addition of reinforcement across the joint a larger joint spacing can be achieved whilst ensuring adequate aggregate interlocking across joints as shown in Figure 3.3. For unreinforced slabs these joints are identical to contraction joints.

A maximum joint spacing of 7.5 meter sawn-tied joints is recommended (Marais & Perrie, 1993). The column layout should also be considered when planning joint spacing.

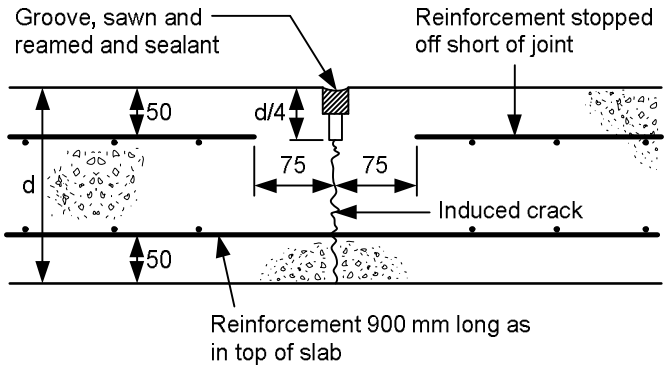

Figure 3.3 Details of typical sawn-tied joint (Marais & Perrie, 1993)

3.3.3 Construction Joints

Construction joints have the same purpose as the joints discussed in the previous sections, but are a joint between different casts. This is a joint type that serves as a day's-work joints and it provides a form of formwork (Marais & Perrie, 1993). These joints can also serve as emergency joints when the concrete sets prematurely or due to interruptions in the construction phase.

Construction joints cannot use aggregate interlocking for load transfer across the joints. Therefore keyways, dowels and tie bars can be used to ensure sufficient vertical load transfer across the joints (Concrete Society Working Group, 2003). See Figure 3.4 for the details of different types of construction joints and methods of allowing load transfer to occur across these joints.

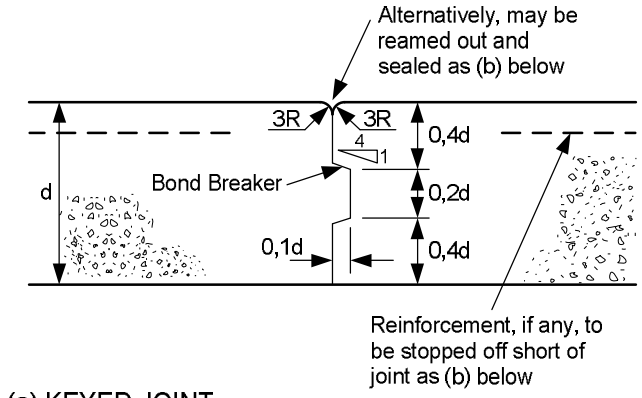

(a) KEYED JOINT

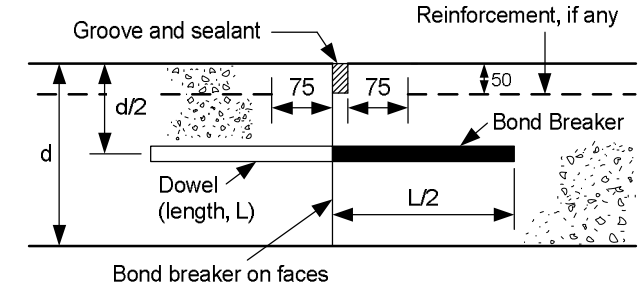

(b) DOWELLED-BUTT JOINT

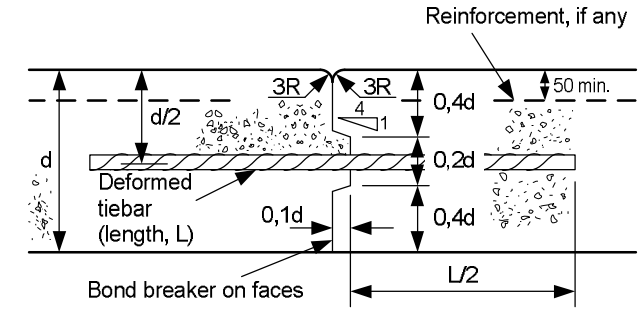

(c) KEYED-AND-TIED JOINT

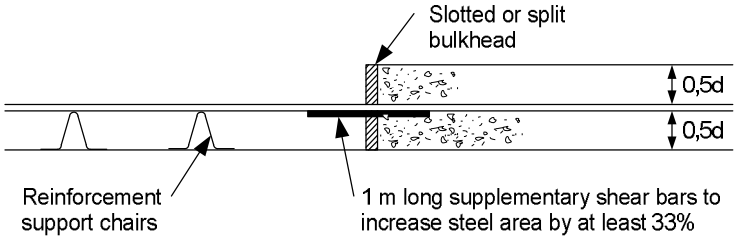

(d) REINFORCED BUTT JOINT

Figure 3.4 Details of typical types of construction joints (Marais & Perrie, 1993)

3.3.4 Isolation Joints

The purpose of isolation joints is to allow horizontal and vertical movement across the joints (Concrete Society Working Group, 2003). These joints are created between the slab and fixed parts of the structure, such as walls, columns, manholes, pits and machinery bases. This prevents the fixed elements from becoming restraints. If such joints are created in trafficked parts, the slab should be thickened by 25% as shown in Figure 3.5.

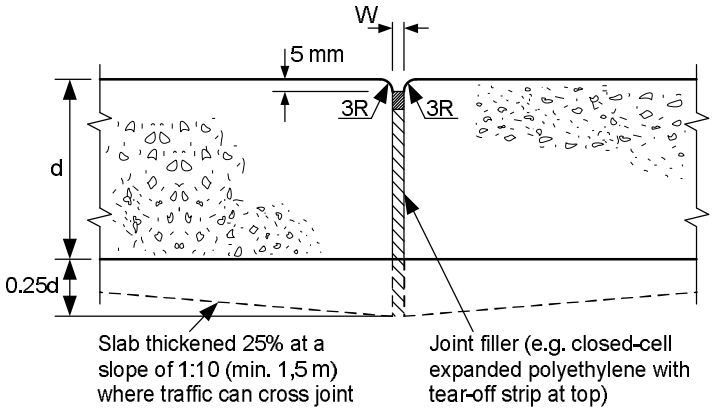

Figure 3.5 Details of typical isolation joint (Marais & Perrie, 1993)

3.4 Design of Slab-on-Grade

The first step in designing a slab-on-grade is to determine a slab thickness which can carry the imposed loads. The next step is to design reinforcement to control DSC or to increase joint spacing. These design methods are discussed in the following sections.

3.4.1 Slab Thickness Design

There are three types of loads that are exerted on a slab-on-grade, such as wheel loads, post loads and distributed loads. The most important factors for determining the slab thickness are the subgrade/sub-base strength, the strength of the concrete of the slab, and the nature and frequency of the imposed loads. The Westergaard's modulus of subgrade reaction (k) is used to represent the stiffness of the subgrade/sub-base (Concrete Society Working Group, 2003).

The objective of the thickness design is to prevent the slab from cracking due to flexural stresses (Sorelli, et al., 2006), to resist bearing stresses on the surface of the slab, to prevent punching shear due to concentrated loads (Marais & Perrie, 1993) and to prevent excessive differential deflections due to settlement of the subgrade.

To design for dynamic loads (Manolis, et al., 1997), wheel loads, the axle load, number of load repetitions, tyre contact area or tyre pressure, and the spacing between wheels and axles are used to determine the slab thickness. In the design for post loads, the maximum post load, the local contact area and the spacing between posts are important. For distributed loads the magnitude of the load, the aisle width between stacks, width of loaded areas and location of joints relative to aisles are considered for the design.

Charts and tables have been developed by Marais & Perrie (1993) to determine the required slab thickness for post loads, wheel loads and distributed loads as shown in Figure 3.6 and 3.7 and in Table 3.3.

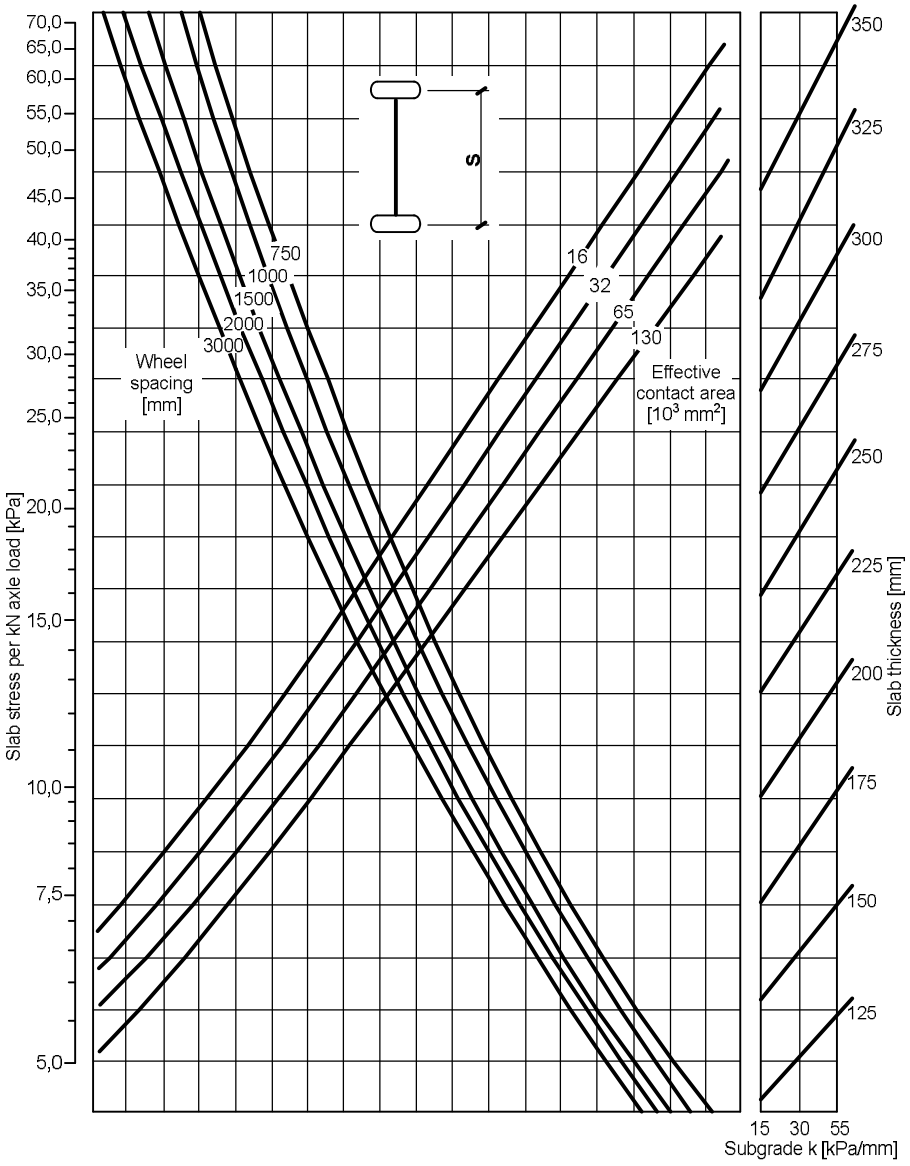

Figure 3.6 Design chart for axles with single wheels (Marais & Perrie, 1993)

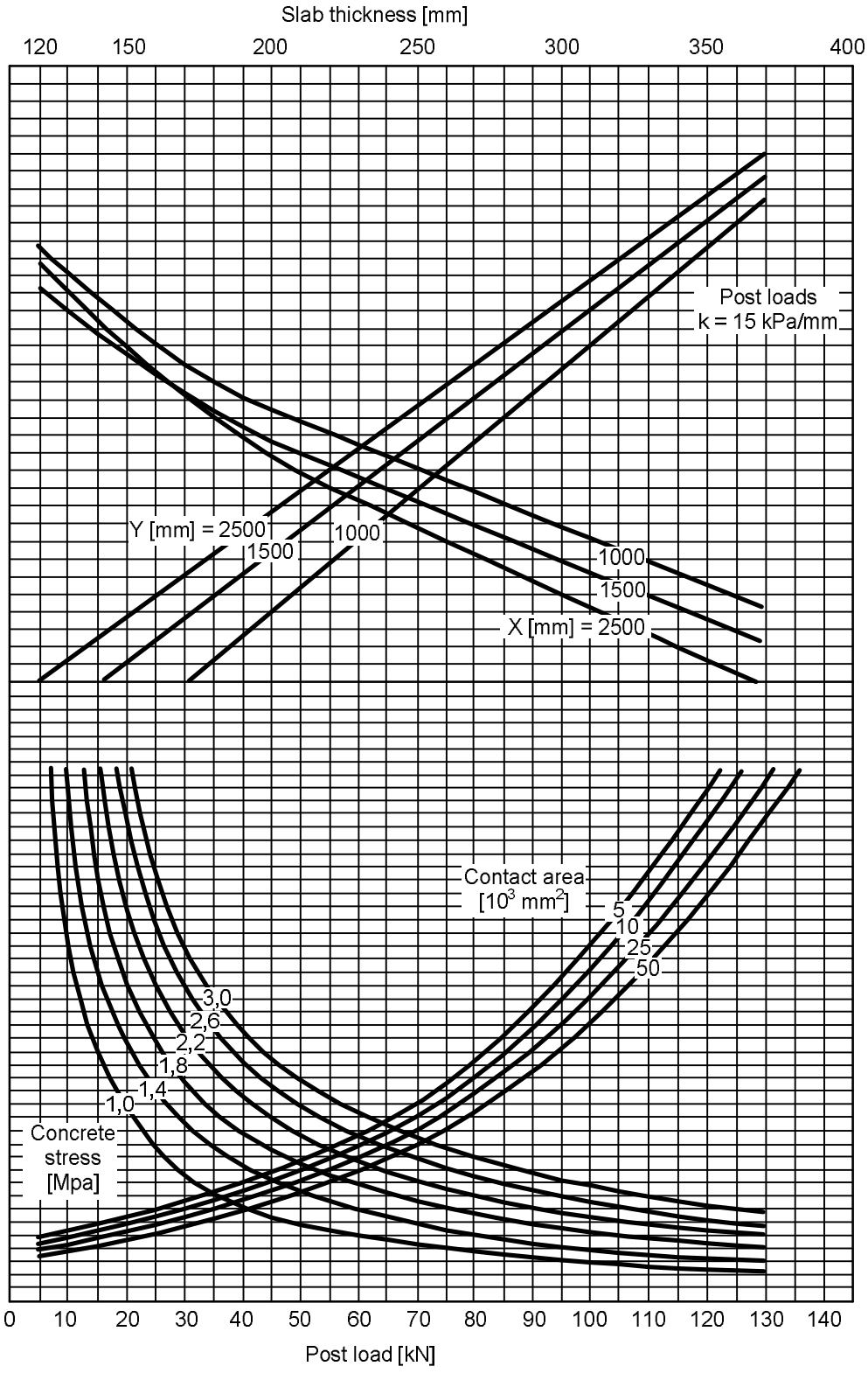

Figure 3.7 Design chart for post loads: k = 15 kPa/mm (Marais & Perrie, 1993)

Table 3.3 Allowable distributed loads [kPa] for variable storage layouts (Marais & Perrie, 1993)

Slab thickness [mm]	Subgrade k [kPa/mm]	Concrete flexural strength [MPa]			
		3.5	4.0	4.5	5.0
120	20	28.0	32.0	36.0	40.0
	40	39.5	45.0	50.5	56.5
	60	48.5	55.0	62.0	69.0
140	20	30.0	34.5	38.5	43.0
	40	42.5	48.5	55.0	61.0
	60	52.0	59.5	67.0	74.5
160	20	32.0	37.0	41.5	46.0
	40	45.5	52.0	58.5	65.0
	60	56.0	63.5	71.5	79.5
180	20	34.0	39.0	44.0	49.0
	40	48.5	55.0	62.0	69.0
	60	59.0	67.5	76.0	84.5
200	20	36.0	41.0	46.5	51.5
	40	51.0	58.0	65.5	72.5
	60	62.5	71.5	80.0	89.0
220	20	38.0	43.0	48.5	54.0
	40	53.5	61.0	68.5	76.5
	60	65.5	74.5	84.0	93.5
240	20	39.5	45.0	50.5	56.5
	40	56.0	63.5	71.5	79.5
	60	68.5	78.0	88.0	97.5
260	20	41.0	47.0	53.0	58.5
	40	58.0	66.5	74.5	83.0
	60	71.0	81.5	91.5	101.5
280	20	42.5	48.5	55.0	61.0
	40	60.0	69.0	77.5	86.0
	60	74.0	84.5	95.0	105.5
300	20	44.0	50.5	56.5	63.0
	40	62.5	71.5	80.0	89.0
	60	76.5	87.5	98.0	109.0
320	20	45.5	52.0	58.5	65.0
	40	64.5	73.5	83.0	92.0
	60	79.0	90.0	101.5	112.5
340	20	47.0	53.5	60.5	67.0
	40	66.5	76.0	85.5	95.0
	60	81.5	93.0	104.5	116.0
360	20	48.5	55.0	62.0	69.0
	40	68.5	78.0	88.0	97.5
	60	83.5	95.5	107.5	119.5

3.4.2 Reinforcement Design

Steel reinforcement is included in slabs-on-grade to improve the tensile and flexural strength of the slab to resist heavier loads and to control DSC in the slab (Ytterberg, 1993). The typical reinforcement used to control the DSC is a steel mesh, as explained in Chapter 2, and is called the distributed reinforcement. The distributed reinforcement is not intended or able to increase the flexural capacity of the slab (Marais & Perrie, 1993). This reinforcement is located in the upper half of the slab height and controls cracking that may occur due to temperature change and shrinkage (Concrete Society Working Group, 2003).

According to the Wire Reinforcement Institute there are five procedures to calculate the required distributed reinforcement area per unit of length (Wire Reinforcement Institute, 2003), namely:

- Subgrade drag procedure
- Confirmed capacity procedure
- Temperature procedure
- Equivalent strength procedure
- Crack restraint procedure

The subgrade drag procedure is generally used with the coefficient of friction determining the amount of reinforcement required. The cross sectional area of steel (A_s) required is measured in square inches per lineal foot of slab width. The allowable stress in the reinforcement (f_s) is measured in pounds per square inch with f_s equal to $0.75f_y$, where the yield stress of the steel (f_y) is measured in pounds per square inch. The coefficient of friction (F) is unitless and the distance between joints (L) is measured in feet. The dead weight of the slab (W) is measured in pounds per square foot which is usually assumed to be 12.5. The area of steel is then calculated using:

$$\boldsymbol{A_s = \frac{FLW}{2f_s}} \tag{3.1}$$

The confirmed capacity procedure is used to determine the minimum required reinforcement to resist a given internal bending moment (Wire Reinforcement Institute, 2003). The cross sectional area of steel (A_s) is measured in the same units as above, and will be the same for all the procedures, and the slab thickness (t) has a unit of inches. The concrete cube compressive strength (f'_c), the yield stress of the reinforcement (f_y) and the modulus of rupture (MOR) is measured in pounds per square inch. The safety factor (SF) in Equation 3.3 is unitless and is normally taken as 2. The following two equations are used to calculate the area of steel required based on this procedure.

$$A_s = \frac{14.5\sqrt{f'_c \times t}}{f_y} \tag{3.2}$$

$$A_s = \frac{4.4 \times MOR \times t}{f_y(SF)} \tag{3.3}$$

The temperature procedure is used to determine the required reinforcement to prevent the cracking of the slab if temperature changes occur (Wire Reinforcement Institute, 2003). The slab thickness (t) has a unit of inches for all procedures that require the slab thickness. The stresses (f_r & f_s) and the modulus of elasticity of the steel (E_s) are measured in pounds per square inch. The range of temperature subjected to the slab (T) is measured in degrees of Fahrenheit and the thermal coefficient, α, has the unit of inch per degree of Fahrenheit. The required area of steel is then calculated using:

$$A_s = \frac{f_r \times 12 \times t}{2(f_s - T\alpha E_s)} \tag{3.4}$$

The equivalent strength procedure is known as the concrete to steel strength ratio and is generally used for airport, taxiways and industrial floors and pavements (Wire Reinforcement Institute, 2003). The units for the symbols are the same as above. The equation used for this procedure to determine the required steel is:

$$A_s = \frac{36\sqrt{f'_c \times t}}{f_s} \tag{3.5}$$

The crack restraint procedure is used to determine the reinforcement requirement to control the maximum amount of shrinkage cracks that may occur (Wire Reinforcement Institute, 2003). The required reinforcement is then calculated using:

$$A_s = \frac{9360t}{f_y} \tag{3.6}$$

The limits of the amount of distributed reinforcement are summarised in Figure 3.8.

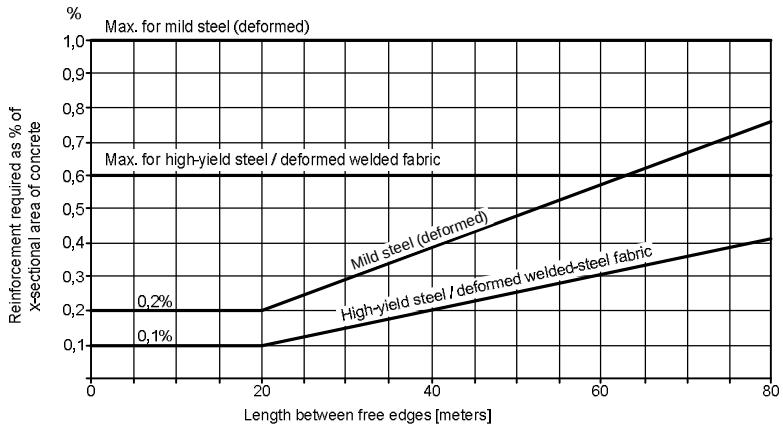

Figure 3.8 Limits of the amount of distributed reinforcement in concrete slabs-on-grade (Marais & Perrie, 1993)

3.5 Concluding Summary

The conventional slab-on-grade was discussed, where the addition of a steel reinforcement mesh and contraction joints are used to control DSC. The sub-layers of the slab-on-grade were investigated, where the soil strength, the concept of plastic index, the uniformity of the subgrade/sub-base and sub-base were discussed. The different joint types were explained, such as contraction joints, sawn-tied joints, construction joints and isolation joints.

Lastly, designing of a slab-on-grade was discussed with the focus on the thickness design and the designing of the reinforcement to control DSC.

Chapter 4 Synthetic-Fibre Reinforced Concrete (SynFRC)

Concrete is strong in compression and weak in tension. This is the main reason for reinforcing concrete structural elements with steel reinforcement, but the rise of cost in building materials, e.g. steel, has started the search for alternative forms of improving the tensile behaviour of concrete. Fibres are a useful reinforcement which improves the concretes post-cracking tensile behaviour and have been researched for more than 40 years (Brandt, 2008).

Different types of fibres have been studied in the past, including steel fibres (Oslejs, 2008) and more recently synthetic fibres (Zheng & Feldman, 1995). Macro synthetic fibres have recently become available, which are used for concrete tunnel linings and industrial concrete floor slabs (Concrete Society Working Group, 2007; Roesler, et al., 2006).

This section deals with the classification, properties and mechanisms of synthetic fibre reinforced concrete and also the mechanical properties of this material in certain loading conditions. The focus of this study is mainly on macro SynFRC.

4.1 Fibre Classification and Properties

The synthetic fibre produced for use in concrete consists of a wide variety of organic polymers. There are different examples of the use of this material in concrete applications, but the focus of this study is on the macro polypropylene fibre. Reports of the experimental application of steel fibres date back to the 1960's, but the use of micro synthetic fibres only started in the 1980's (Concrete Society Working Group, 2007). The micro fibres have much smaller diameters and are intended to enhance the plastic properties of the concrete, and typically these fibres have a Young's Modulus of about 4-6GPa.

Historically these fibres suffered from relatively poor bond properties. Polymer fibres with a higher Poisson's ratio have lower bond because of the effect of tension. This is the property that composite materials rely on mostly. More recently the interest in polymer fibres has led to an increase in Young's Modulus to about 10GPa. The fibre's bond with the concrete has also been increased with a variety of anchorage mechanisms (Richardson, 2005).

4.1.1 Classification

The BS EN 14889 divides polymeric fibres, like polypropylene, polyethylene, polyester, nylon, poly-acrylic and aramids, into two main classes. This classification is made based on the physical properties of the fibres, with Class I: Micro fibres and Class II: Macro fibres shown in Figure 4.1. Micro fibres can be either mono-filamented (Class 1a) or fibrillated (Class 1b). The BS EN 14889

states, “Class II fibres are generally used where an increase in residual (post-cracking) flexural strength is required”, but they give no guidance on the use of such fibres. The BS EN 14889 focusses more on the properties of FRC than on the properties of the fibres themselves (British Standards Institution, 2006). The ASTM is currently working on a standard that classifies FRC for both steel fibres and synthetic fibres (Concrete Society Working Group, 2007).

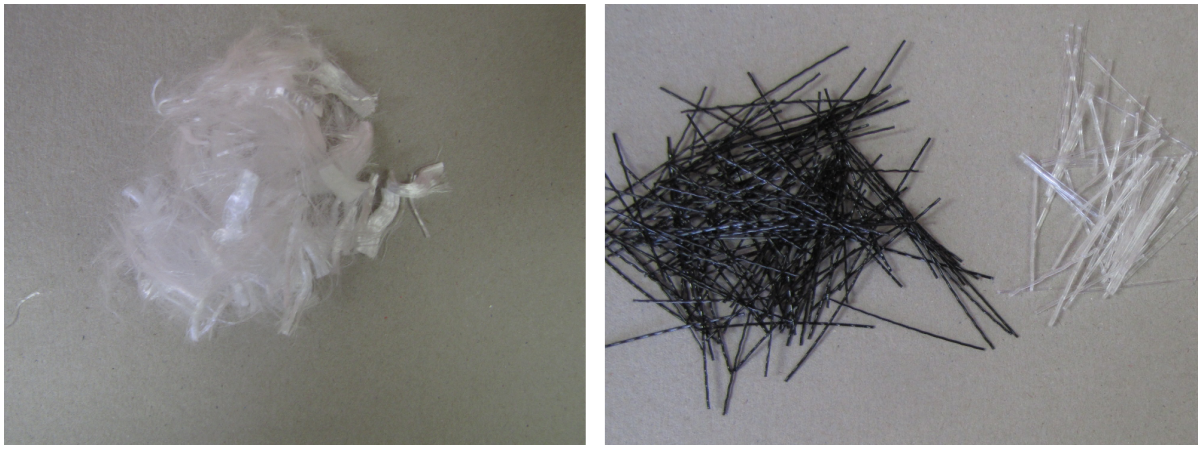

a) Class I: Micro synthetic fibres b) Class II: Macro synthetic fibres

Figure 4.1 Classification of synthetic fibres according to the BS EN 14889 (2006)

4.1.2 Physical Properties

The properties that are most important for using fibres in concrete are the strength, elongation, stiffness and its specific gravity. These properties of different types of synthetic fibres are summarised in Table 4.1. Also of importance is the durability of the fibres, which includes the resistance of the fibres against water or alkalis and its thermal properties. The durability properties of different types of synthetic fibres are shown in Table 4.2.

Table 4.1 Physical properties of synthetic fibres (Zheng & Feldman, 1995)

Fibre Type	Specific Gravity	Tensile strength [MPa]	Elastic Modulus [GPa]	Ultimate elongation [%]
Acrylic	1.17	207-1000	14.6-19.6	7.5-50
Aramid I	1.44	3620	62	4.4
Aramid II (high modulus)	1.44	3620	117	2.5
Nylon	1.16	965	5.17	20
Polyester	1.34-1.39	896-1100	17.5	
Polyethylene	0.96	200-300	5.0	3.0
Polypropylene	0.90-0.91	310-760	3.5-4.9	15

Table 4.2 Durability of synthetic fibres for FRC (Zheng & Feldman, 1995)

	Environmental durability		Thermal resistance	
Fibre Type	**Water resistance**	**Alkali resistance**	**Behaviour at high temperatures**	**Temp. at which all strength is lost [°C]**
Aramid	Good	Good	Progressive loss in tensile strength at 200°C	400-500
Nylon	Good	Good	Progressive loss in tensile strength at 100°C	180-200
Polyethylene	Good	Good	Progressive loss in tensile strength at 100°C	100-130
Polypropylene	Good	Good	Progressive loss in tensile strength at 100°C	120-150
Poly(vinyl alcohol)	Good	Good	Progressive loss in tensile strength at 100°C	200-240
Pitch-based carbon	Good	Good	Gradual decrease in tensile strength at 300-350°C	500-600
Pan-based Carbon	Good	Good	Gradual decrease in tensile strength at 300-350°C	500-600

The fibre type that is the focus of this study is the macro polypropylene fibre which is less dense than water with a specific gravity of 0.90-0.91. The tensile strength of this type of fibre varies between 100-650MPa and the elastic modulus between 2-10GPa. Typical dosages of these fibres are between 0 and 12 kg/m^3, which is about 1.35% by volume of concrete (Concrete Society Working Group, 2007).

4.1.3 Mechanical Properties

Concrete is a brittle material that cracks when it is subjected to a tensile force. Concrete exhibits a limited elastic response which is followed by micro cracking, and thereafter a localised macro crack forms that is followed by rupture (Hughes, et al., 1990). This is shown in Figure 4.2 with the red line representing the behaviour of normal concrete. The introduction of synthetic fibres to the concrete will not alter the elastic response or the stress at which the concrete cracks, but it will enhance the post-cracking behaviour (Oh, et al., 2004).

The volume of fibres added to a concrete matrix determines the behaviour of the post cracking tension behaviour of the concrete (Concrete Society Working Group, 2007). The critical volume of fibres is when the post-cracking strength of FRC becomes more than the tensile strength of the concrete matrix. A volume of fibres less than the critical volume will result in a strain-softening post cracking

response and a volume higher, will result in a strain-hardening post cracking response, see Figure 4.2. This response is measured against the crack mouth opening displacement (CMOD) of the specimen.

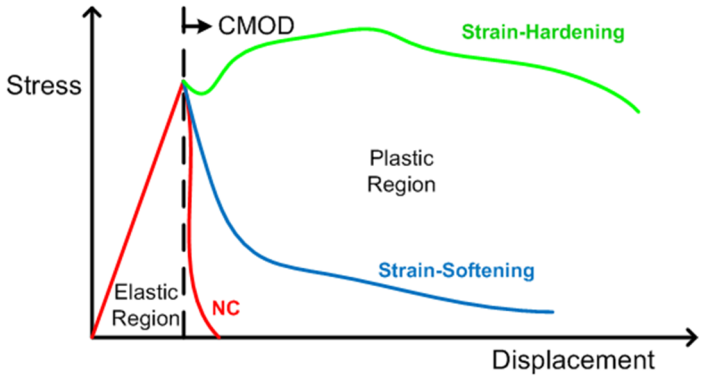

Figure 4.2 Flexural/Tensile behaviour of a crack of FRC

The bending of FRC is even more complex because it is not elastic and it is possible to obtain a deflection-hardening effect with a fibre volume of less than the critical fibre volume in tension (Hannant, 1978). This is due to concrete being stronger in compression than in tension and the movement of the neutral axis towards the compression block of the section. The reason for this will be discussed in more depth in Section 4.2.2.

The FRC performance is therefore determined by the volume of fibres added to the concrete and the physical properties of the fibres. The physical properties in Section 4.2.1 will determine the failure mechanism that occurs across a crack in the concrete and will be discussed in depth in Section 4.3.

4.2 Mechanisms Inducing Crack Control in FRC

There are different mechanisms that occur in FRC composites either across a crack or within the concrete matrix. The mechanism which may occur in the matrix is micro cracking of the concrete matrix between fibres. Across a crack the mechanisms of the fibres within the concrete matrix are fibre breakage, fibre pull-out, fibre bridging and fibre de-bonding, shown in Figure 4.3 from the left hand side.

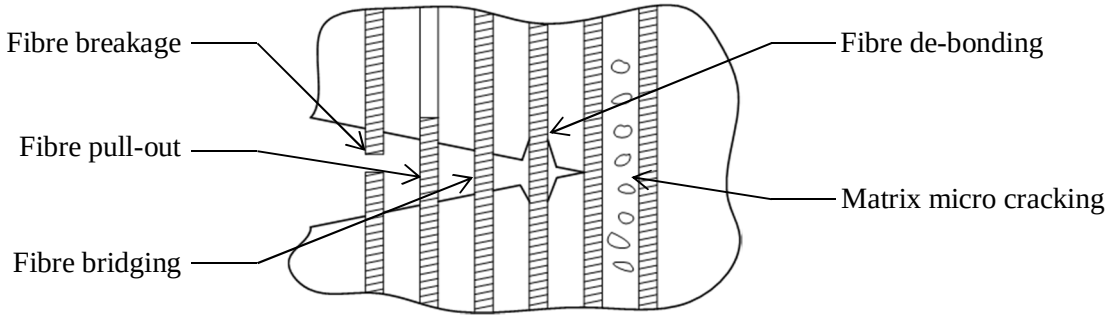

Figure 4.3 Mechanisms that occur within FRC (Zollo, 1996)

Fibre breakage occurs when there is sufficient bond strength on both side of the crack which leads to the fibre strength being exceeded resulting in failure of the fibre. Fibre pull-out is when the bond strength is not sufficient at one or either side of the crack and the fibre pulls out of the concrete matrix. Fibre bridging occurs before fibre breakage occurs, which is when the fibre has sufficient bond strength and the fibre yield strength has not been exceeded. Fibre de-bonding is when the fibre diameter changes and de-bonds from the matrix, which can be due to a chemical reaction between the fibre and the mix constituents. Therefore fibre durability is important when deciding on which fibre type to use within concrete (Zollo, 1996). The Poisson's ratio of the fibre when under a constant tension force may also lead to fibre de-bonding.

4.2.1 FRC in Uniaxial Tension

Performing a tensile test on concrete specimens is uncommon because of the difficulties in performing such tests. It is far more common to use an indirect test method, where a beam is tested in flexure and an inverse analysis is conducted to determine the tensile behaviour of the concrete (Ozcan, et al., 2009). The inverse procedure can be performed in flexural or splitting tests (Esler, et al., 1996).

Fibres are introduced into concrete to improve the post-cracking behaviour of the concrete and will usually result in an FRC that has a strain-softening behaviour. For this reason, if strain-hardening behaviour is required, then it will be more efficient controlling the tensile forces with the addition of steel reinforcement or a wire mesh (Concrete Society Working Group, 2007). This is due to costs.

Direct or indirect tensile tests are sometimes performed with a load controlled test, but this does not show the post-cracking response of a strain-softening FRC. Therefore these tests should be performed using a displacement controlled procedure to obtain the post-cracking response of FRC. Figure 4.4 shows different FRC tensile behaviours which could be obtained through uniaxial tension tests.

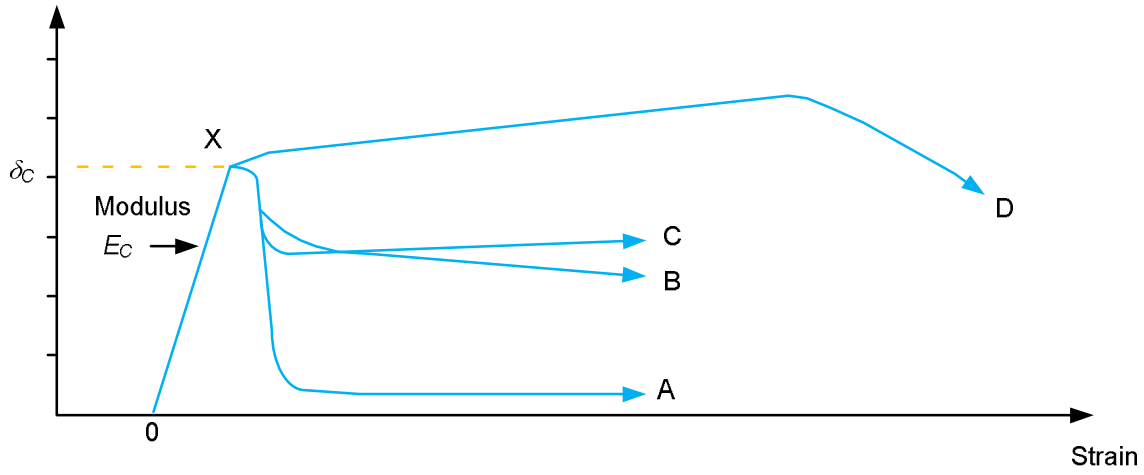

Figure 4.4 Indicative stress strain curves in uniaxial tension (Concrete Society Working Group, 2007)

Curve A is the case of a very low volume of FRC or where a good bond between fibres and matrix can lead to fibre breakage. Curve B is the case where a higher volume of fibres is used for FRC and fibre pull-out is the main mechanism that occurs in the crack. Curve C shows typical behaviour of a macro synthetic fibre with a high modulus of elasticity and high tensile strength, as well as high volume of fibres in concrete. Macro synthetic fibres with a low modulus of elasticity and strength will have a tensile response between curves A and C. Curve D is not that of a synthetic fibre reinforced concrete, but glass or steel fibre that has a fibre volume higher than the critical fibre volume. After the initial cracking, more cracking occurs, forming multiple cracks that contribute to a strain hardening effect (Brandt, 2008). Therefore a maximum tensile force is reached that is followed by a strain-softening response which is determined by the contribution of fibre pull-out and breakage.

The uniaxial tension test is a fundamental procedure in characterising the tensile stress vs crack opening behaviour of FRC, which is used in advanced design methods. These tests are difficult to conduct and there are not many standard methods providing guidance in the performance of such tests. These tests should be conducted by using a displacement controlled procedure. Recently RILEM provided guidance on the uniaxial test method (RILEM, 2001) and a corresponding design methodology for steel FRC (RILEM, 2002).

4.2.2 FRC in Flexure

FRC is a non-linear material in both tension and compression and therefore the elastic beam theory is not applicable to this material after cracking has occurred. There is a big difference between the post-cracking behaviour of FRC composites in bending and in uniaxial tension for all types of fibres (Soroushian, et al., 1998). This is due to the post-cracking tensile behaviour that exists within the FRC, adding to the tensile capacity of concrete, hence modifying the elastic beam theory. This increases the moment capacity of the section and shifts the neutral axis towards the compression side

of the section, leading to higher bending forces than tensile forces. The tensile behaviour also changes with crack widths. Therefore no linear equation can be used to transform bending stresses to tensile stresses directly.

The tensile behaviour of FRC is a combination of fibre pull-out and elastic extension that were discussed in previous sections. At a crack the fibres within the concrete represent many point forces which hold the two sections over the crack together. It is a complex procedure to determine the individual fibre stresses (Wang, et al., 1988). These stresses are determined with the shear bond strength, orientation and the embedment length of each fibre, as well as the distance of the fibre from the neutral axis of the section.

This is the reason why it is common to add a tensile stress block (Hannant, 2003) when the flexural response of the concrete is determined, see Figure 4.5. These analyses also assume that the compression stress remains elastic, which is not entirely accurate because concrete may yield in compression. The ultimate flexural tensile strength, known as the modulus of rupture (MOR), is commonly determined using an elastic stress block as in Figure 4.5a, which is also not the correct method in the case of FRC. Hannant (2003) has made the suggestion of using a rectangular stress block to represent the tensile behaviour of the FRC. This rectangular block method assumes that the compressive block is at a quarter of the depth of the section, which makes this method conservative, see Figure 4.5b. These figures show the theories using a rectangular section.

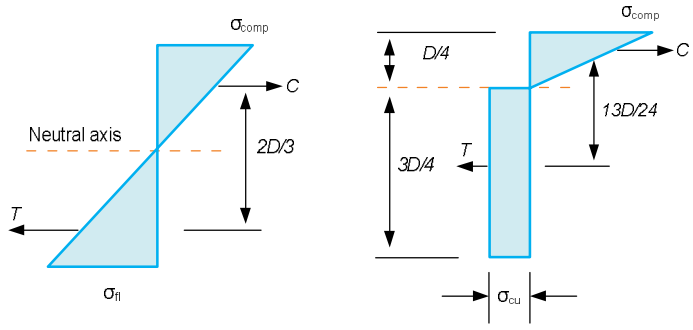

a) Elastic flexural stress block b) Stress block proposed by Hannant

Figure 4.5 Stress blocks used in beam theory for FRC (Concrete Society Working Group, 2007)

Theoretically the neutral axis moves upwards when the flexural response on the beam becomes inelastic, because FRC is much stronger in compression than tension and forces need to be in equilibrium. Therefore the neutral axis moves towards the compression to increase the tension block. Hannant showed that the flexural behaviour of FRC composites is always higher than the uniaxial tension behaviour (Hannant, 2003). In Section 5.3 a method for determining the tensile behaviour of a FRC composite can be established by using an inverse analysis from the results of the flexural behaviour of the FRC.

Typical flexural behaviours of sprayed concrete, tested with 100x100mm beams are shown in Figure 4.6, and more recent curves from load deflection curves of round panel tests are shown in Figure 4.7. Both the steel and macro synthetic fibre concrete curves show linear elastic response up to a point where the concrete cracks, also known as the MOR. After this the fibres contribute to the ductile behaviour seen in Figures 4.6 and 4.7.

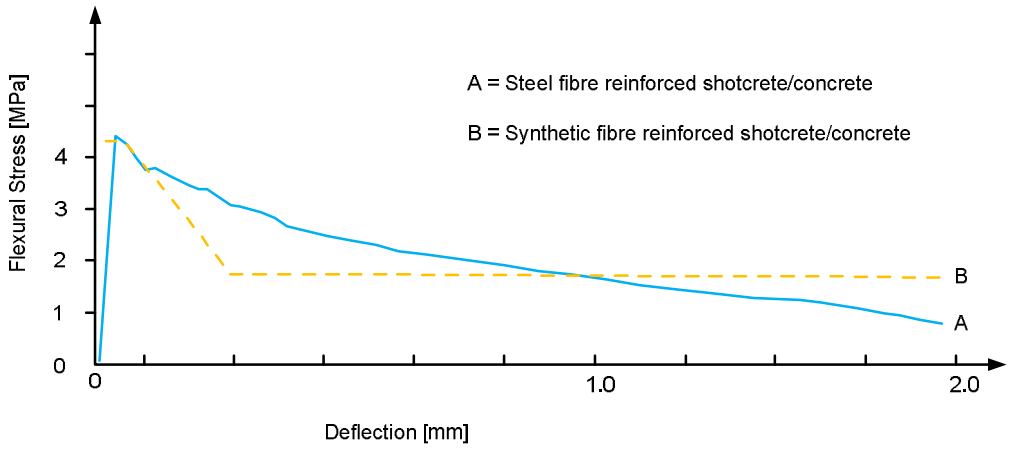

Figure 4.6 Generic stress-deflection curves using 100x100mm beams (Heere & Morgan, 2003)

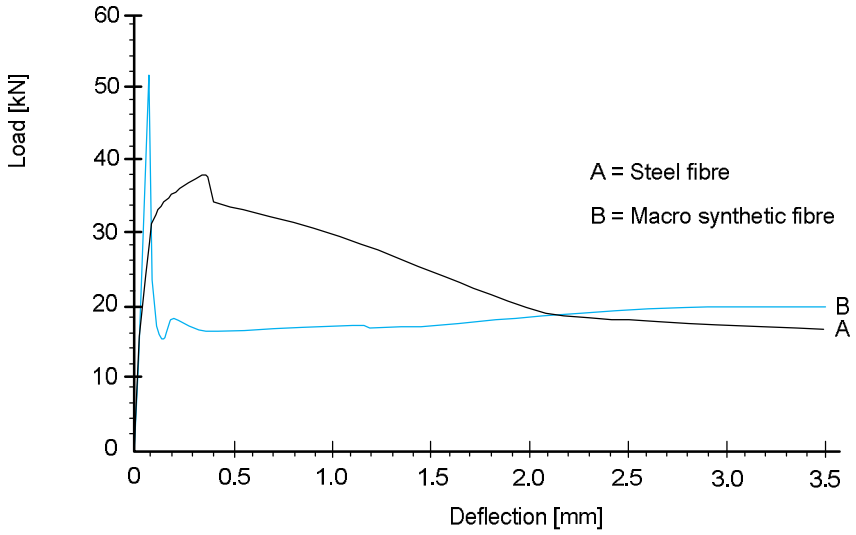

Figure 4.7 Load-deflection curves for steel and macro synthetic fibres from panel tests (Ratcliffe, 2006)

There are a few methods to test fibre reinforced concrete in flexure. One method is performing a three or four point bending test. There is some guidance on how to perform these specific tests (FIB Special Activity Group 5, 2010; ASTM, 1997). Another relatively new method is the round panel test (Bernard, 2000). All of these tests use a displacement controlled process to show the fibre behaviour in the post-cracking of the specimens.

4.3 Mechanical Properties of Fibres Controlling Cracking

When concrete is subjected to drying shrinkage and is restrained against movement, tensile stresses develop within the concrete and cracking occurs. After a crack initiates due to tensile forces, the concrete does not provide any tensile resistance and the fibres are the only resistance against the tensile forces bridging the crack. It is important to note that fibres only start contributing to the resistance of tensile forces when the concrete has cracked. A fibre bridging a crack and the mechanisms of fibre bridging which controls crack widths are shown in Figure 4.8. The mechanical properties of the fibre and the concrete as well as the bond strength between the two determine the performance of the FRC.

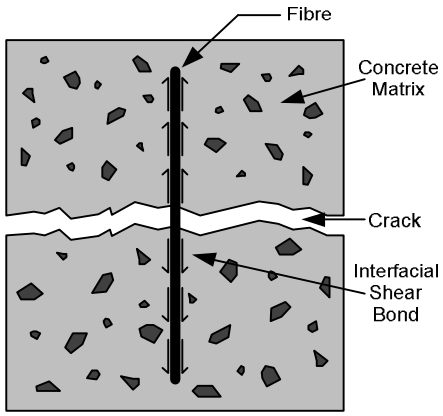

Figure 4.8 Mechanism of a fibre bridging a crack plane

The factors contributing to fibre bridging, as shown in Figure 4.8, are the interfacial shear bond, the fibre volume and the fibre aspect ratio (Hannant, 1978). These factors are discussed in the following sections.

4.3.1 Interfacial Shear Bond Stress

An interfacial shear bond stress is necessary between the fibre and the concrete matrix to allow any tensile force transfer from the concrete to the fibre (Richardson, 2005). If there is no interfacial shear bond between the fibre and the concrete then no tensile resistance will develop within the fibres and the tensile capacity of the matrix will only rely on the concrete (Johnston, 2001).

Adhesion, friction and mechanical interlocking are the mechanisms responsible for the interfacial shear bond. These factors depend on the fibre type and the anchorage system incorporated into the fibre type. Most macro synthetic fibres are crimped or corrugated to increase the bond strength of the FRC through a form of interlocking, see Figure 4.9. Also shown in Figure 4.9 are different techniques to improve the interlocking mechanism between the fibres and the concrete. These fibres do not have any chemical reaction with the concrete and therefore no adhesion develops between the fibres and

the concrete. However, the fibres have a lower strength than the concrete aggregate and this allows the small aggregate particles to slightly penetrate the fibres, which increase the frictional effect, see Figure 4.10. (Richardson, 2005)

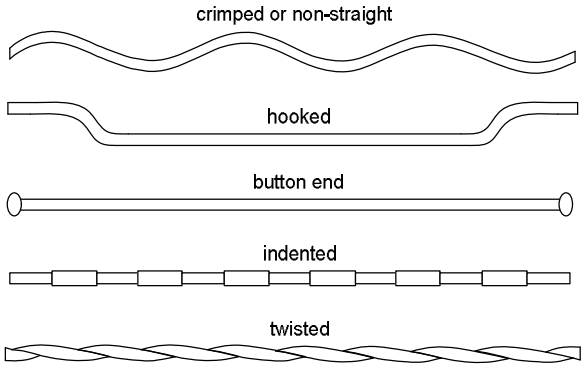

Figure 4.9 Examples of deforming fibres to increase interlocking (Brandt, 2008)

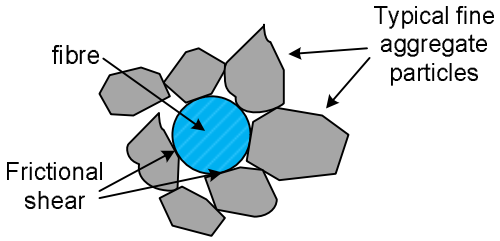

Figure 4.10 Frictional shear caused by fine aggregates

4.3.2 Fibre Volume

The quantity of fibres used in a concrete mix is usually expressed as a percentage of the volume of the concrete mix. This is to simplify the comparison between different types of fibres since all fibres do not have the same relative densities. Therefore two different types of fibres with the same size and volume percentage within a mix will have a different total mass. (Hannant, 1978)

Theoretically, the increase of fibre volume will increase the number of fibres that bridge a crack plane, see Figure 4.11. This requires each fibre to transfer a smaller load between the two sections of the concrete. This leads to a lower force in each fibre that will decrease the bonding required, ultimately leading to a higher tensile load capacity across a crack.

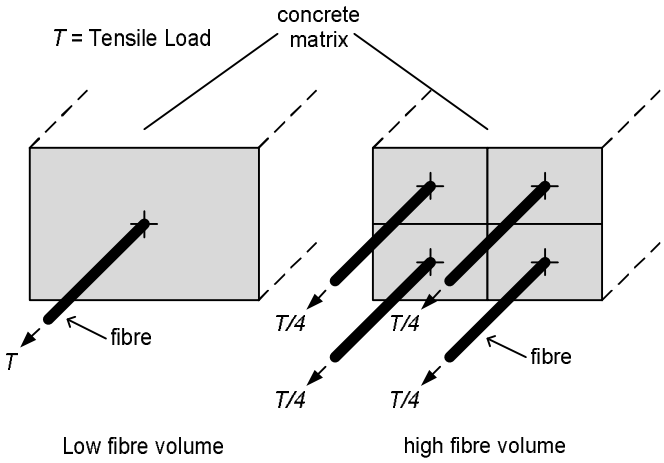

Figure 4.11 Effect of increasing fibre volume on the tensile load per fibre

4.3.3 Fibre Aspect Ratio

The fibre aspect ratio, also known as the L/d ratio, is the ratio between the fibre length and the fibre diameter. Accordingly a longer fibre with a small diameter will have a larger aspect ratio than a short fibre with a larger diameter.

If two fibre types with the same length and fibre content, but with different fibre diameters are used in concrete, it is possible for the smaller diameter fibre to be more effective. The reason for this is that the overall surface area of the smaller diameter fibre is larger than that of the larger diameter fibre (Bagherzadeh, et al., 2001). The smaller diameter fibre will also have more fibres crossing a crack plane at the same volume of fibres. This results in smaller spaces between fibres which reduce the stress concentration and improve the crack stress resistance (Banthia & Gupta, 2006). When the fibre diameter becomes too small, the surrounding particles cannot interact with the fibre and insufficient interfacial shear bond develops between the fibre and the matrix.

4.4 Concluding Summary

The focus of this chapter is on macro synthetic fibres and the behaviour in concrete composites. Firstly the fibre properties and the classification of the different synthetic fibres were investigated. Then the physical and mechanical properties between the fibres and the concrete mix were discussed to get a better understanding of fibres.

The mechanisms that are responsible for crack control within FRC were discussed, with the focus on the uniaxial tension and flexural behaviour. The mechanical properties of the fibres that control the cracking of the concrete were discussed. These properties are the interfacial shear bond, the fibre volume and the aspect ratio of the specific fibre.

Chapter 5 Material Parameter Characterisation

Fibre reinforced concrete (FRC) is a specialised material with material properties that depend on the fibre properties, the matrix properties and the interface between the fibres and the matrix. The fibre properties include the fibre length, diameter, anchorage mechanism, strength and elastic modulus. The matrix properties depend on the mix constituents and their properties, as well as the matrix strength and elastic modulus. These properties were discussed in Chapter 4.

Before any experimental work or modelling can be performed on FRC, the material properties should be characterised. In order to characterise the FRC, tests need to be performed. The following sections describe the tests performed to characterise FRC.

5.1 Experimental Framework

The FRC material behaviours that are of interest for the analyses performed in Chapter 6 are the tension and compressive behaviour. The tensile behaviour was determined using flexural tests and an inverse analysis procedure (Section 5.3). Most of the other material properties and factors required for these analyses are obtained from literature, as will be discussed in Chapter 6.

The material behaviours that are of interest for the analyses performed in Chapter 6 are the tensile-, shrinkage- and friction behaviour of FRC. The following sections discuss the tests that were performed to obtain these properties.

5.1.1 Test Objectives

Experimental tests were performed to achieve the following two objectives:

Objective 1

The first set of experimental tests was performed to determine the flexural behaviour of macro SynFRC to be used in the inverse analysis procedure. These would be used to perform the finite element analyses (FEAs) discussed in Chapter 6.

Objective 2

The second group of experimental tests were performed to determine the flexural, compressive, friction and shrinkage behaviour of the macro SynFRC used in the full scale tests discussed in Chapter 7.

5.1.2 Test Program

Compressive Tests

Compressive tests were performed on 100x100x100mm cubes of macro SynFRC in accordance to SABS method 863:1994. The first set of tests was performed to estimate the compressive strength of the three different polypropylene FRC composites used for analysis in Chapter 6. These include a micro fibre (Chryso Fibre Plus) and two types of macro fibres (Fibsol Rockstay CXO 40, Geotex GRO 50). The first set of tests was performed on specimens at an age of 7 days, which were placed in curing tanks 24 hours after the casting(directly after demoulding them) and tested an hour after the specimens were removed from the curing tanks. The curing tanks were kept at a temperature of 23±1°C. The second set of tests was performed to estimate the compressive strength development of the SynFRC used for the full scale tests discussed in Chapter 7. These cubes were cast the same time as the slabs discussed in Chapter 7. A set of four cubes were tested at three different ages: 3, 7 and 28 days.

The second set of cubes was not cured, to ensure that the concrete cast in the slabs and the cubes were hardened under the same conditions. The cubes were demoulded 24 hours after casting and stored between the slabs, see Figure 5.1. The large slabs discussed in Chapter 7 were not cured, because they were tested for shrinkage. Therefore the cubes were not cured.

Figure 5.1 Cubes stored between slabs to experience the same environmental conditions

Flexural Tests

Flexural tests were performed on 150x150x700mm beams of micro- and macro SynFRC. The fibres used for all the tests were polypropylene fibres. These tests were performed to determine material behaviour to be used in the analyses discussed in Chapter 6.

The first set of tests was performed with three different fibre types which include a micro- (Chryso Fibre Plus) and two types of macro polypropylene fibres (Fibsol Rockstay CXO 40, Geotex GRO 50). These fibres will be discussed in Section 5.1.4. The contents used for the micro SynFRC beams were 0.1, 0.2 and 0.3% by volume, and 0.2, 0.3 and 0.4% by volume for the macro SynFRC beams. These beams were all tested at an age of 28days.

The second set of tests was all performed with the Geotex macro polypropylene fibre, with a fibre dosage of 0.266% by volume. These beams were cast the same time as the full scale slabs discussed in Chapter 7, hence the fibre content difference. The flexural tests were performed on the beams at three different ages: 3, 7 and 28days. All of the beams were demoulded after 24 hours and placed in curing tanks at a temperature of 23±1°C. The beams were removed from the curing tanks 24 hours before testing and placed in a temperature controlled room which is kept at a temperature of 23±1°C. The only time the beams were removed from the curing tank, was when the beams were notched. The saw used for the notching is shown in Figure 5.2. The notching was performed at a concrete age of 2 days and required the beams to be removed from the curing tank for 2 hours. The beam notch was cut 25mm deep and 3mm in width.

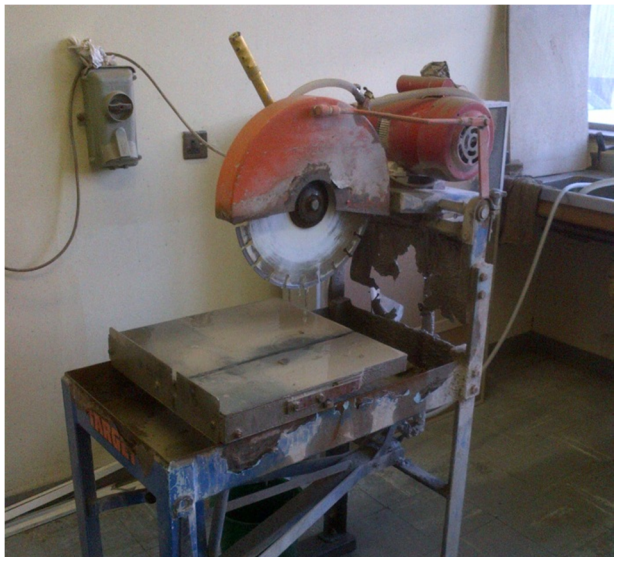

Figure 5.2 Machine used for notching of beam specimens

Friction Tests

Friction tests were performed on 100x100x100mm cubes that were cast using normal concrete without any fibres. The concrete cubes were cast directly on to a wooden surface and were left to set for 24 hours after which the moulds were removed. The wooden surface was used for the full scale tests discussed in Chapter 7. Therefore these cubes were cast on a variety of wooden surfaces to determine which surface to use. The moulds used for these cubes are shown in Figure 5.3.

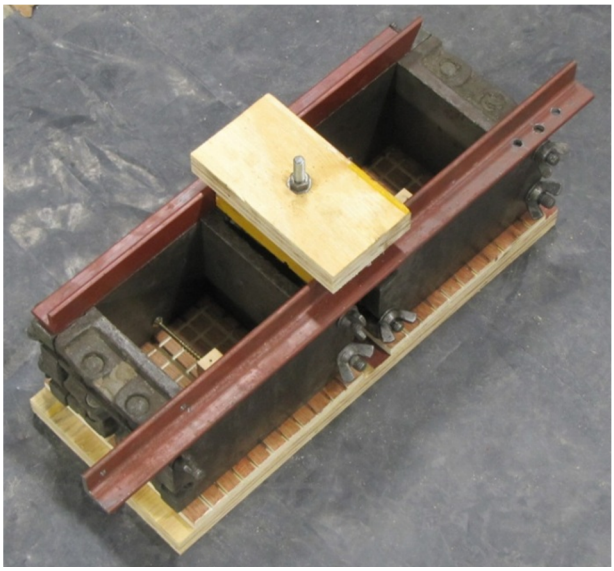

Figure 5.3 Moulds used for casting the friction test specimens

Before casting, wooden blocks were placed in the mould which will provide a surface to anchor the cable to the cube. This cable was used to pull the concrete cube across the wooden surface to determine the force vs displacement diagrams for these tests. These blocks were anchored into the cube with the aid of chipboard screws turned into the sides of the wooden block, see Figure 5.4.

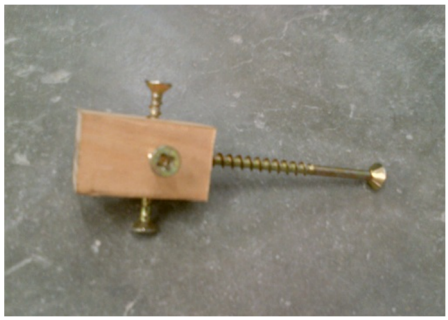

Figure 5.4 Wooden blocks that were placed within concrete cubes for friction tests

The first set of friction tests was performed to determine the friction between concrete and a wooden surface, with different types of grooves to enhance the friction bond between the concrete and the wood. These grooves were added to increase the friction for the full scale tests discussed in Chapter 7. Afterwards a surface type was selected to be applied to the test setup discussed in Chapter 7. These tests were performed on specimens with an age of 7 days. The cubes were not cured to avoid the wood surface from soaking up water that might cause swelling of the wood and create a weakness in the bond between the wood and the concrete.

The second set of friction tests was performed to determine the friction development between the concrete and the wood surface that was selected based on the first set of tests. These tests were

performed at concrete ages of 7 and 28 days. The cubes were not cured, again to avoid the wood from swelling, but also to ensure the cubes were in the same condition as the large slabs.

Shrinkage Tests

Shrinkage tests were performed on 100x100x500mm beams of macro SynFRC used for the full scale tests discussed in Chapter 7. The fibre content was 0.266% the same as the full scale tests. The tests were performed to determine the free shrinkage strain that occurred within the concrete specimens. The beams were sealed on the sides and the bottom to prevent moisture from escaping. This was also done for the full scale tests. This ensured that evaporation could only occur from the top surface, which is the case for slabs-on-grade. The beams were not cured to provide exactly the same hardening conditions for the full scale slabs and the free shrinkage beams.

5.1.3 Test Setups and Procedures

Compressive Tests

The compression tests were performed in accordance with the SANS 5863:2006. Each of the cubes was weighed and dimensions were recorded before testing. The weight and dimensions of each cube was then used to determine the concrete density. Each cube was placed in a Contest compression machine and compressed to determine the maximum compressive force of each cube.

Flexural Tests

The flexural tests were performed in accordance with the FIB 2010 Model Code. Each of the beams was measured to determine the dimensions of the beam specimen. These dimensions were used to determine the cross sectional area where the cracking occurs. Plastic blocks were attached with epoxy to the sides of each beam, which allows linear variable displacement transducers (LVDTs) to be secured, as well as at the top of the notch to measure crack mouth opening displacement (CMOD), shown in Figure 5.5.

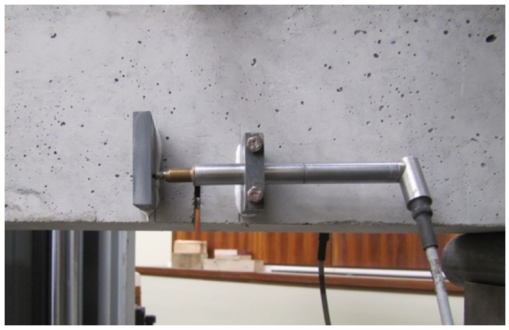

Figure 5.5 LVDT secured to the side of beam to measure CMOD in flexural tests

Each beam was then placed into the Zwick Z250 test machine, shown in Figure 5.6, which was set up for a three point flexural test in which the beam has a span length of 500mm. The test was performed using closed loop control where the CMOD measured in the LVDT on the front face of the beam, was used. The CMOD rate selected for the flexural test was 1.2 mm/min. The flexural results obtained will be discussed in detail in Section 5.2.2.

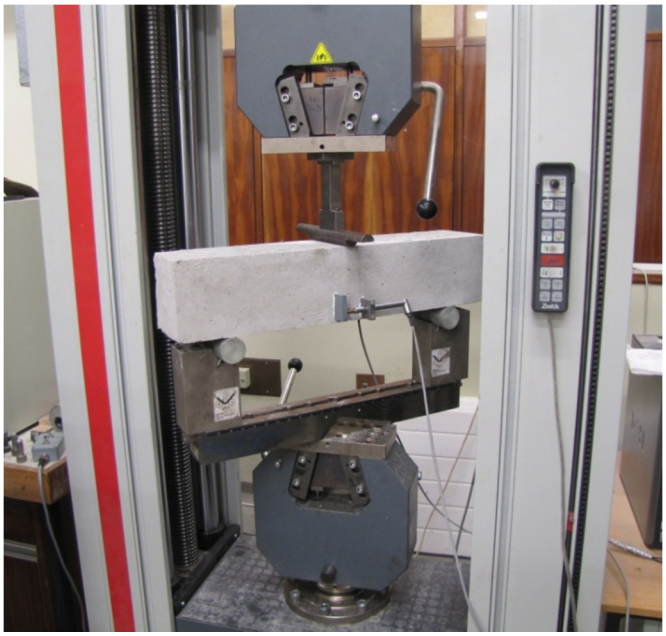

Figure 5.6 Test setup for 3 point flexural tests within the Zwick Z250 test machine

Friction Tests

The friction test setup was designed to apply a tension force to the side of a cube with the aid of a cable and pulley system that develops a friction shear between the concrete cube and the wood base. The test was performed with the Zwick Z250 test machine and is shown in Figure 5.7.

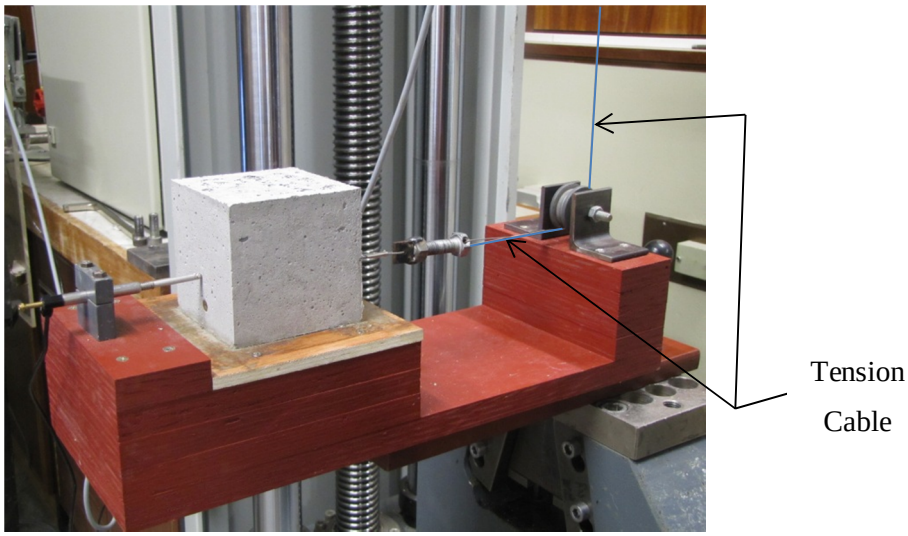

Figure 5.7 Friction test setup within the Zwick Z250 test machine

The pulley allowed the vertical force applied by the test machine to be redirected into a horizontal force, which was measured with a load cell connected between the test machine and the cable, see Figure 5.8. The cable was attached to the cube with a small piece of angle iron with a bolt and a few nuts connected to it, shown in Figure 5.8. The displacement was measured with the LVDT connected to the back of the test setup as shown in Figure 5.7. This results in a graph providing the force versus the displacement of the cube on top of the wooden surface. The cubes were weighed after each test to determine the coefficient of friction between the cube and the wooden surface.

Figure 5.8 Details of connections used for the friction test setup

Shrinkage Tests

The shrinkage tests were performed by placing the beam specimens on rollers between the slabs cast for the test setup discussed in Chapter 7. This allowed the specimens to move freely without the interference of any external restraint. Markers were placed on all four faces of the beam, which were used to take measurements at chosen time intervals, see Figure 5.9. The markers were placed 100mm apart and at the centre of the beam.

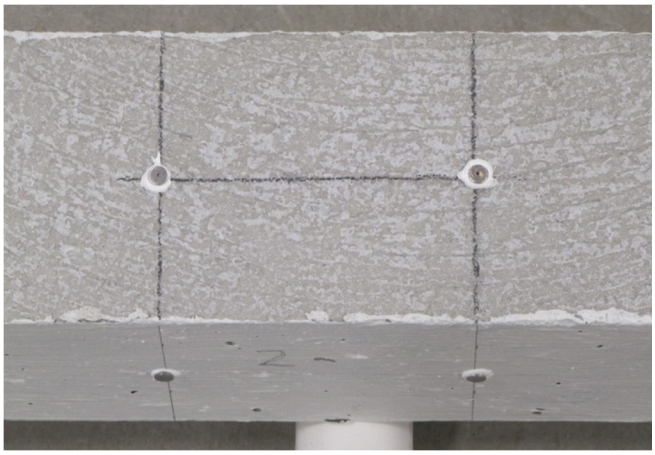

Figure 5.9 Marker placed on the sides of the shrinkage beam specimens

Measurements were taken with the aid of an LVDT connected to an apparatus with two sharp points that fits within the marker centres, see Figure 5.10.

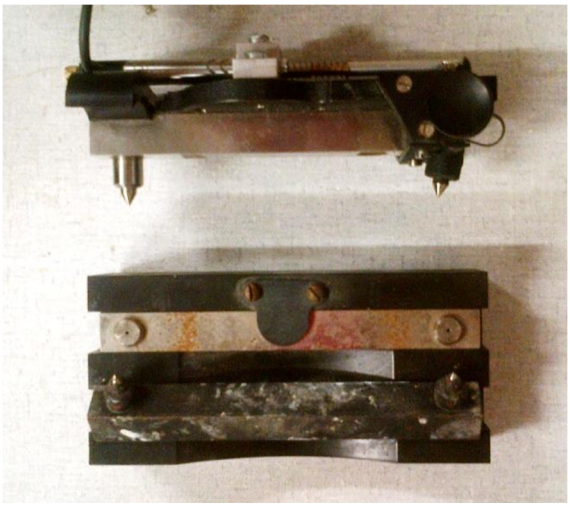

Figure 5.10 Strain measurement apparatus used to determine shrinkage strain

The shrinkage strain was then determined by dividing the change of length between the markers with the original length that the markers had been apart (100mm). Measurements were repeated three times to ensure a dependable value. The measurement was taken to the nearest 0.0025mm. The shrinkage strain was determined using:

$$\varepsilon_{sh} = \frac{L_{ti} - L_{t0}}{L_{t0}} \quad \textbf{(5.1)}$$

where L_{ti} = measured length at time i

L_{t0} = measured length at time 0

The markers were attached to the beams with epoxy after the beams had been removed from their moulds, which was 24 hours after casting the beams. The epoxy was allowed to set for 2 hours after which the zero measurements were taken. In the first month measurements were then taken every 12 hours for the first 2 days and daily afterwards. For the next month measurements were taken every 2 to 3 days and for the last month the measurements were taken weekly. The specimens were thus allowed to shrink for 3 months.

5.1.4 Material Properties

The material properties of all the fibres used for this study were discussed in this section. The three different fibre types used were the micro polypropylene fibre supplied by Chryso and the macro polypropylene fibres supplied by Geotex and Fibsol. The important material properties of the polypropylene fibres used are summarised in Table 5.1. These values were obtained from the manufacturers.

Table 5.1 Important fibre properties for polypropylene fibres used

Fibre Type	Class	Length [mm]	Diameter [mm]	Tensile Strength
Chryso Fibre Plus	Ia	12	0.020-0.035	36 cN/tex
Fibsol Rockstay CXO 40	II	40	0.8	300N/mm^2
Geotex GRO 50	II	50	0.9	295N/mm^2

The first set of tests was performed using the materials available in the concrete lab at Stellenbosch University and the second set of tests used a standard 35MPa floor mix supplied by Lafarge-Ready mix. The first set of tests was used for the analyses discussed in Chapter 6. The second set of tests was to determine the material properties and behaviour of the full scale tests discussed in Chapter 7.

5.1.5 Mix Proportions

The first two concrete mixes were used for the first group of tests which were performed to obtain material parameters for the analyses discussed in Chapter 6. These are shown in Table 5.2.

Table 5.2 Mix designs and fibre dosages for first group of tests

Material		Micro FRC [kg/m^3]			Macro FRC [kg/m^3]		
Water	Tap	200			180		
Binder	CEM I 52.5N	308			277		
Stone	13mm Greywacke	800			975		
Sand	Malmesbury	1055			965		
Plasticiser	Plast 900	1.00			1.00		
Fibre content [%]		0.1	0.2	0.3	0.2	0.3	0.4

The third mix was used for the full scale slabs tested for DSC discussed in Chapter 7. This mix was designed and supplied by Lafarge Ready mix. The fibres were added into the mixing drum of the concrete truck before casting, which is discussed in Chapter 7. In Table 5.3 the mix proportions for this standard floor mix from Lafarge are shown.

Table 5.3 Mix design and fibre dosage for second group of tests

Material		[kg/m^3]
Water	Tap	175
Binder	CEM I 52.5	140.7
	Slag	140.7
Stone	19mm Greywacke	740
	13mm Greywacke	306
Sand	Super Sand	360
	Dune Sand	519
Admixture	OMEGA 154	1.5
Fibres content [%]	Geotex GRO 50	0.27%

5.2 Experimental Results & Discussion

The experimental results discussed in this section are from compression-, flexural-, friction- and shrinkage tests. All of these tests were performed to obtain the behaviour and characteristics of SynFRC, and also to determine parameters that were used in FEA.

5.2.1 Compressive Tests

The densities and the compressive strength of the three different types of polypropylene FRC at an age of 7 days are shown in Table 5.4.

Table 5.4 Density and Compressive stress of different types of polypropylene FRC with different fibre content

Fibre Type	Fibre Volume [%]	Density [kg/m^3]	7 day	
			Strength [MPa]	COV [%]
Chryso (micro)	0.1	2271	26.3	10.8
	0.2	2222	23.7	1.1
	0.3	2183	21.2	4.0
Fibsol (macro)	0.2	2346	26.2	7.7
	0.3	2342	28.4	6.1
	0.4	2335	27.5	11.4
Geotex (macro)	0.2	2328	27.3	13.2
	0.3	2316	27.3	9.4
	0.4	2317	24.0	6.2

It is interesting to notice that the compressive strength of the micro FRC decreases with the increase of fibre volume and that this is not the case for both the macro FRCs. The concrete mixes were designed to obtain a compressive strength of 30MPa and all of the mixes surpassed this strength at 28 days assuming that the 7 day strength is equal to 70% of the 28 day strength.

The densities and the compressive strengths of the macro SynFRC used for the full scale tests discussed in Chapter 7, at ages of 3, 7 and 28 days are shown in Table 5.5.

Table 5.5 Density and Compressive stress of macro SynFRC at different ages

Age [days]	Density [kg/m^3]	COV [%]	Strengh [MPa]	COV [%]
3	2389.0	0.5	21.10	4.0
7	2387.9	0.8	30.32	5.2
28	2353.6	0.6	43.12	1.9

The compressive strength of the concrete forms an expected trend, shown in Figure 5.11, which shows an increase with age. The density of the concrete is decreasing with age, this shows a loss of volume with age, which is due to the effect of drying.

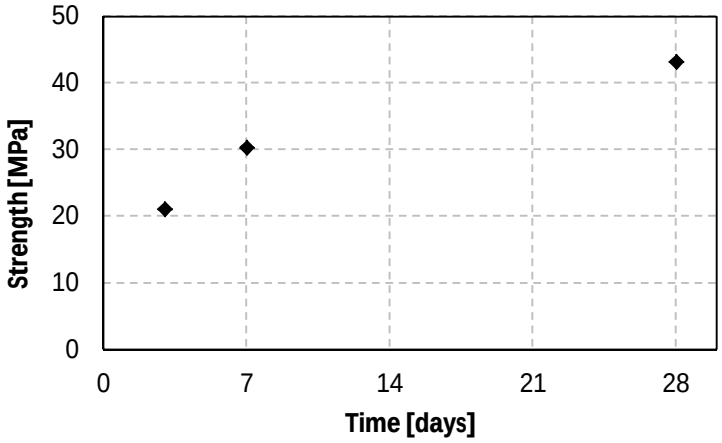

Figure 5.11 Compressive strength development with age of macro SynFRC

The concrete mix was designed to represent a compressive strength of 35MPa which was surpassed between 7 and 28 days, and progressed to a compressive strength of 43MPa. Therefore the concrete passed the compressive strength requirements.

5.2.2 Flexural Tests

The results of the first set of tests are shown in Figures 5.12 to 5.14, which include the micro and macro polypropylene FRC considered for this study. The average results for each of the fibre contents are presented in this section and the individual specimen results are shown in Appendix A.

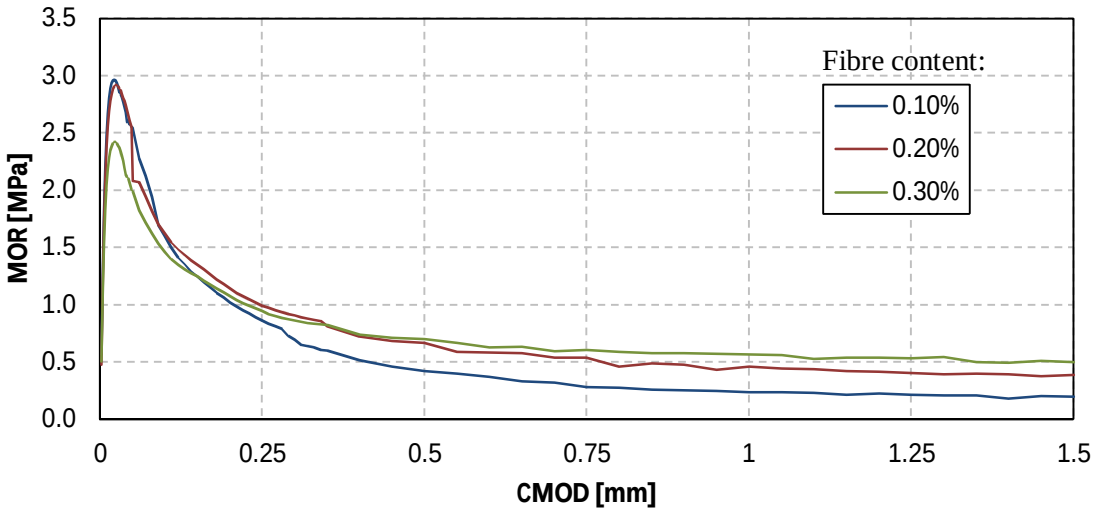

Figure 5.12 Flexural results for micro polypropylene FRC using Chryso fibres

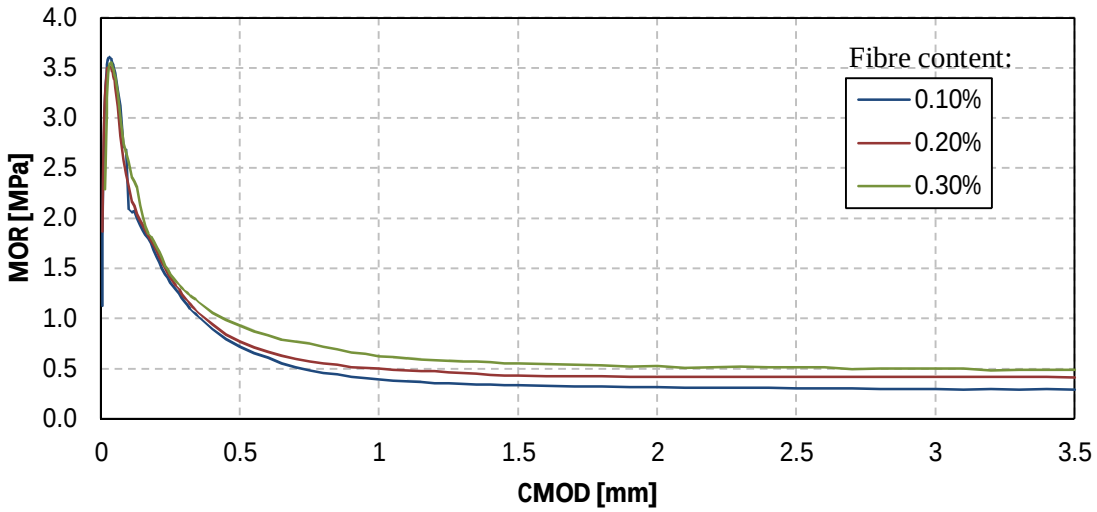

Figure 5.13 Flexural results for macro polypropylene FRC using Fibsol fibres

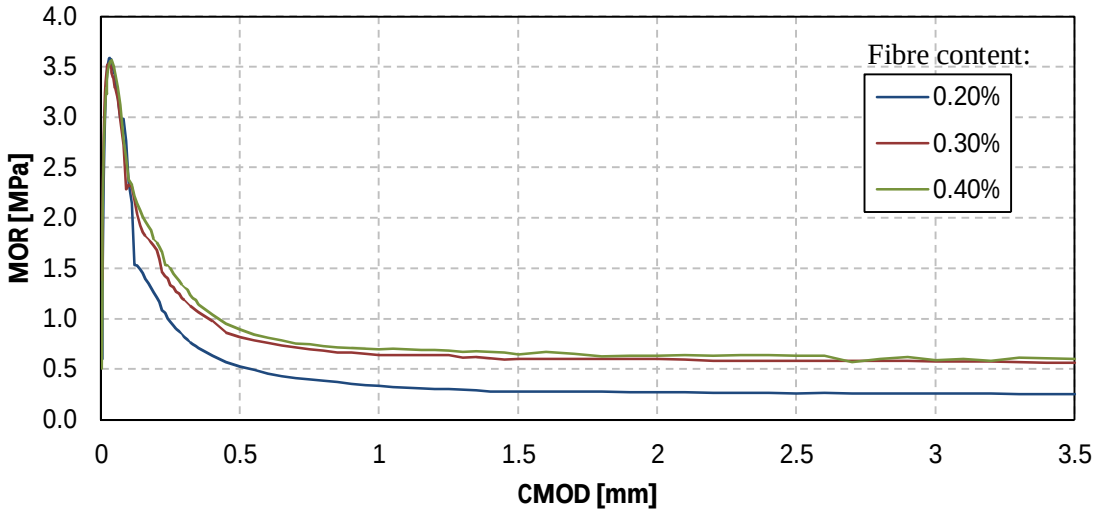

Figure 5.14 Flexural results for macro polypropylene FRC using Geotex fibres

A small difference in the maximum MOR between the micro and macro FRC is observed, with the MOR of the micro FRC at about 3.0MPa and the macro FRC at about 3.5MPa.

The $R_{e,3}$ values of the macro polypropylene fibres were calculated from the above results and are shown in Figure 5.15. The reason for not calculating the $R_{e,3}$ values of the micro FRC is because the flexural tests of this FRC were only performed to a CMOD of 1.5mm (due to the short fibre lengths, to prevent the beams from failing completely and damaging lab equipment) and a crack width of 3.333mm (L/150 = 500/150 = 3.333) was required to calculate these values (Concrete Society Working Group, 2003).

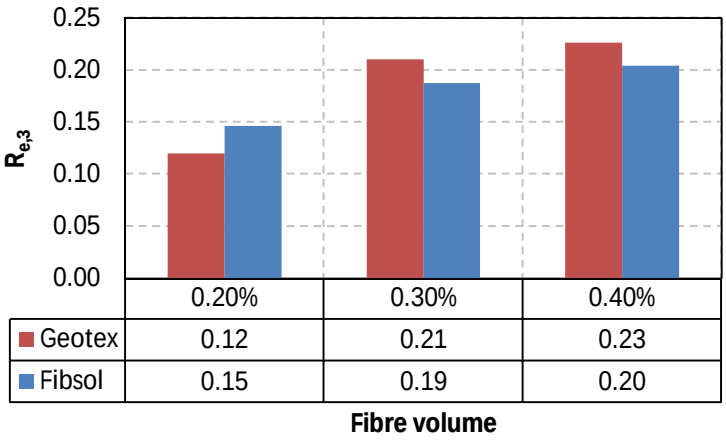

Figure 5.15 $R_{e,3}$ values for the macro polypropylene FRC

The average results of the second set of tests are shown in Figure 5.16, which contained the macro polypropylene FRC produced by Geotex. These tests which were performed at concrete ages of 3, 7 and 28 days, were performed to determine the flexural development of the FRC. This was to determine the flexural development of the SynFRC used for the full scale tests discussed in Chapter 7. The individual results of each beam specimen are shown in Appendix A.

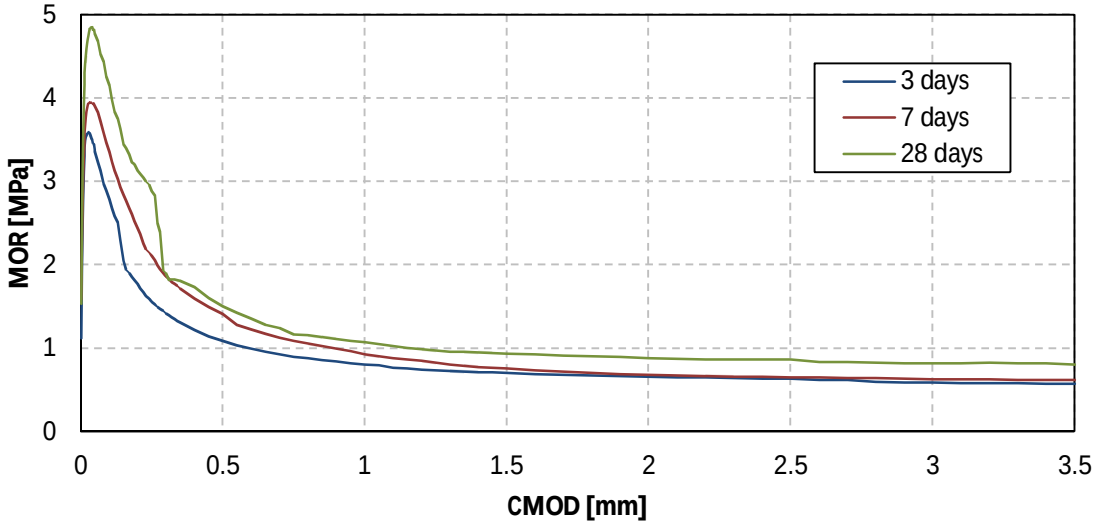

Figure 5.16 Flexural development results of Geotex macro polypropylene FRC with 0.266% fibre content

As the concrete matures the maximum force applied increases and also the post-cracking flexural strength. Between 3 and 7 days the post-cracking flexural force stays the same, but an increase in this force is seen in the curve of the 28 day tests. For each of the flexural tests the amount of fibres and broken fibres across the cracked surface were counted (after the beams were split into two parts) and these results are shown in Figures 5.17 and 5.18. The area of crack surface for each fibre was then calculated from the amount of fibres and the beam dimensions, shown in Figure 5.19.

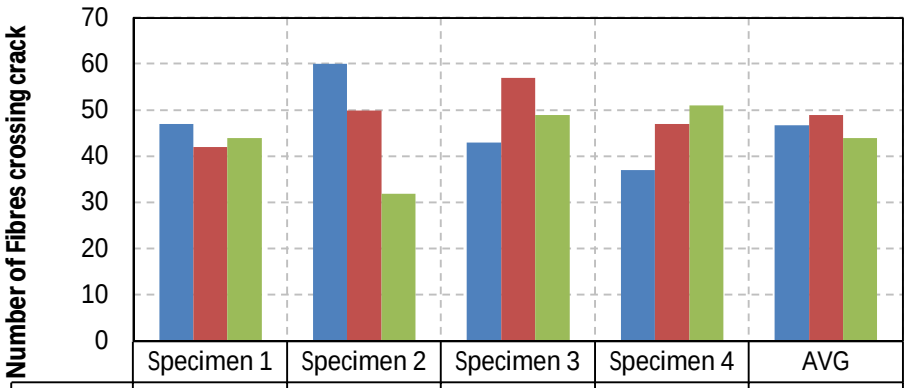

	Specimen 1	Specimen 2	Specimen 3	Specimen 4	AVG
3 Days	47	60	43	37	47
7 Days	42	50	57	47	49
28 Days	44	32	49	51	44

Figure 5.17 Chart showing the number of fibres counted crossing the crack of each beam specimen tested in flexure, using the Geotex macro polypropylene FRC with 0.266% fibre content

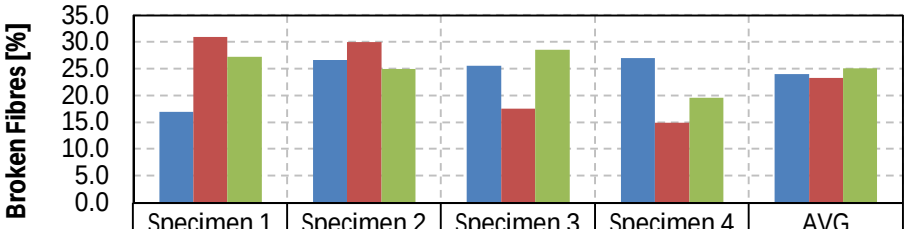

	Specimen 1	Specimen 2	Specimen 3	Specimen 4	AVG
3 Days	17.0	26.7	25.6	27.0	24.1
7 Days	31.0	30.0	17.5	14.9	23.3
28 Days	27.3	25.0	28.6	19.6	25.1

Figure 5.18 Chart showing the percentage of broken fibres counted on within the crack of each beam specimen tested in flexure, using the Geotex macro polypropylene FRC with 0.266% fibre content

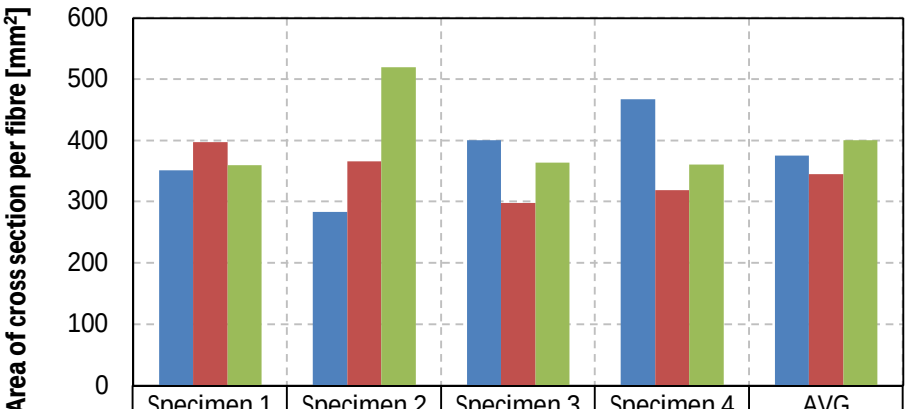

	Specimen 1	Specimen 2	Specimen 3	Specimen 4	AVG
3 Days	352	283	401	468	376
7 Days	397	366	298	319	345
28 Days	360	520	364	361	401

Figure 5.19 Chart showing the average cross Section area for each fibre bridging the crack of each beam specimen tested in flexure, using the Geotex macro polypropylene FRC with 0.266% fibre content

Two things that are noticed from these results are that the distribution of the fibres within the concrete is random. The flexural results from this section are used in Section 5.3 to determine the tensile behaviour of the SynFRC.

The flexural results showed a desired strain softening curve as in Chapter 4.

5.2.3 Friction Tests

Preliminary friction tests were performed to estimate which wood surface to use for the large slab tests presented in Chapter 7. The friction coefficients obtained from these tests are shown in Figure 5.20.

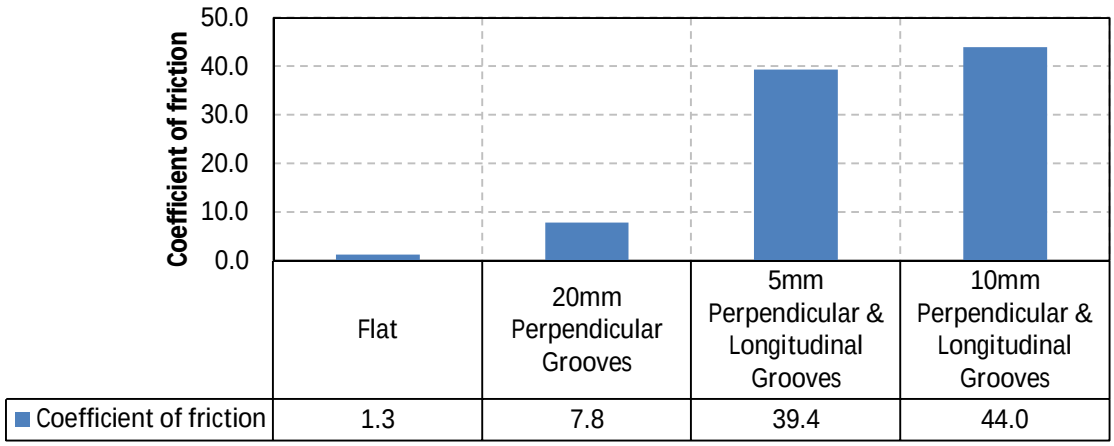

Figure 5.20 Coefficient of friction for various wood surfaces

The coefficient of friction between the flat wood surface and the concrete is somewhere between the coefficient of friction of sand/granular subgrade and the concrete, see Figure 2.7. When grooves are added perpendicularly to the direction of movement, the coefficient is increased, but much higher than any natural subgrade. When more grooves are added in the direction of movement as well, then this coefficient drastically increases. The reason why the 10mm spacing between grooves shows a higher coefficient than the 5mm is due to the wood shearing off in the case of the 5mm spacing. The 10mm grooves in both directions were then selected for the large slab tests because a high coefficient of friction was required, according to the theory that higher restraints cause more DSC. The development of the coefficient of friction was then tested on 7 and 28 days with the concrete mix used in the large slabs, see Figure 5.21.

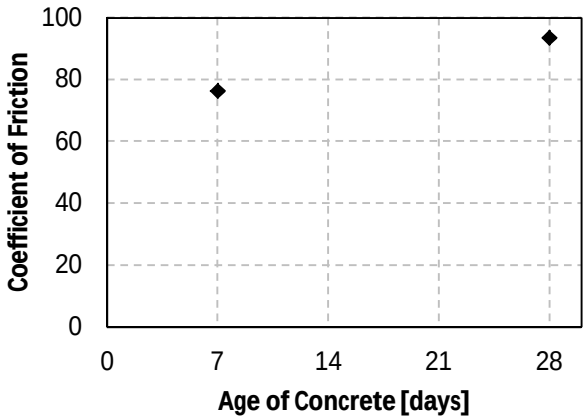

Figure 5.21 Development of the coefficient of friction between concrete and a grooved wooden board

From Figure 5.21 an increase in the coefficient of friction is observed over time. The coefficient of friction is much higher than those obtained in preliminary tests, which is due to a different type of concrete used with a better grading and workability. These friction results represent the friction coefficients between the full scale slabs and their wooden bases discussed in Chapter 7. The individual coefficients of friction obtained from all the friction tests performed to estimate friction bond development, are shown in Appendix B.

5.2.4 Shrinkage Tests

The results of the free shrinkage tests performed in accordance with the full scale slab tests discussed in Chapter 7, are shown in Figure 5.22.

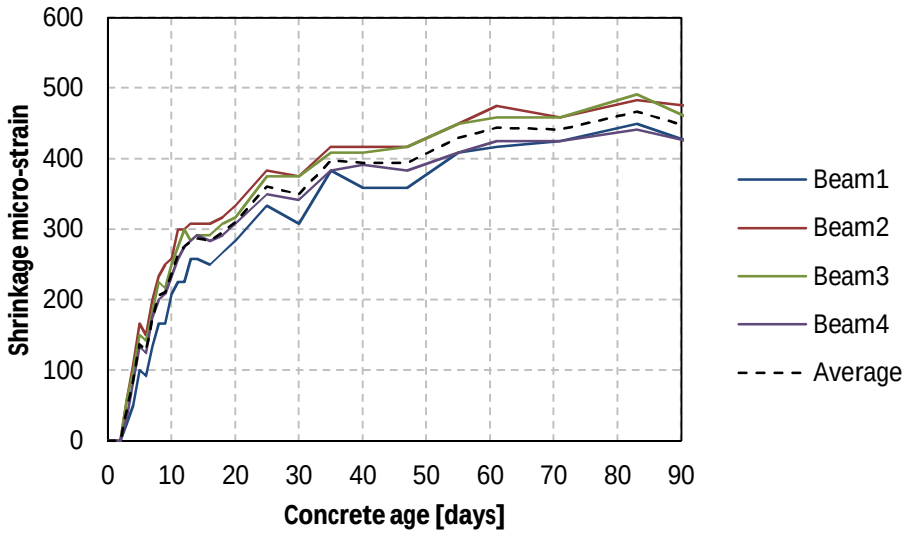

Figure 5.22 Average free shrinkage results obtained from beam specimens

The average relative humidity and the average temperature the beams experienced were 61.5% and 19.8°C respectively. The recordings of these values and the individual marker results from each beam are shown in Appendix C. The measured shrinkage strain curves follow an expected trend and reach a shrinkage micro-strain of almost 500, which is relatively high at an age of 90 days compared to the prediction model results. A trend line was fitted to the average shrinkage strain curve and was then used for the analysis discussed in Chapter 7.

5.3 Inverse Analysis

To determine the post-cracking tensile behaviour of FRC a uniaxial tension or a flexural test may be performed. In the case of the flexural test an inverse analysis procedure must be performed. The procedure used for the inverse analysis is discussed in this section and also the results obtained.

5.3.1 Inverse Analysis Procedure

The inverse analysis was performed with the aid of the software package Matlab. The program was used to speed up the iterative process. Hand calculations were performed throughout the iterative process to ensure that it gives the correct results. In Chapter 4, the procedure of adding a stress block to the flexural stress distribution diagram used in beam design theory was discussed. This is not the actual behaviour that occurs in flexure as the tensile behaviour of the FRC follows mostly a strain softening path. Therefore the diagrams shown in Figure 5.23 were used to get a better estimate of the true material behaviour. There are different phases that may occur within the flexural stress distribution diagram, see Figure 5.23. The method used assumes that the compression block stays linearly elastic.

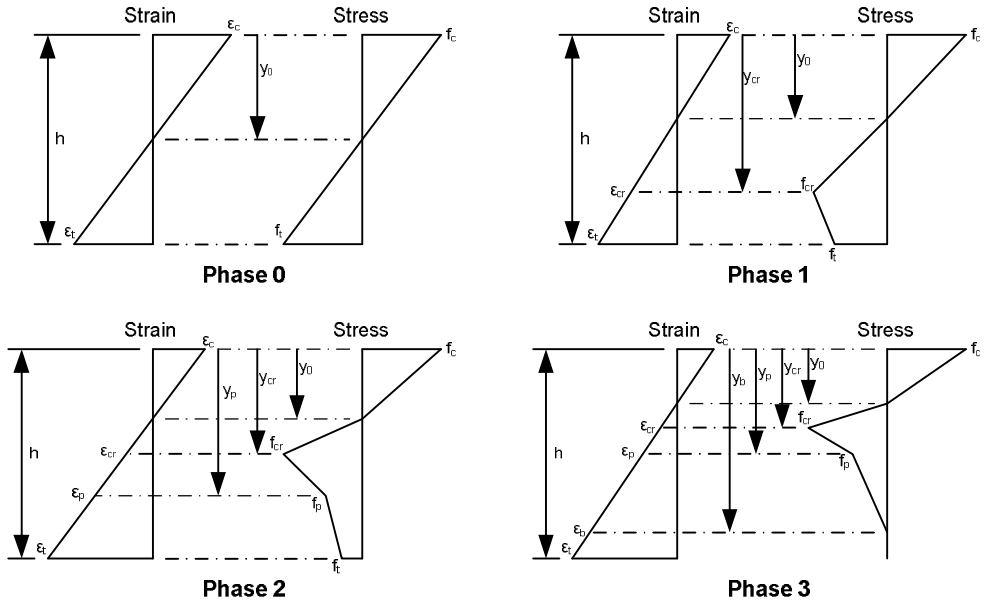

Figure 5.23 Strain and stress diagrams in different phases of flexure used to perform inverse analysis

In Phase 0 the concrete is in the elastic phase and has not cracked. In Phase 1 the concrete cracked, but there is still some aggregate interlocking across the crack, hence the relatively high tensile stress still existing over the crack. In Phase 2 the concrete is cracked and the crack has grown to a point where the fibres are the only mechanism bridging the crack, hence the relatively constant tensile stress in the bottom of the beam specimen across the crack. In Phase 3 the concrete is cracked and has grown to a point where there is no resistance left within the fibres, hence the zero stress across the crack in the bottom of the beam specimen.

The Young's modulus was assumed to be 28GPa, for the first set of tests used for the analyses discussed in Chapter 6, which is normally the case for concrete with a strength of 30MPa (South African Bureau of Standards, 2000). This was adjusted for the analyses conducted on the second set of tests with a compressive strength of 35MPa. The only unknowns left to solve are the factors that describe the post-cracking tensile behaviour of the FRC, shown in Figure 5.24.

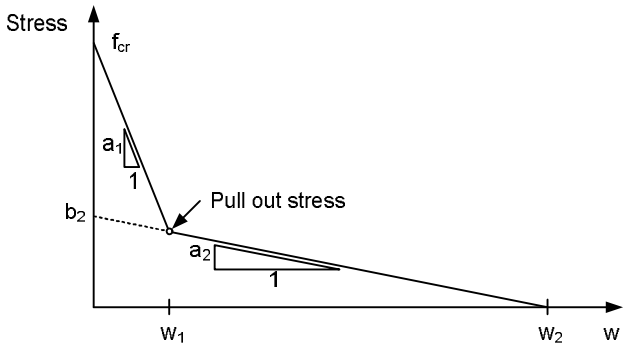

Figure 5.24 Unknowns describing the post-cracking tensile behaviour of the FRC with w the crack width

These unknowns are the only values required to solve the two linear equations that describe the tensile behaviour. The following equation represents the bi-linear curve:

$$\sigma(w) = \begin{cases} -a_1 \cdot w + f_{cr} & for \;\; 0 \le w < w_1 \\ -a_2 \cdot w + b_2 & for \;\; w_1 \le w < w_2 \\ 0 & for \;\; w \ge w_2 \end{cases} \tag{5.2}$$

where a_1 = the gradient of Line 1

f_{rc} = the maximum tensile strength of the concrete

b_2 = force where Line 2 intersects the force axis

w = crack width

σ = tensile stress in [MPa]

The first part of the inverse procedure is to develop a tensile force to CMOD curve for a given FRC post-cracking tensile behaviour. To do this the neutral axis height should be determined at a certain CMOD by ensuring equilibrium between the compression and tension forces. The next step is to determine the moment of the section at this CMOD. Thereafter the force required to induce this moment on the beam can be determined with the following:

$$\boldsymbol{F = 4M/L} \tag{5.3}$$

where F = the force being applied to specimen

M = the moment within the specimen

L = the specimen span length

This equation applies to the three point flexural test only.

When the forces for a number of CMOD values are calculated, a force to CMOD curve can be plotted together with the force to CMOD curve obtained from the flexural test. The aim is then to determine the unknowns mentioned earlier by decreasing the difference between the curves. These analyses were applied to the flexural results discussed in Section 5.2.2 and the results obtained are discussed in the next section.

5.3.2 Results & Discussion

These results (key elements) in the analyses are discussed in both Chapters 6 and 7. The results were obtained from performing inverse analyses on the flexural test results. The first set of results, used in Chapter 6, is shown in Figures 5.25 to 5.27. Shown are the average indirect tensile results. The results from each individual beam specimen are shown in Appendix D.

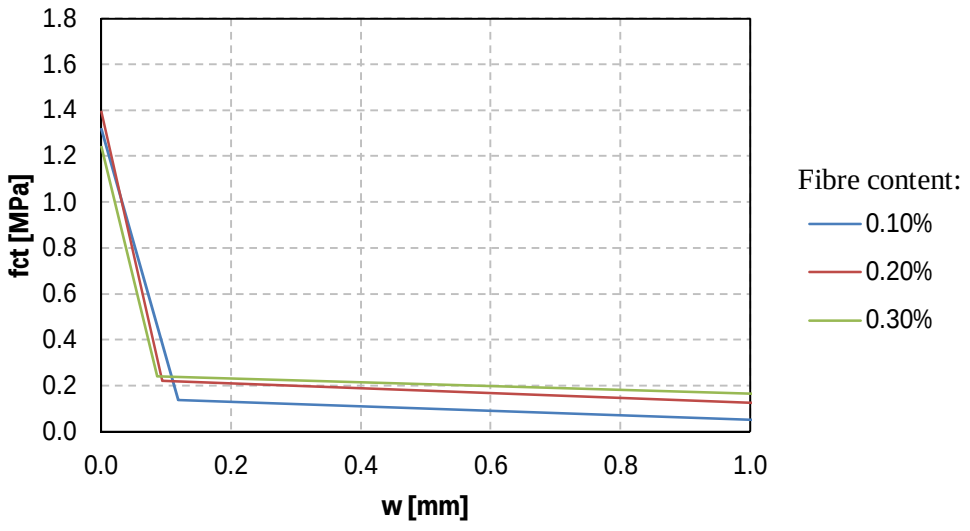

Figure 5.25 Indirect tensile results for the micro polypropylene FRC from Chryso

The Chryso micro polypropylene FRC showed a slight increase in tensile performance with increased fibre content. The first gradient does not show any significant difference between the different fibre contents, although an increase of the input energy beneath the second part did increase with a small fraction. The average tensile cracking strength (f_{cr}) was just below 1.4MPa, with pull out stresses ranging between 0.1 and 0.2MPa.

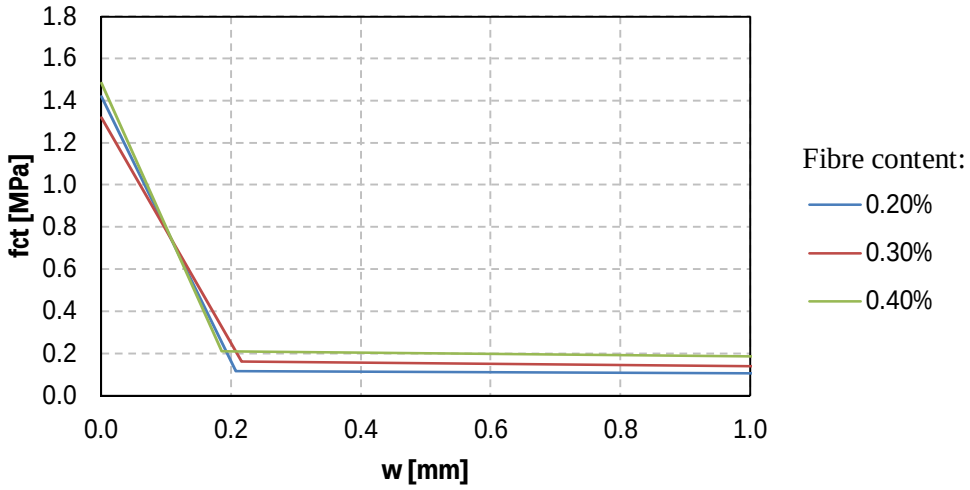

Figure 5.26 Indirect tensile results for the macro polypropylene FRC from Fibsol

Higher Fibsol macro fibre content shows much better tensile performance in the first section of the curve than the micro Chryso polypropylene FRC, with the first gradient also not showing any large differences between fibre contents. The second part of the curve shows a significant increase with the increase of fibre contents. The average tensile cracking strength was about 1.4MPa, with the pull out stresses also ranging between 0.1 and 0.2MPa. The only major difference noted between the tensile behaviour of the Fibsol- and Chryso FRC, is the gradients of the curves.

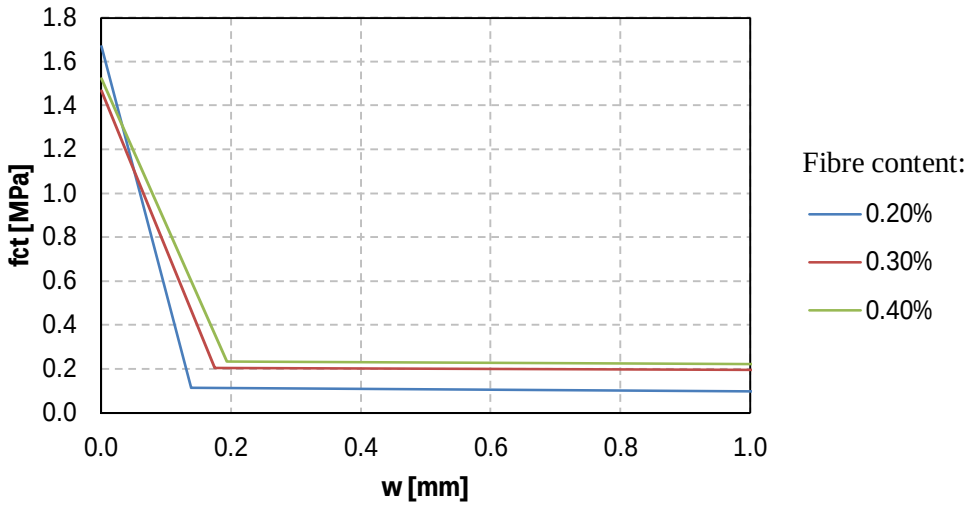

Figure 5.27 Indirect tensile results for macro polypropylene FRC from Geotex

The Geotex macro polypropylene FRC shows results between the Chryso micro and Fibsol macro FRC discussed above. The first line section shows a definite increase in gradient with the increase of fibre content. The second part of the curve also shows an increase in tensile stress capacity with the increase of fibre content. The average tensile cracking strength is about 1.5MPa, which is slightly higher than the other FRCs, but this is due to small differences in the concrete strength itself and not due to an improvement of the fibres. It was mentioned in Chapter 4 that the fibres only start to work after the concrete has cracked. The pull out stress of the FRC ranged between 0.1 and 0.23MPa for different fibre dosages, which is slightly better than the previous results, which may be due to higher concrete strength.

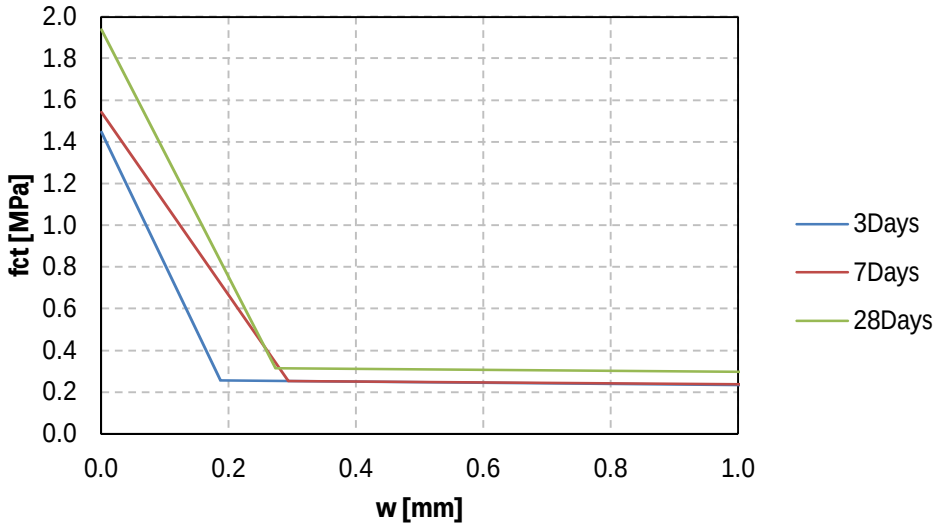

Figure 5.28 Indirect tensile development results for macro polypropylene FRC from Geotex

There is a difference in the tensile cracking strength of the SynFRC results between the first and second set of tests, because a different concrete matrix was used for these tests. These results also show the development of the post-cracking tensile behaviour of the SynFRC over the concrete age. For the tests performed on concrete of a 3 day age, the results relatively similar to the Geotex 0.4% fibre content of the previous concrete mixtures' results. At 7 days age there is a slight increase of the cracking strength and on 28 days the cracking strength again increases. As time progresses, the amount of input energy beneath the first section increases, which also occurred in the second section at 28 days shown in Figure 5.28.

The tensional results behaved in a strain softening manner as desired, and are therefore a good representation of the tensile behaviour of the SynFRC.

5.4 Concluding Summary

The various tests performed to characterise the SynFRC used were discussed in this chapter. The tests' objectives, programmes, setups and procedures were discussed. The tests were performed to determine the compressive strength, the flexural behaviour, the friction behaviour and the shrinkage of the SynFRC used for the analyses and tests discussed in Chapter 6 and 7. Then the material properties of the different fibres and the mix proportions used for the specific tests were provided. The results from these tests were then provided and discussed.

Next the tensile behaviour of the different SynFRC composites were determined by performing an inverse analysis procedure to the flexural results obtained from experiments. The inverse analysis procedure was briefly discussed and the results were provided and discussed. These results are used in the analyses discussed in Chapter 6 and 7.

Chapter 6 FEA of Drying Shrinkage Cracking

Finite element analyses (FEA) were performed on a slab-on-grade with contraction joints at particular spacing, to determine the cracking behaviour of the slab due to drying shrinkage. This is a common problem for slabs-on-grade due to the friction restraint of the subgrade/sub-base. The SynFRCs that were discussed in Chapter 5 were used for the slab material and the subgrades used were obtained from literature (Marais & Perrie, 1993). A 2D finite element model (FEM) was used to determine cracks widths and crack spacings depending on different geometry layouts and material properties. The analyses were conducted with the aid of the software package Abaqus. The objectives, procedure and results from these analyses are discussed in this section.

6.1 Analysis Objectives

These finite element analyses were performed to obtain the following objectives:

Objective 1

Determine and compare the maximum crack widths that develop within a slab-on-grade of normal concrete (NC) and SynFRC.

Objective 2

Determine the spacing between the cracks and the number of cracks forming within the slab-on-grade for NC and SynFRC.

Objective 3

Determine the difference in crack width and spacing of cracks for different SynFRC types, fibre content, slab thicknesses, friction types, joint spacing and ambient relative humidity.

6.2 Analysis Setup and Procedure

The procedure followed for the analysis of the DSC in a slab-on-grade is discussed in this section. First the different components, the assembly of these components and the mesh type and mesh layout are discussed. The material properties of the components, the friction between them and the boundary conditions are provided. Lastly the different combinations used to evaluate the effect of DSC on the slab-on-grade are discussed.

6.2.1 Components, Assembly and Mesh

The model consists of two main components, which are the slab and the subgrade shown in Figure 6.1. Only one crack can be simulated for a specific analysis because of the procedure used for the analysis. An assumption was made that the first crack that forms after the cracking of the joints is at the centre between two joints. The next crack then forms in the centre between the joint and this crack. It is therefore assumed that a new crack always initiates midway between two joints, a joint and a crack, or in the middle of two cracks. Analyses were performed for each individual crack as cracking progress throughout the slab. The joint was also added to the slab component to represent initial cracking at the joint.

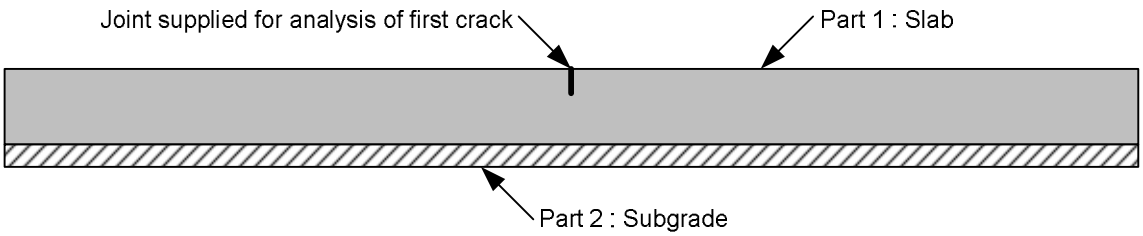

Figure 6.1 Component assembly for FEA of DSC

The mesh type used for the analysis is a coupled thermal-displacement mesh type, which allows the effects of temperature to be analysed at steady state and also allows expansion strains to be applied to the model. For the analysis temperature was used as the variable for time. Thus the change of temperature was used to apply the shrinkage strain to the slab-on-grade. The shrinkage strains were applied by changing the thermal coefficient of expansion alongside temperature change. The shrinkage strains were determined by the prediction model discussed in Chapter 2 (FIB Special Activity Group 5, 2010). Strains were converted to thermal coefficients of expansion using the following:

$$\boldsymbol{\alpha} = \frac{\boldsymbol{\varepsilon_{sh}}}{\boldsymbol{\Delta T}} \tag{6.1}$$

where ε_{sh} = shrinkage strain

α = thermal coefficient of expansion in [1/°C]

ΔT = change within temperature in [°C]

The temperature was then linearly increased and the thermal coefficient of expansion (α) was adjusted (with Equation 6.1) with the change in temperature. In this manner the shrinkage strain was applied with time. The thermal coefficient of expansion (α) is then calculated by dividing the shrinkage strain (at a certain concrete age) with the change in temperature (at the same concrete age). In order for this to work according to the model expectations, the Poisson's ratio of the concrete had to be zero. This

is because the Poisson's ratio does not comply with the method used to apply the strains and increases the strain being applied. Since the effect of Poisson's ratio was not important for the type of analyses, it was not an issue.

The 2D coupled thermal-displacement elements used for the analyses have degrees of freedom which are shown in Figure 6.2.

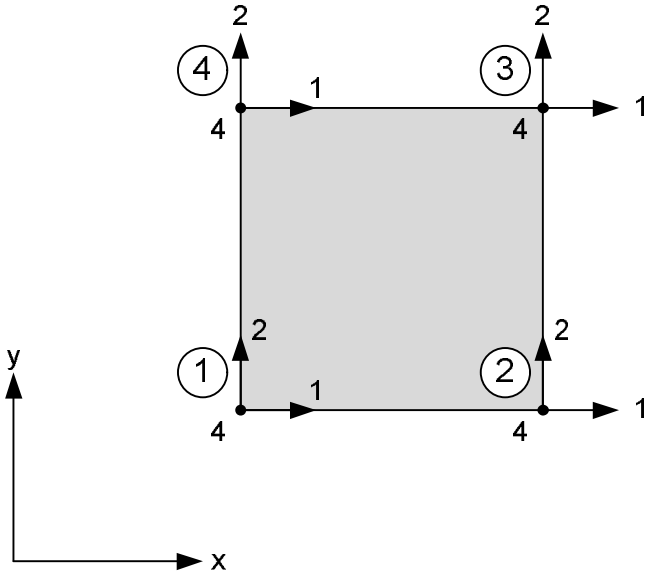

Figure 6.2 Degrees of freedom of the coupled thermal-displacement element

The element has two displacement degrees of freedom (1 to 2) and one temperature degree of freedom (4). The node numbers are indicated by the circled numbers. Degree of freedom 1 to 2 corresponds to the local axis directions x to y, respectively.

The maximum and minimum slab length was 10 and 0.1m, respectively. The maximum and minimum slab thicknesses were 200 and 75mm, respectively. Following a sensitivity analysis an element size of 5mm x5 mm was chosen. The 5mm were then also used for the width of the crack section supplied in the slab, shown in Figure 6.3. This was relatively small to the global analysis and was selected following a sensitivity analyses.

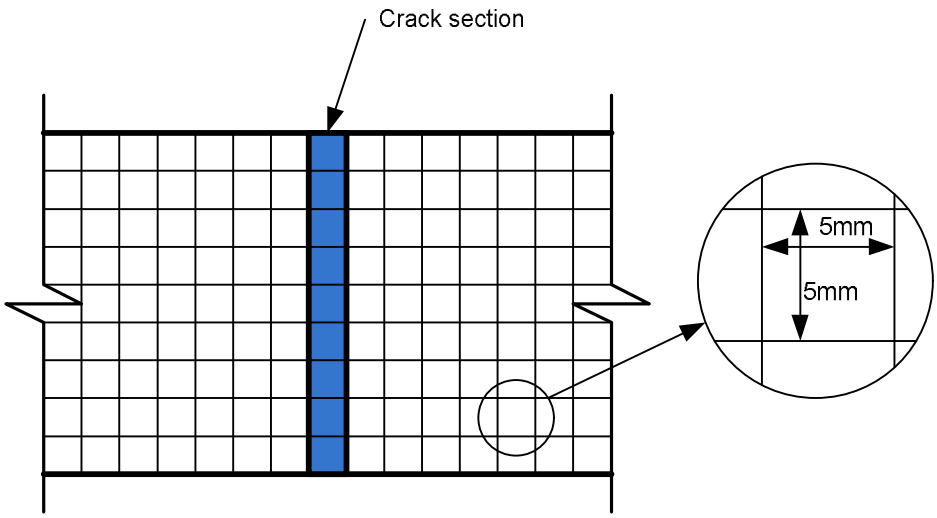

Figure 6.3 Mesh layout, size and crack Section of FEA of slab Section

The same mesh size was used in the subgrade section, but the subgrade was only 10mm thick and the same length as slab section. The friction between the slab and the subgrade was the important factor for the subgrade modelling. Consequently the compaction of the subgrade was not of importance and a thin subgrade acceptable. Therefore the subgrade provided rigid vertical support to the concrete slab model.

6.2.2 Material properties

The different material properties used for the analyses and the friction behaviour selected for these analyses are discussed in this section.

The concrete material properties for the un-cracked sections are shown in Table 6.1. The uncracked concrete behaves in a linear elastic way and has no limit in compression or in tension. The assumption was made that as soon as the tensile capacity for the concrete is reached, a new crack forms within the slab, and a new analysis should be performed to model the new crack.

Table 6.1 Un-cracked concrete Section material properties

Material Property	Value	Unit
Density	2400	kg/m^3
Young's Modulus	28	GPa
Poisson's ratio	0	

The cracked concrete material properties were assumed to be the same as for the uncracked concrete, but with the tensile material properties shown in Figure 6.4. These properties were included into a concrete damage plasticity model. The assumption was made that the concrete will not fail in compression and will always behave linearly elastic. The inverse analysis results obtained in Section 5.3.2 were used in the analysis of DSC in slabs-on-grade, together with the three estimated curves shown in Figure 6.4. The estimated behaviours were analysed to predict the behaviour of FRC that consists of higher content of synthetic fibres. The $R_{e,3}$ values of these curves are also shown in Figure 6.4.

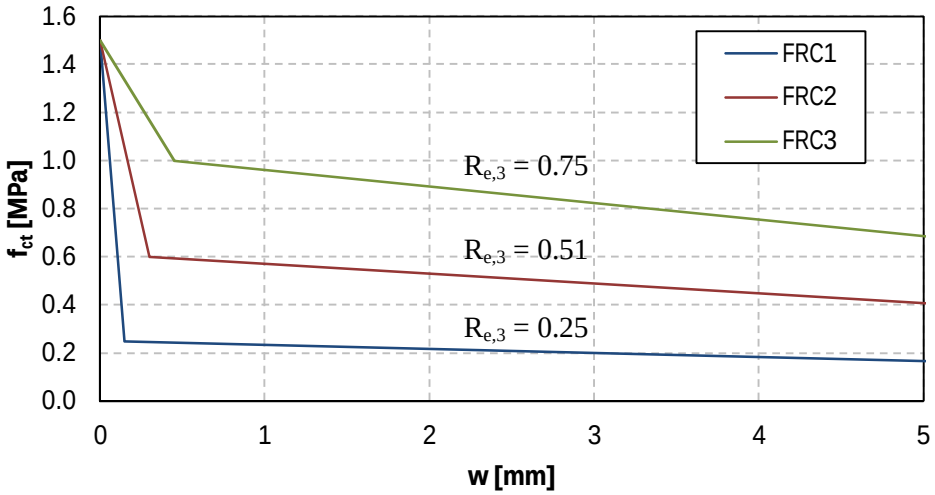

Figure 6.4 Post cracking tensile behaviour of selected FRC behaviours for cracked section of concrete

An example of the thermal coefficient of expansion added to concrete material behaviour is shown in Figure 6.5, with the temperature also representing concrete age within the analysis.

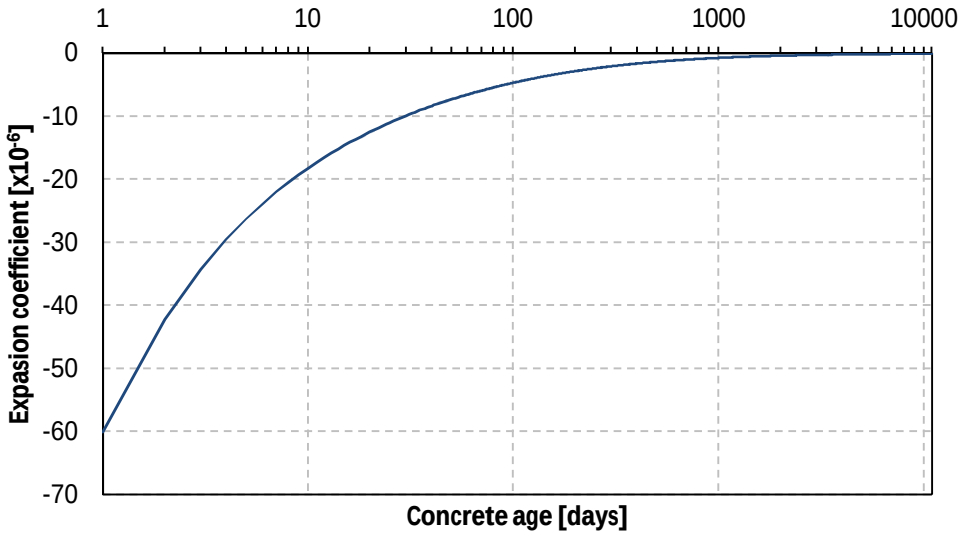

Figure 6.5 Expansion coefficient behaviour for applying shrinkage strain to slab on grade within FEA

The subgrade is only created as a component applying the friction interaction between the slab and the subgrade. Therefore it had no density, thermal coefficient of expansion or conductivity, and a Young's modulus of 10 000GPa was used to make the subgrade a rigid component. The friction behaviour used for the analysis was a static and kinetic friction model. This model adds the kinetic frictional effects into the model to provide accurate slip distances. An elastic slip value was provided to the frictional behaviour, which allows the object to move a small distance before it reaches its maximum frictional resistance and starts slipping. This friction model was discussed in Chapter 2. The friction coefficients used for the various analyses were obtained from Figure 2.7 and are summarised in Table 6.2.

Table 6.2 Coefficients of friction used in the FEA of the DSC in slabs-on-grade

	Movement	
Subgrade Material	1st	average 2nd
Polyethylene sheeting	0.90	0.50
Sand layer	1.00	0.75
Granular subbase	1.70	0.85
Washed sand & gravel	1.95	1.35
Plastic Soil	2.05	1.30

6.2.3 Boundary conditions

The analysis procedure aims to model a slab-on-grade with equal joint spacings in both directions as shown in Figure 6.6. The analysis model could only take into account one crack at a time. Therefore the model contained several analyses to determine the cracking of the slab over time.

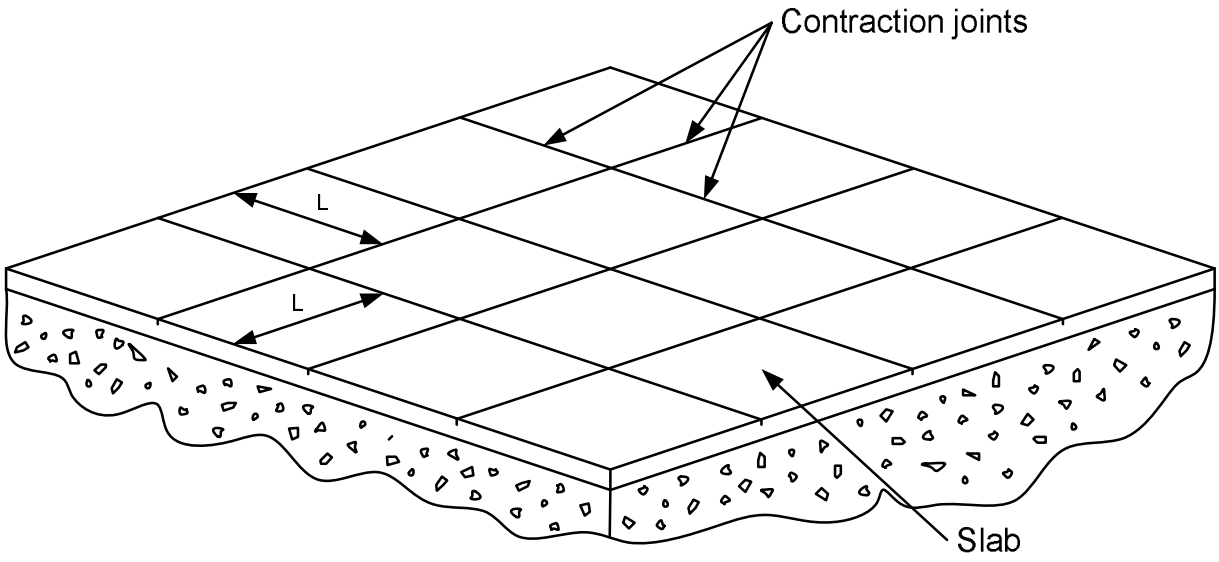

Figure 6.6 Conventional slab-on-grade with contraction joint modelled in FEA

The analyses were performed on a cut section of the slab-on-grade, with a 2D FEA. The sections used to analyse the slab are shown in Figure 6.7. Each crack is analysed on its own, with the assumption that the concrete slab does not move at a section in the middle of two cracks and that symmetry may be applied in these sections. Figure 6.7 shows in what order the analyses were performed and the order of cracking assumed. The first analysis modelled the first crack, the second analysis the second crack and the third analysis the third crack, etc. Analyses were performed up to a point where no further cracking occurred.

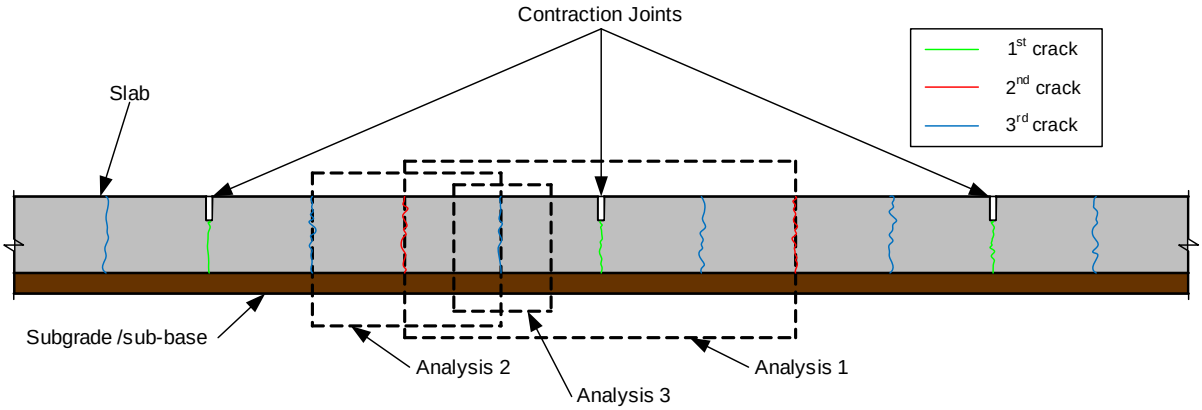

Figure 6.7 Cut-sections used for the analysis of the slab-on-grade and the order of analyses performed

Figure 6.8 shows the cut-sections of the analysis process used to analyse a slab-on-grade. The analyses correspond to Figure 6.7. The first crack is analysed until the tensile capacity of the concrete is reached at the ends of the analysis. This is indicated by the grey areas encircled in Figure 6.8. This process was repeated until the concrete slab did not crack again. Then the results of these analyses were processed to provide the maximum crack width within the slab at any concrete age.

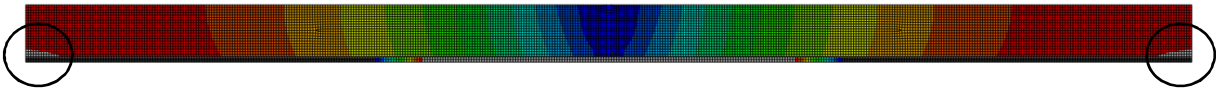

Analysis 1

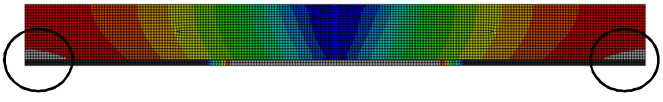

Analysis 2

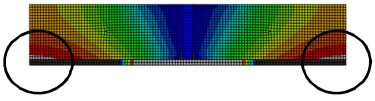

Analysis 3

Figure 6.8 Cutt-Sections to explain the analysis procedure

Crack width results were obtained from the top surface of the slab-on-grade. The maximum crack width is assumed to be the crack width of the first crack until the second crack forms. It is then assumed that the first crack will not grow if the second crack's width is smaller than the first crack's, and that the first and second crack will have the same crack width if the second crack width passes the first crack's maximum width. This process is continued until the slab does not crack again or until the concrete reaches an age of 30 years.

The boundary restraints of the analyses are shown in Figure 6.9. Symmetry boundary restraints were applied to the sides of the slab and the subgrade, and with a vertical boundary restraint beneath the subgrade.

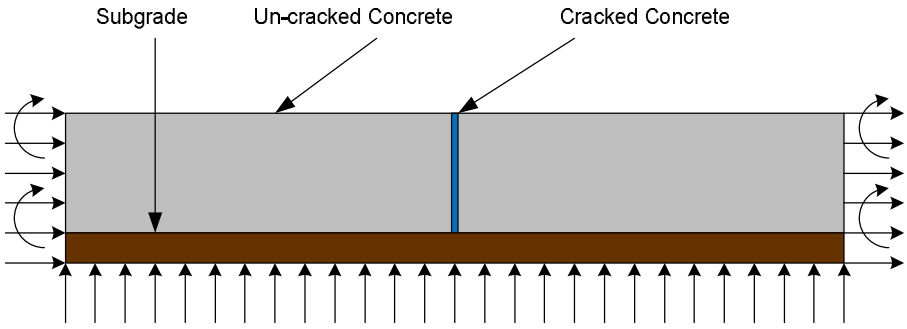

Figure 6.9 Boundary conditions applied to slab-on-grade analyses

6.2.4 Different combinations analysed

The analyses were performed on a variety of slab models by varying the slab thickness, joint spacing, relative humidity, fibre type, fibre content, coefficient, α, of friction and elastic slip of friction. Figure 6.10 is a diagram showing the various analyses conducted, to determine which of these factors will affect the performance of the NC and FRC slabs as well as the difference in crack widths that result from varying the parameters.

The factors shown with the large dots in Figure 6.10 and linked with the dashed line were used as the control analysis. The different parameters were varied from the control to investigate the effects of each parameter on cracking of the slab. For each FRC analysis a NC analysis was also performed. The 0.5mm elastic slip value was selected as the control value and was obtained from literature (Gaedicke, et al., 2012). The remainder of the values selected as the control analysis is a slab thickness of 100mm, a joint spacing of 4.5m, a relative humidity of 60%, a granular sub-base and the Geotex macro polypropylene fibres with a content of 0.3% by volume. The results of these analyses are shown and discussed in the next section.

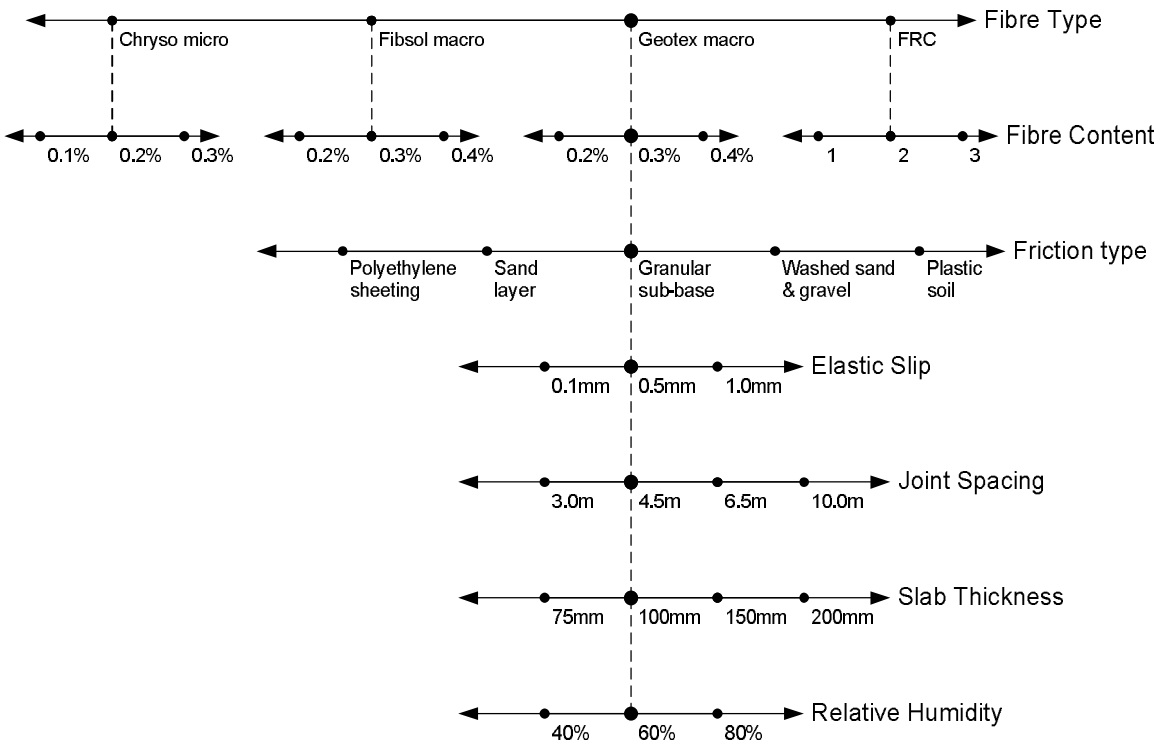

Figure 6.10 Diagram showing different FEA performed for DSC in a slab-on-grade

6.3 Results & Discussion

This section focusses on the results of the different analyses conducted. The results of the analyses are those performed on different types of SynFRC, fibre content, friction types, elastic slip values for friction, joint spacings, slab thicknesses and ambient relative humidities. The results of the cracking behaviour and the maximum crack width of NC and the FRC are discussed in this section. The results for the average crack widths are presented on a logarithmic and normal time scale in Appendix E.

6.3.1 SynFRC Type

The three types of polypropylene FRC discussed in Chapter 5 were used to analyse the effects of shrinkage on the cracking behaviour of slabs-on-grade. Analyses were also performed on estimated SynFRC tensile behaviours that were discussed in Section 6.2.2. The results from these analyses are presented in this section.

Chryso micro polypropylene FRC

Figure 6.11 presents the crack spacing of the Chryso SynFRC slab-on-grade.

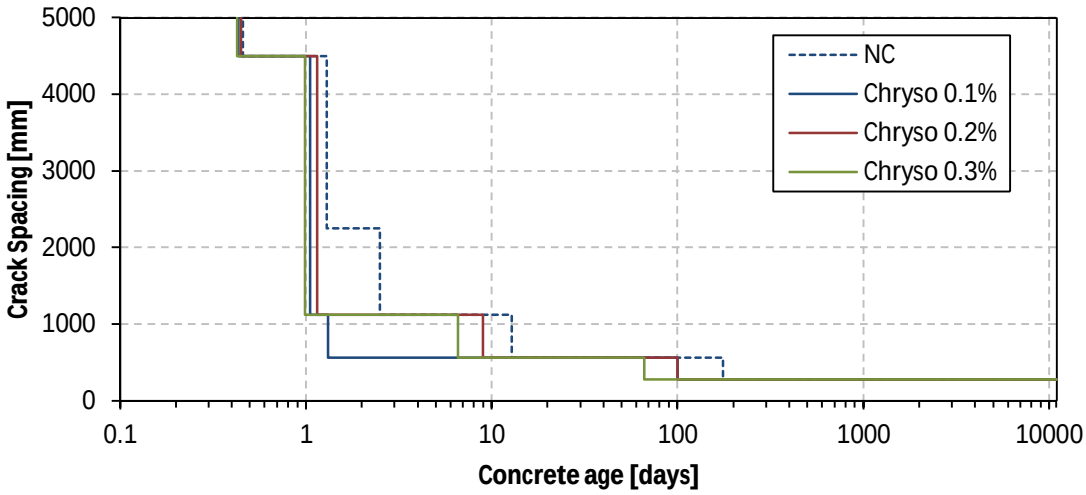

Figure 6.11 Spacing between cracks, as cracking occurs for the different fibre content of the Chryso SynFRC

The micro SynFRC and NC cracking occurred at different ages whereas the first cracks of the SynFRC and NC occurred at exactly the same time. This is due to the fact that the SynFRC and NC have the same initial tensile cracking stress. The SynFRC has a post cracking tensile behaviour which induces cracking earlier than the NC for the NC has no post cracking tensile behaviour. The smallest crack spacing reached between the cracks is 281.25mm. This was reached for both the NC and all the fibre contents of the micro SynFRC. In Figure 6.12 the results of the maximum crack width over the concrete age of the Chryso SynFRC slab-on-grade analyses are presented.

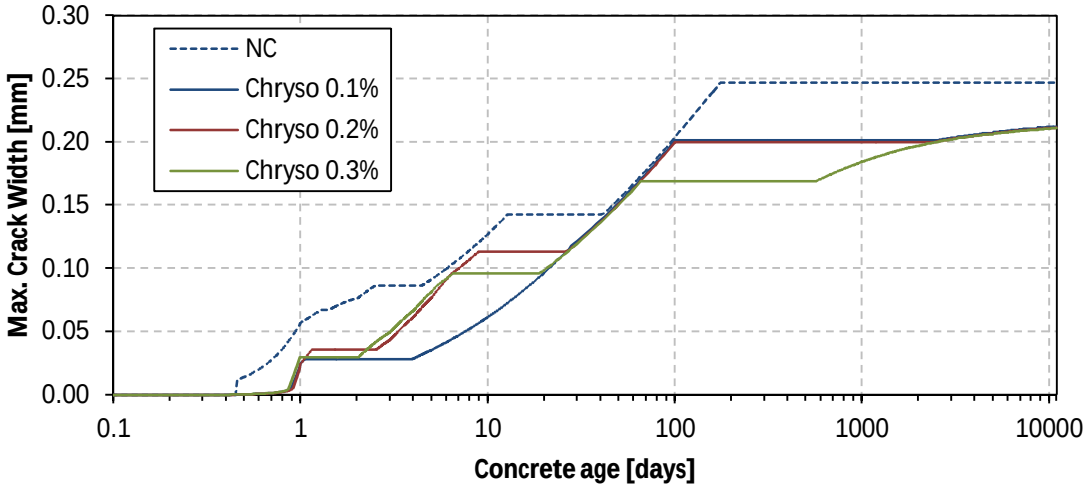

Figure 6.12 Development of the maximum crack width within the slab-on-grade of the Chryso SynFRC

The NC reached a maximum crack width of almost 0.25mm whilst the micro SynFRCs reached a maximum crack width of 0.21mm, as shown in Figure 6.12. This is not a significant improvement between the FRC and the NC. There is, however, an improvement in crack widths at ages less than

10 days and then a small improvement beyond 170 days. Between these ages the SynFRC and NC behaved almost identically.

Fibsol macro polypropylene FRC

Figure 6.13 presents the crack spacing of the Fibsol SynFRC slab-on-grade.

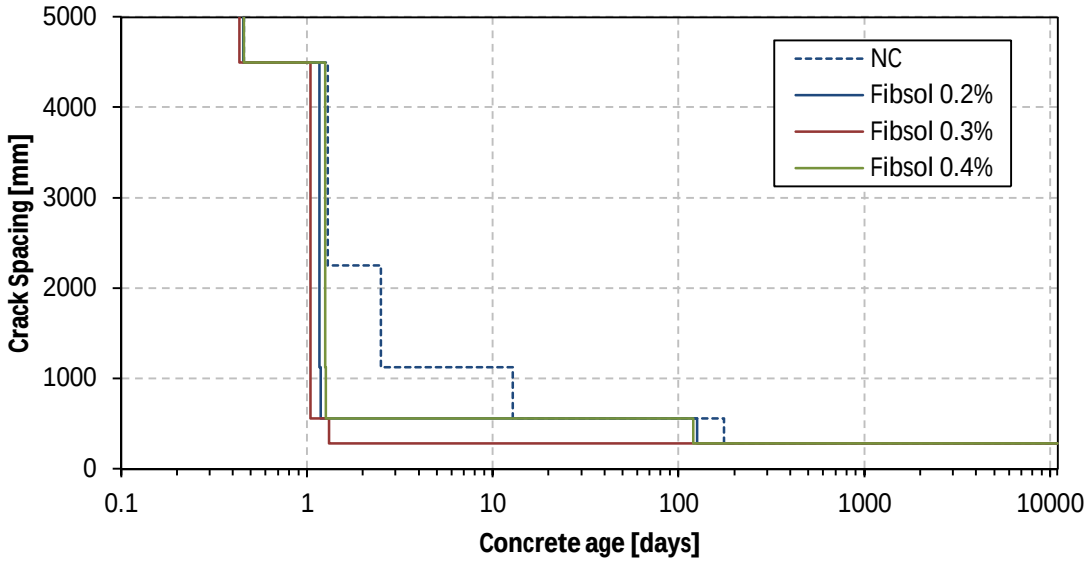

Figure 6.13 Spacing between cracks as cracking occurs for the different fibre content of the Fibsol SynFRC

The macro SynFRCs cracking occurred at different ages than the cracking of the NC. All the cracks of the SynFRC with the 0.3% fibre content formed at an earlier age. For all models analysed the smallest crack spacing was 281.25mm. The NC reached this crack spacing at an age of 175 days, and the 0.2 and 0.3% dosage of the Fibsol FRC reached this spacing at ages of 120 days and just beyond 1day, respectively. In Figure 6.14 the results of the maximum crack width over the concrete age of the Fibsol SynFRC slab-on-grade analysis are shown.

The NC reached a maximum crack width of almost 0.25mm and all the micro SynFRCs reached a maximum crack width of between 0.21 and 0.22mm, as shown in Figure 6.14. This is not a significant difference between the FRC and the NC, although the 0.3% fibre content showed a reasonable improvement in crack width up to an age of 160 days. From there on the difference in response became less pronounced.

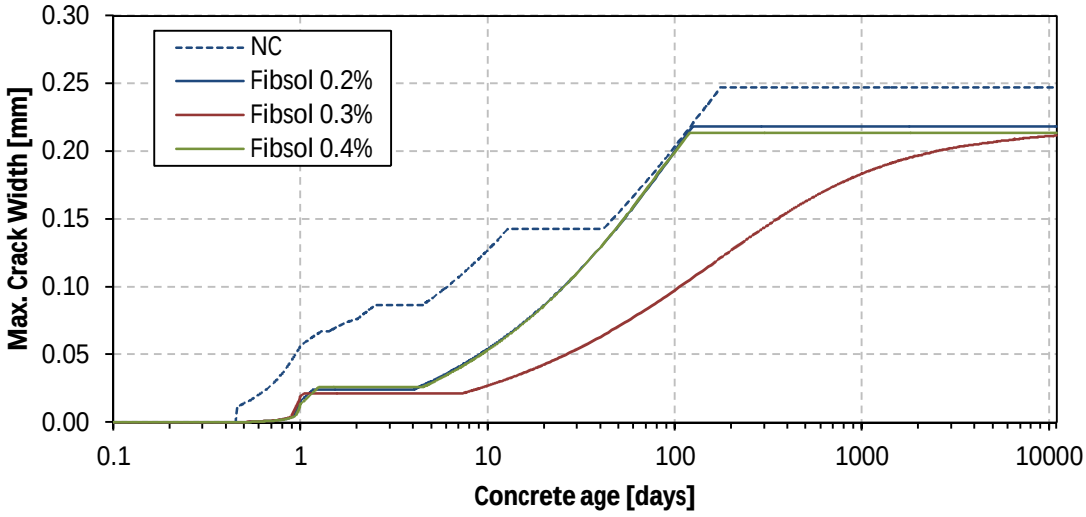

Figure 6.14 Development of the maximum crack width within the slab-on-grade of the Fibsol SynFRC

Geotex macro polypropylene FRC

Figure 6.15 presents the crack spacing of the Geotex SynFRC slab-on-grade.

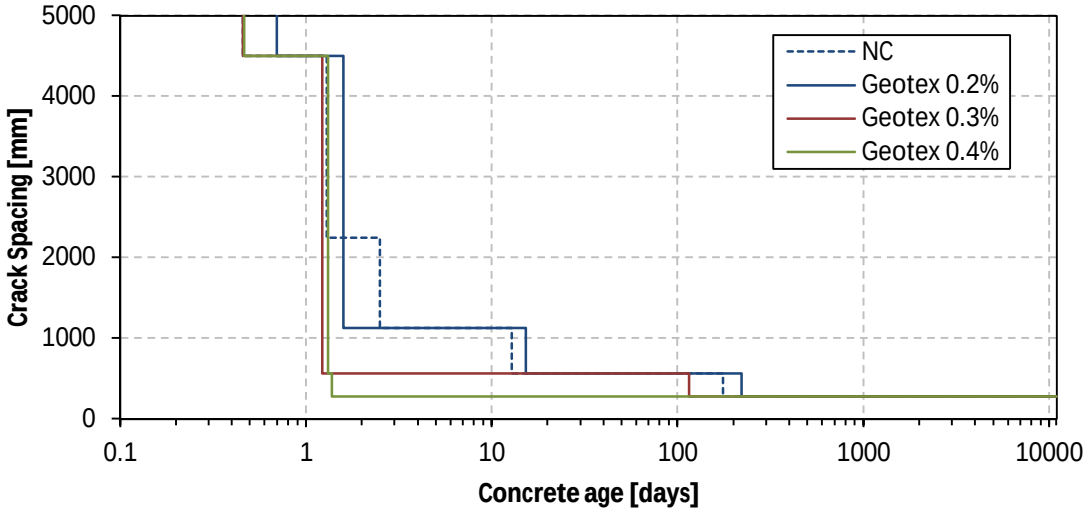

Figure 6.15 Spacing between cracks as cracking occurs for the different dosages of the Geotex SynFRC

The SynFRC slab with the 0.4% fibre content resulted in cracking at an earlier age than the NC slab, whereas the SynFRC slab with the 0.2% dosage of fibres showed cracking at a later age than the NC slab. This is due to the tensile cracking stress of the 0.2% fibre dosage being larger than that of the NC and the remainder of the fibre dosages. This is why different ages are noticed for the first cracking at the joints. The smallest crack spacing reached between the cracks is again 281.25mm. This was reached for both the NC and all the macro SynFRC fibre content.

The NC reached this crack spacing at an age of 175 days whereas the 0.2%, 0.3% and 0.4% fibre dosage of the Fibsol SynFRC reached this spacing at ages of 220 days, 115 days and just beyond 1day, respectively. In Figure 6.16 the results of the maximum crack width over the concrete age of the Geotex SynFRC slab-on-grade analysis is presented.

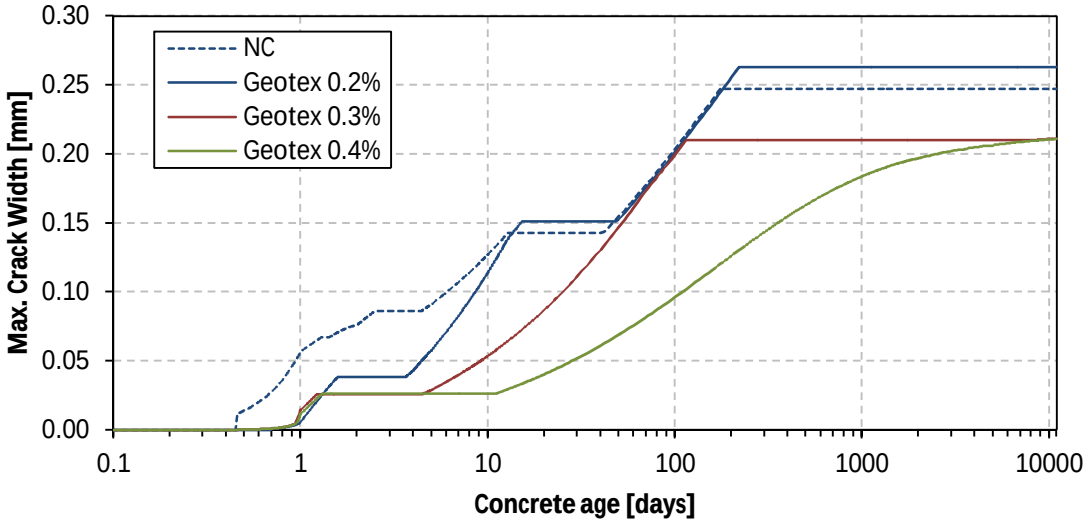

Figure 6.16 Development of the maximum crack width within the slab-on-grade of the Geotex SynFRC

The earlier the cracking can occur, the smaller the crack widths are and this is what the SynFRC aims to do. Through cracking and the forming of multiple cracks of the SynFRC (these cracks are very small compared to the cracks of NC slabs), stress on the slab will be reduced.

Estimated FRC

Figure 6.17 presents the crack spacing of the estimated SynFRC slab-on-grade.

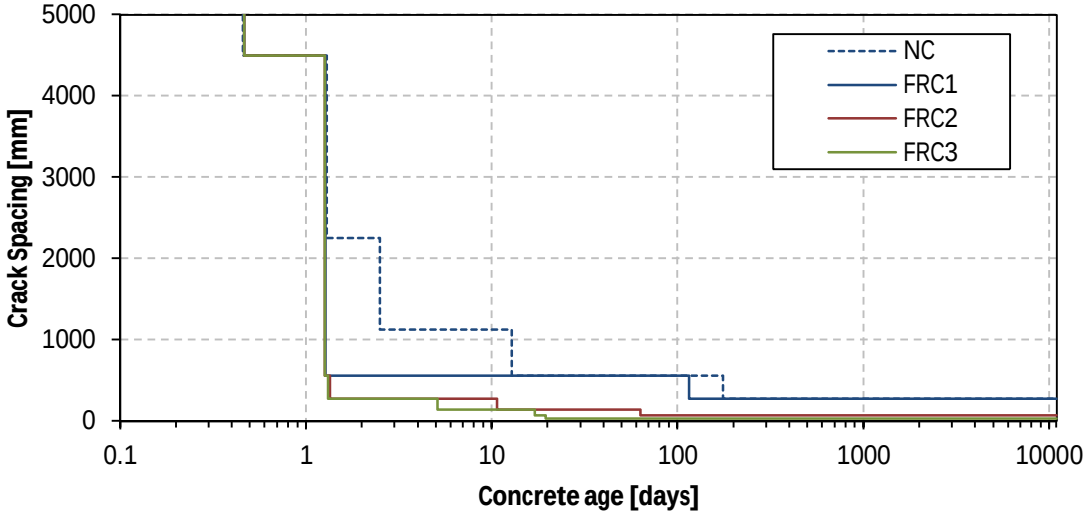

Figure 6.17 Spacing between cracks as cracking occurs for the different fibre content of the estimated SynFRC

The estimated SynFRC responses that were analysed, cracked at different ages than the NC, with a decrease in the age of each crack as the tensile fracture strength was increased. The first cracking, at the joints, are again at the same age for both the NC and SynFRC. The crack spacings reached between the cracks are 281.25mm, 70.31mm and 35.16mm for FRC1, FRC2 and FRC3, respectively. The NC reached this crack spacing at an age of 175 days and the FRC1, FRC2 and FRC3 reached the minimum spacings at ages of 115 days, 63 days and 20 days, respectively. In Figure 6.18 the results of the maximum crack width over the concrete age of the estimated SynFRC slab-on-grade analysis is presented.

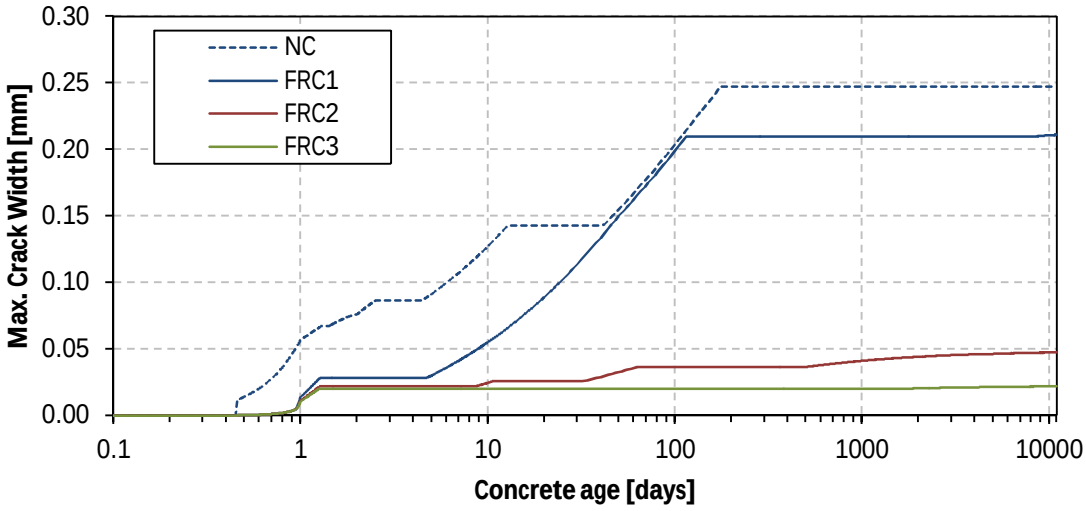

Figure 6.18 Development of the maximum crack width within the slab-on-grade of the estimated SynFRC

Excellent results were obtained from the analyses performed on the estimated tensile behaviours for SynFRC. This shows that larger polypropylene fibre content controls the DSC through cracking earlier, but keeping the cracks small with the aid of the polypropylene fibres bridging the crack. In Figure 6.18 it is observed that the SynFRC with an $R_{e,3}$ value of 0.25 did not significantly improve the response compared to NC. The SynFRC with $R_{e,3}$ values of 0.51 and higher clearly improved the response by decreasing the crack width from 0.25mm to less than 0.05mm.

This means that the desired outcome can be reached, because it shows that polypropylene FRC can control DSC with an $R_{e,3}$ value of 0.51 or higher. The SynFRC with the $R_{e,3}$ value of 0.25 shows a slight long term improvement, but the two higher $R_{e,3}$ values analysed show continuous improvement over the age of the concrete.

6.3.2 Friction Type

The effects of the coefficient, α, of friction and the elastic slip of friction (stickiness) were analysed. This was done to determine the effect on the crack widths obtained from the DSC in a slab-on-grade. The results of these analyses are presented and discussed in this section.

Coefficient of Friction

Figure 6.19 presents the crack spacing of the cracking within the slab-on-grade by changing the friction type.

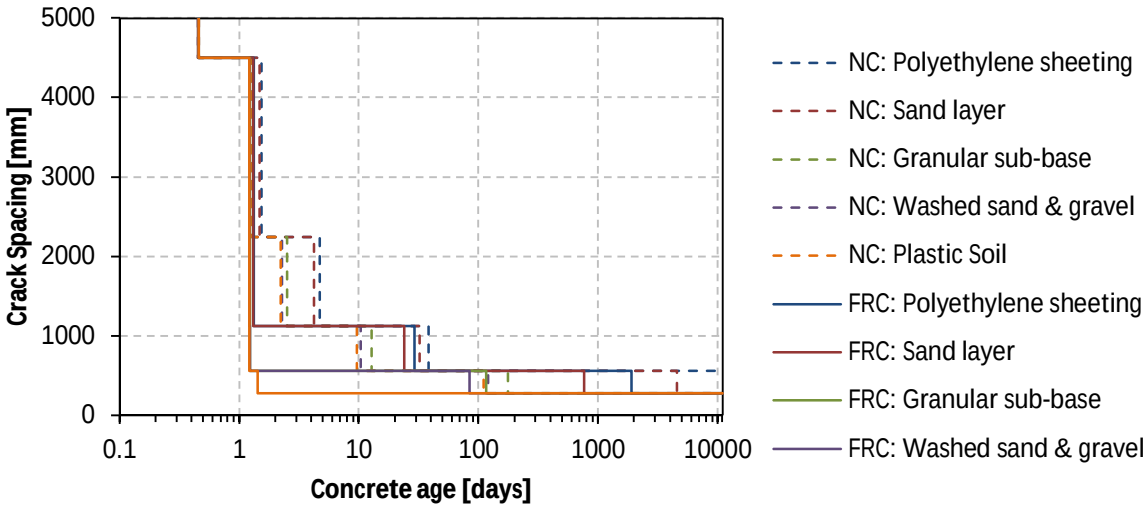

Figure 6.19 Spacing between cracks as cracking occurs for the different coefficients of friction

The coefficient of friction has an effect on the rate at which cracking occurs, which is shown in Figure 6.19. As was expected, the coefficient, α, of friction and the rate of occurrence of cracking are directly proportional to each other. As the coefficient, α, of friction increases, the occurrence of cracking accelerates. The minimum crack spacing obtained was 281.25mm for all the SynFRC analyses and four of the five NC analyses. The NC on polyethylene sheeting reached a crack spacing of 562.5mm. In Figure 6.20 the results of the maximum crack width over the concrete age of the slab-on-grade analysis where the friction type was varied, are presented.

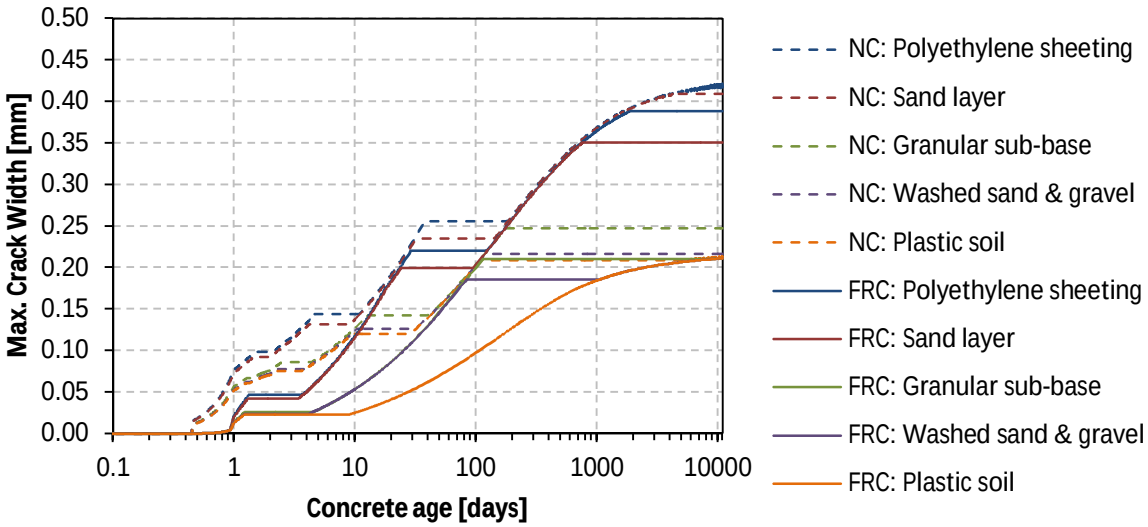

Figure 6.20 Development of the maximum crack width within the slab-on-grade for different coefficients of friction

As discussed, more cracks with smaller crack widths are more favourable than fewer cracks with larger crack widths, except when the large cracks occur at joints. This was not observed for the NC on polyethylene sheeting. Should NC on polyethylene sheeting be used, then the joints would be required every 560mm to avoid cracks forming between joints for the 100mm thick control slab thickness, which is less than the 4.5m suggested by Marais & Perrie (1993).

From Figure 6.19 it is observed that with the decrease in the coefficient of friction there is an increase in the maximum crack width. This shows that the coefficient, α, of friction and the maximum crack width are not directly inverse proportionally to each other. This was expected, because the slab is allowed to move more freely. The polyethylene sheeting between the slab and the subgrade caused a maximum crack width of about 0.41mm whereas the plastic soil beneath the slab, a crack width of about 0.21mm. The coefficient, α, of friction had a small effect on the behaviour of the SynFRC, meaning that the improvement, due to the SynFRC was not significantly enhanced by the change of the coefficient, α, of friction.

Elastic Slip

Figure 6.21 presents the crack spacing of the cracking within the slab-on-grade by changing the elastic slip value of the friction.

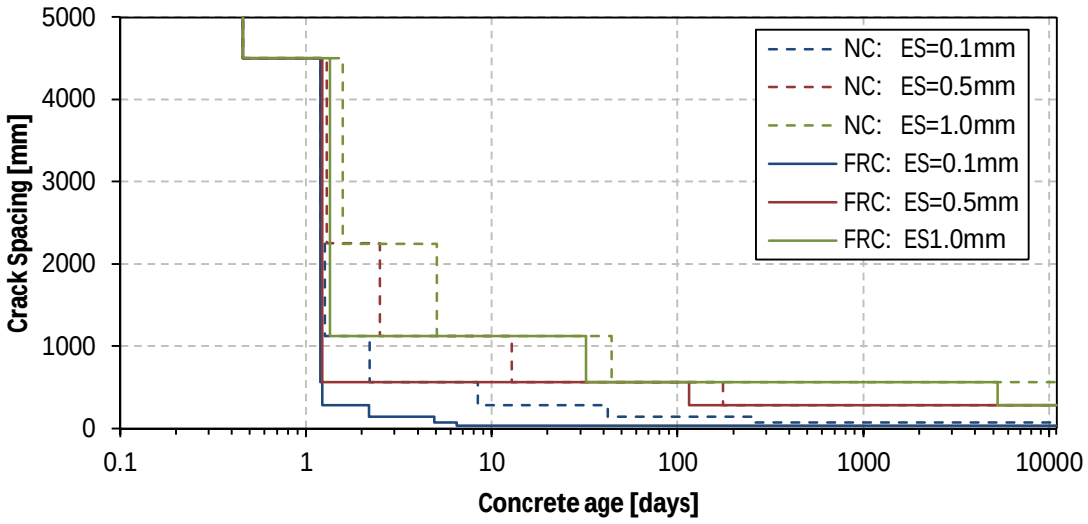

Figure 6.21 Spacing between cracks as cracking occurs for the different elastic slip values

From Figure 6.21 it is observed that the elastic slip value had an effect on the rate of cracking and the number of cracks that occurred. Therefore the elastic slip of friction is more important than the coefficient, α, of friction when designing a slab-on-grade. The stickier the friction (and hence, the smaller the elastic slip value) the earlier the slab model cracked and multiple cracks occurred. It is observed that there is a slight increase in the rate and number of cracks between the SynFRC and the

NC with a decrease in the elastic slip value. The SynFRC with the elastic slip value of 0.1mm had the smallest crack spacing of 35.16mm. The NC with an elastic slip value of 1.0mm had the largest crack spacing of 562.5mm. Figure 6.22 presents the results of the maximum crack width over the concrete age of the slab-on-grade analysis where the elastic slip value of the friction was varied.

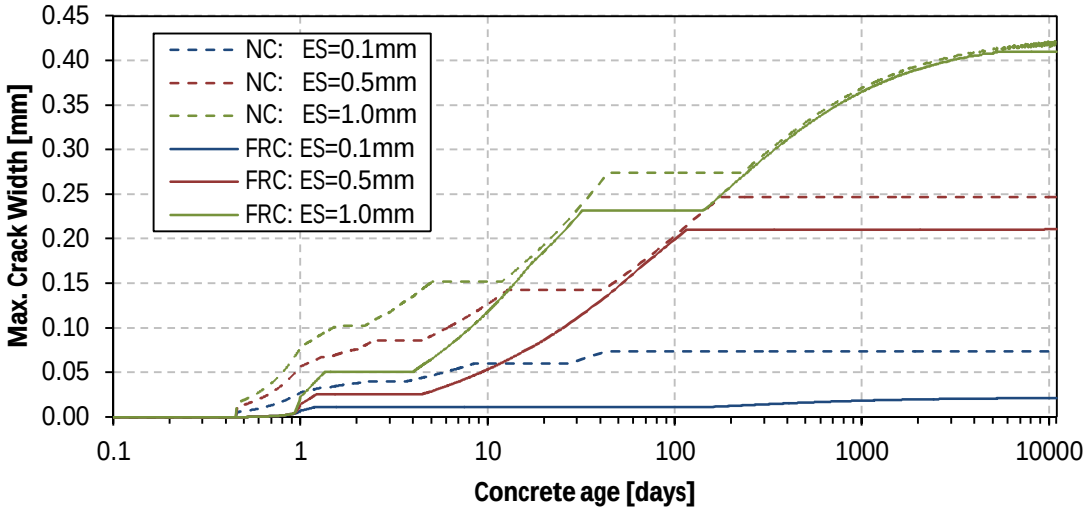

Figure 6.22 Development of the maximum crack width within the slab-on-grade for different elastic slip values

The elastic slip value had an effect on the maximum crack width obtained within the slab, because of its effect on the number of cracks that occurred. The smaller the elastic slip value (and hence, the stickier the friction), the smaller the maximum crack width was within the slab (Figure 6.22). With an elastic slip value of 1.0mm there was no long term difference between the NC and SynFRC in maximum crack width. For the elastic slip value of 0.1mm the SynFRC reached a crack width of 0.02mm after 30 years. This is a relatively big improvement from the NC that reached a maximum crack width between 0.07mm and 0.08mm after 30 years. These are very small cracks and would be hard to spot with the naked eye, which is the case for low coefficients of friction.

The difference between NC and SynFRC in the case of multiple cracking is that the SynFRC will have fibres bridging the cracks which will keep the cracks small.

6.3.3 Joint Spacing

Figure 6.23 presents the crack spacing of the cracking within the slab-on-grade by changing the joint spacing.

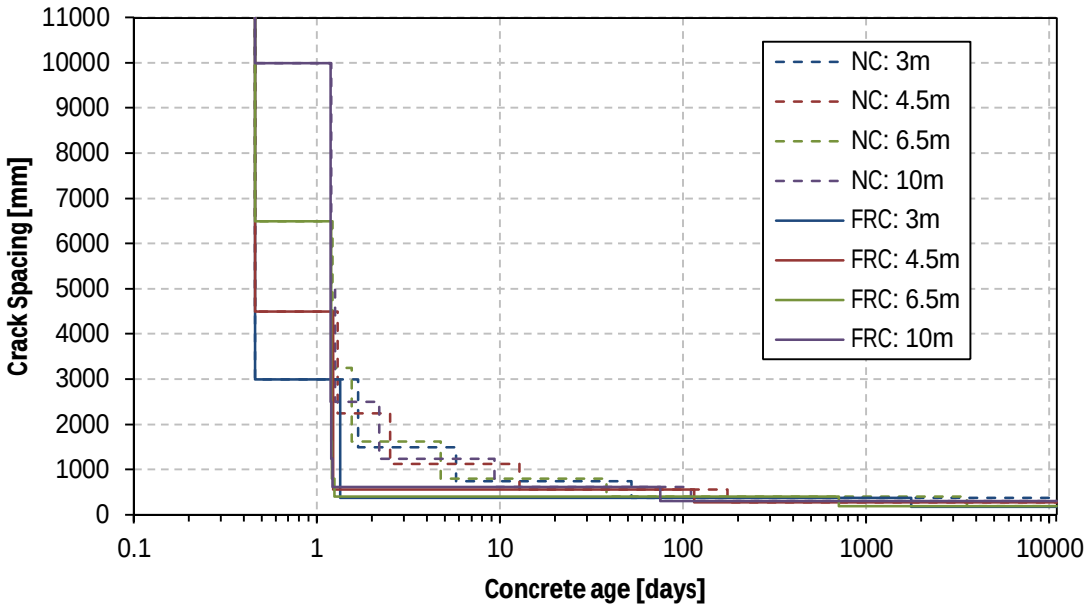

Figure 6.23 Spacing between cracks as cracking occurs for the different joint spacings

The joint spacing does not have any significant effect on the crack spacing after 30 years or the number of cracks per length of slab, and it affects only the number of cracks that may occur between joints. In Figure 6.23 it is seen that the 3.0m and 6.5m follow the same response when the cracking occurs and the spacing only differs slightly. This was also the case for the 4.5m and 10.0m joint spacings. In Figure 6.24 the results of the maximum crack width over the concrete age of the slab-on-grade analyses where the joint spacing were varied, are shown.

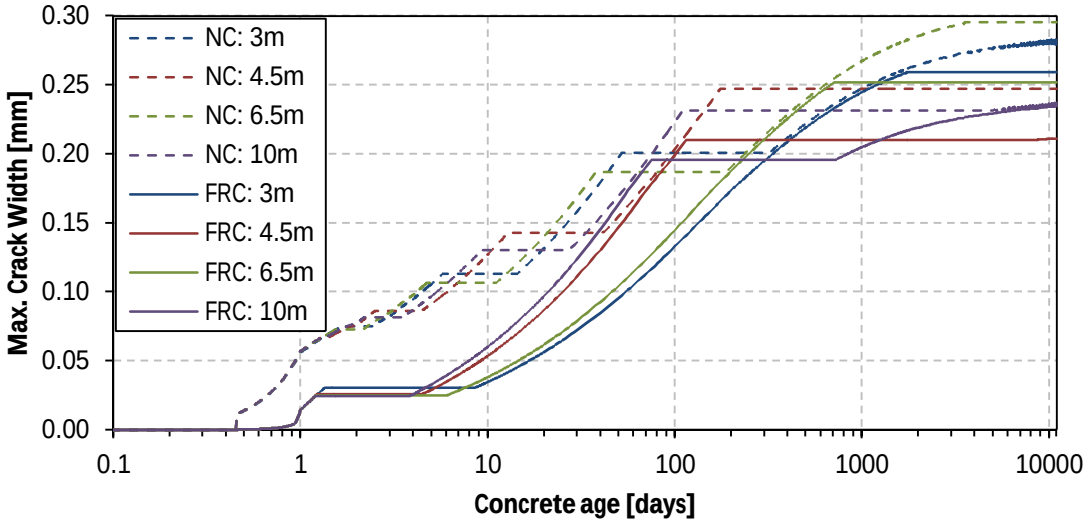

Figure 6.24 Development of the maximum crack width within the slab-on-grade for different joint spacings

The long term maximum crack width between NC and SynFRC was only slightly improved in the early ages of the concrete. The crack widths at a concrete age of 30 years ranged between 0.21mm

and 0.30mm. The SynFRC only improved the long term cracking by ±0.04mm, but only for joint spacings of 3.0m and 4.5m.

6.3.4 Slab Thickness

Figure 6.25 presents the crack spacing of the cracking within the slab-on-grade by changing the slab thickness.

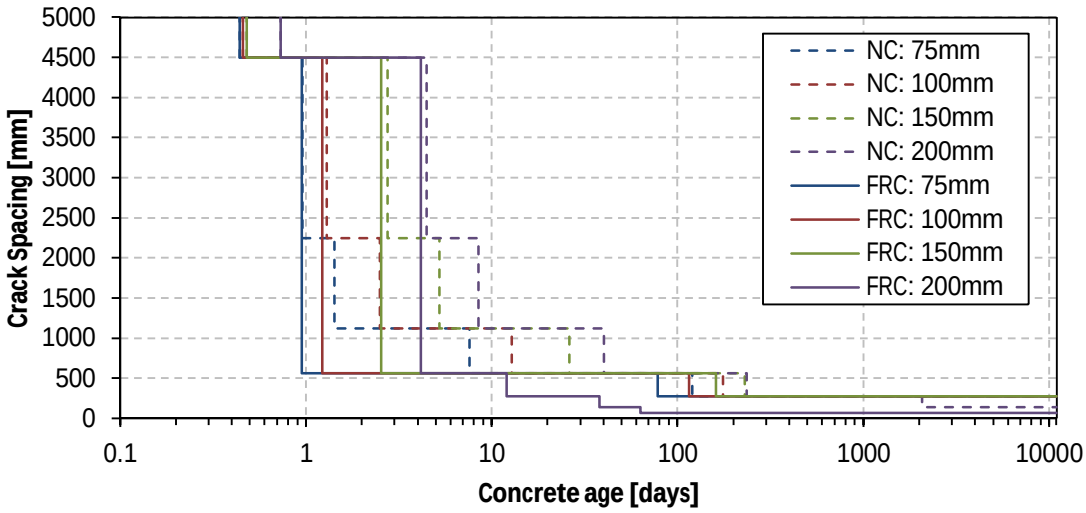

Figure 6.25 Spacing between cracks as cracking occurs for the different slab thicknesses

With the exception of the 200mm thick slab the increase in slab thickness caused the slab to crack more slowly, after 10 days. This was due to the added gravity that increased the friction force between the slab and the subgrade, due to the increased slab thickness. The increase of slab thickness caused a decrease in the amount of shrinkage strain that occurred within the slab.

All the slab thicknesses reached a crack spacing of 281.25mm after 1 year, except the 200mm thick slab with SynFRC which reached a crack spacing of 70.31mm. This was an interesting result, because initially the 200mm thick slab cracked more slowly than the thinner slabs and then the rate of cracking increased. The same was noted for the NC slab with a thickness of 200mm. The NC slab with a 200mm thickness reached a crack spacing of 140.63mm. In Figure 6.26 the results of the maximum crack width over the concrete age of the slab-on-grade analyses, where the slab thickness was varied, are shown.

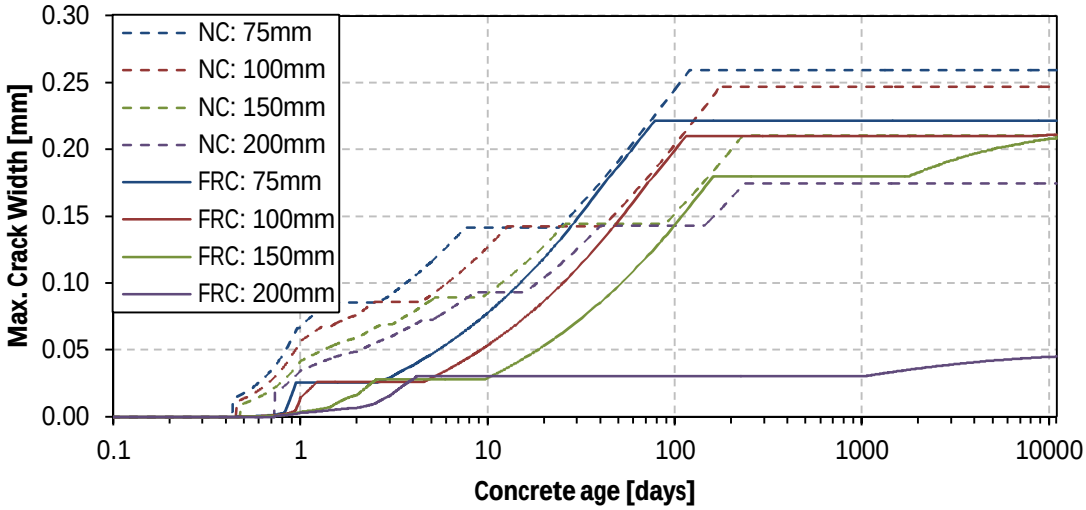

Figure 6.26 Development of the maximum crack width within the slab-on-grade for different slab thicknesses

As presented in Figure 6.26, the maximum crack widths decreased with the increase of slab thickness, due to smaller shrinkage strains. The 200mm thick slab with the SynFRC reached much smaller crack widths than the NC slab with the same thickness. This was due to the number of cracks that were formed at an early age of the concrete. These results show that with an increase of slab thickness, it may be possible to decrease the polypropylene fibre content and still be able to control the DSC.

The 200mm thick NC slab reached a maximum crack width of 0.17mm and the SynFRC a crack width of only 0.04mm; a significant improvement in maximum crack width.

6.3.5 Ambient Relative Humidity

Figure 6.27 presents the crack spacing of the cracking within the slab-on-grade by changing the ambient relative humidity.

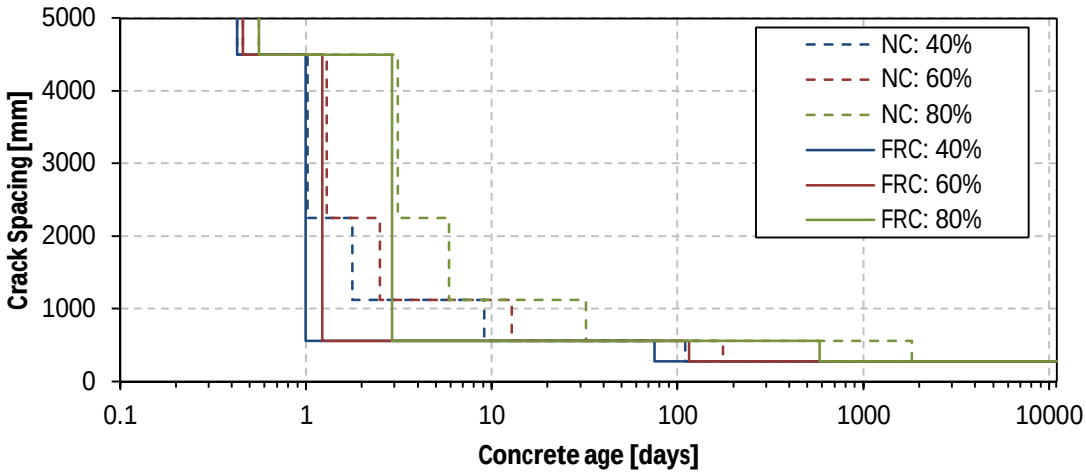

Figure 6.27 Spacing between cracks as cracking occurs for the different relative humidities

The ambient relative humidity has an effect on the shrinkage strain that occurs within the slab-on-grade. Therefore with a low relative humidity the DSC occurred more rapidly as shown in Figure 6.27. The minimum crack spacing reached after 30 years for all the analyses was 281.25mm. In Figure 6.28 the results of the maximum crack width over the concrete age of the slab-on-grade analyses, where the ambient relative humidity was varied, are shown.

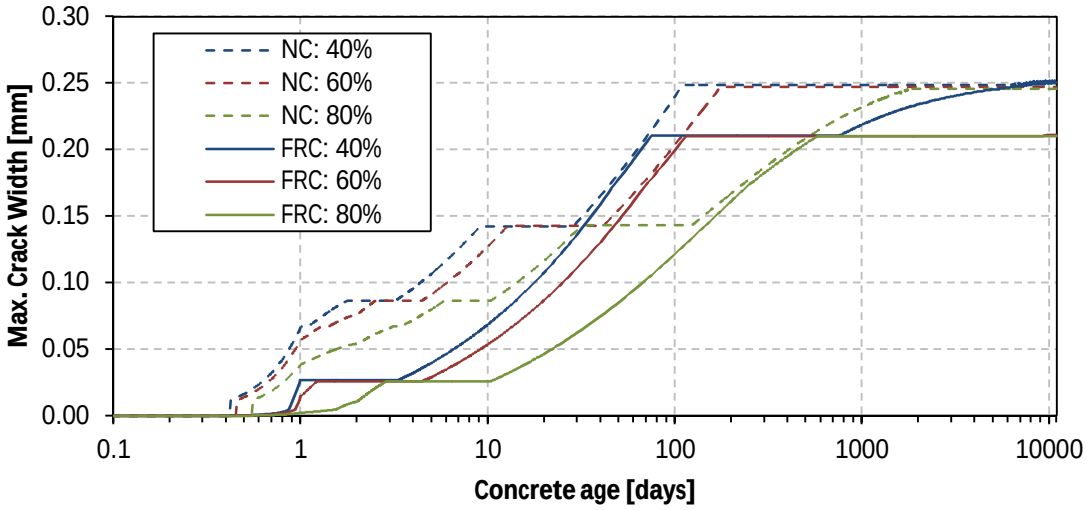

Figure 6.28 Development of the maximum crack width within the slab-on-grade for different relative humidities

There is no significant difference between the ultimate maximum crack widths of the NC and the SynFRC slabs-on-grade. At lower relative humidities the improvement of maximum crack width by adding fibres to the concrete mix, last a bit longer at early ages of the concrete, see Figure 6.28. The NC slabs all reached a maximum crack width of 0.25mm and this crack width was also reached for the SynFRC slab-on-grade model subjected to 40% ambient relative humidity. There was only an insignificant difference between the maximum crack width for the SynFRC models subjected to the relative humidities of 60% and 80%. These slabs reached a maximum crack width of 0.21mm.

6.3.6 Results Summary

In this section the results obtained from the analyses at concrete ages of 6 months and 30 years are summarised by showing the maximum crack widths.

SynFRC Type

Figures 6.29 and 6.30 present the maximum crack widths obtained, at concrete ages of 6 months and 30 years for the different fibre types and fibre dosages, respectively, with the DSC analyses performed on slabs-on-grade.

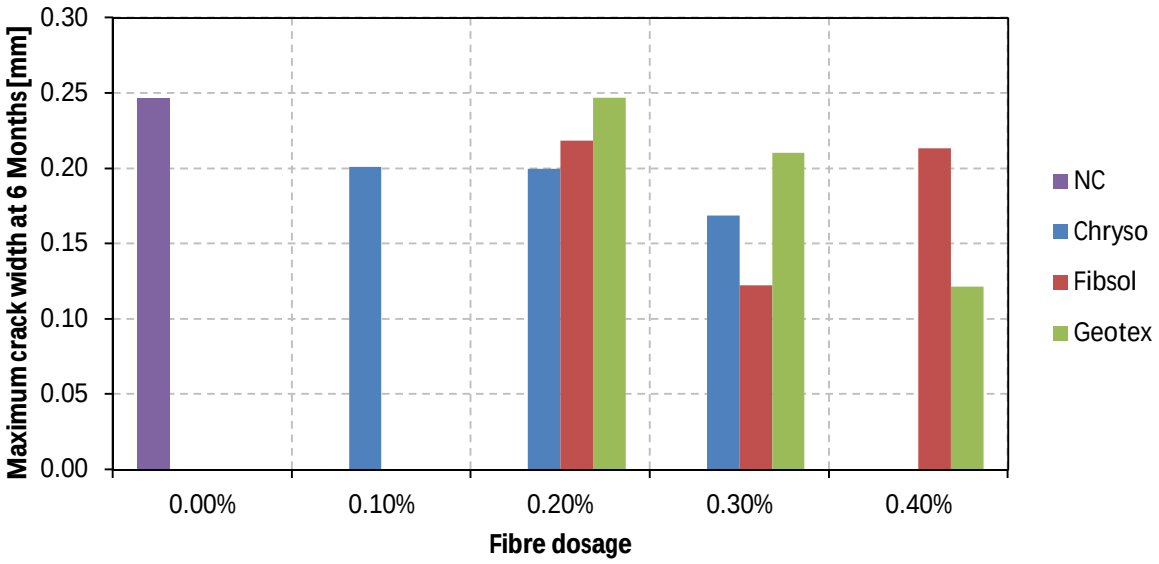

Figure 6.29 Maximum crack widths at a concrete age of 6 months of slabs-on-grade with different fibre types and percentages

Figure 6.29 shows that increased fibre content tends to decrease the maximum crack width of the slab. The Fibsol SynFRC with 0.3% fibre content was the only outlier, but the number of samples tested are too small to prove this. This was not the case for the crack widths obtained at a concrete age of 30 years. In Figure 6.30 shows that the maximum crack widths within the slab with the fibre content of less than 0.4% did not differ significantly from the NC. It is also noted that the maximum crack width between the SynFRC with fibre content ranging between 0.1% and 0.4% did not improve significantly at a concrete age of 30 years.

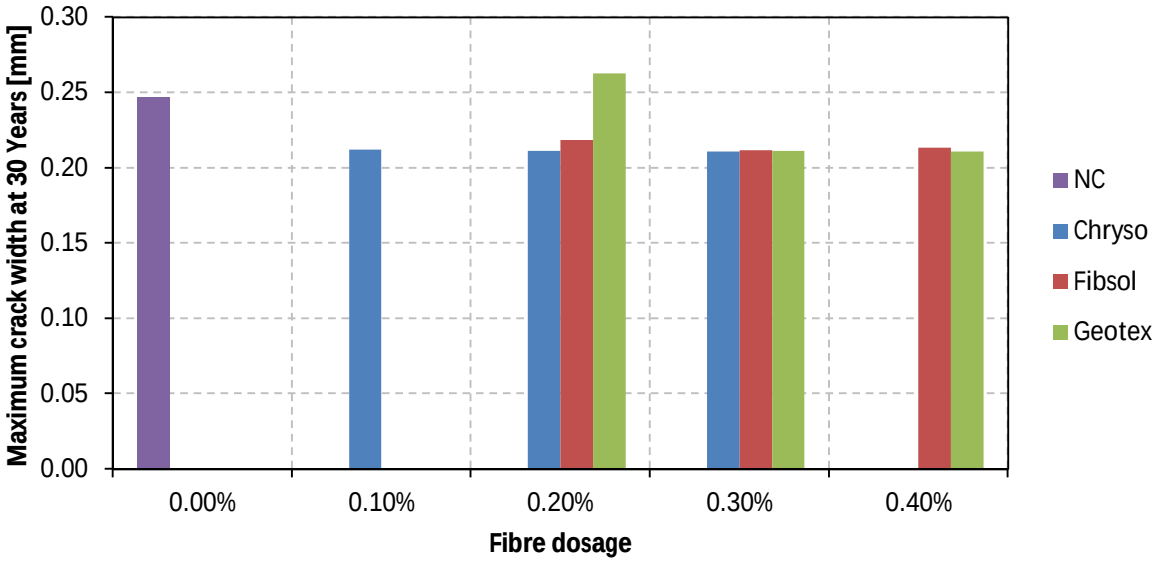

Figure 6.30 Maximum crack widths at a concrete age of 30 years of slabs-on-grade with different fibre types and percentages

Shown in Figure 6.31 are the maximum crack widths obtained, at concrete ages of 6 months and 30 years. This was for the different estimated SynFRC tensile behaviours, with the DSC analyses performed on slabs-on-grade.

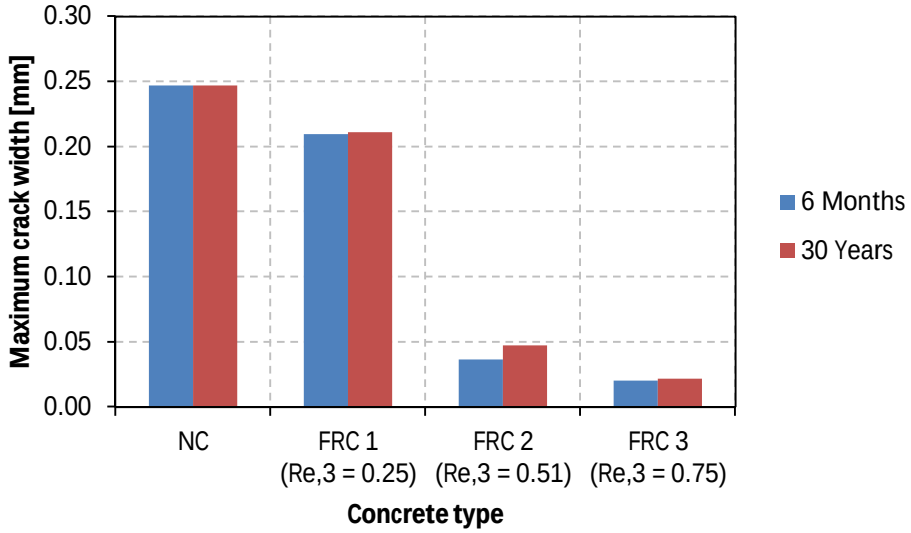

Figure 6.31 Maximum crack widths at concrete ages of 6 months and 30 years of slabs-on-grade with different estimated tensile behaviours

Figure 6.30 shows that the concrete almost reached its maximum crack width at a concrete age of 6 months. This was the case for both the NC and the SynFRC. The maximum crack width was significantly reduced with increased SynFRC post cracking energy ($R_{e,3}$). Figure 6.32 presents the maximum crack widths obtained, at the concrete age of 30 years, for SynFRC with different $R_{e,3}$ values.

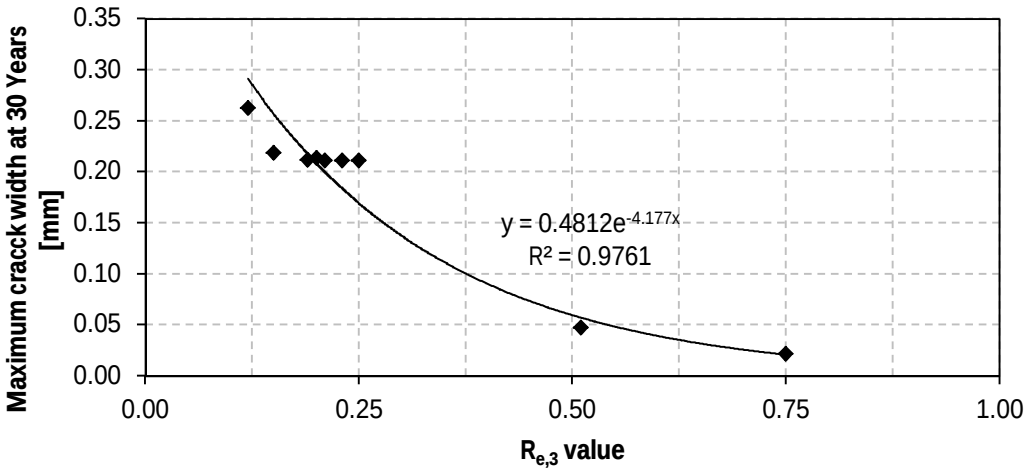

Figure 6.32 Maximum crack widths at a concrete age of 30 years of slabs-on-grade with different $R_{e,3}$ values

Series1 shown in Figure 6.32 were subjected to an exponential regression shown by the solid line. The R^2 value and the regression line equation are shown just above this line.

Friction Type

Figures 6.33 and 6.34 present the maximum crack widths obtained at the concrete ages of 6 months and 30 years, respectively. This was done for different friction types, with the DSC analyses performed on slabs-on-grade.

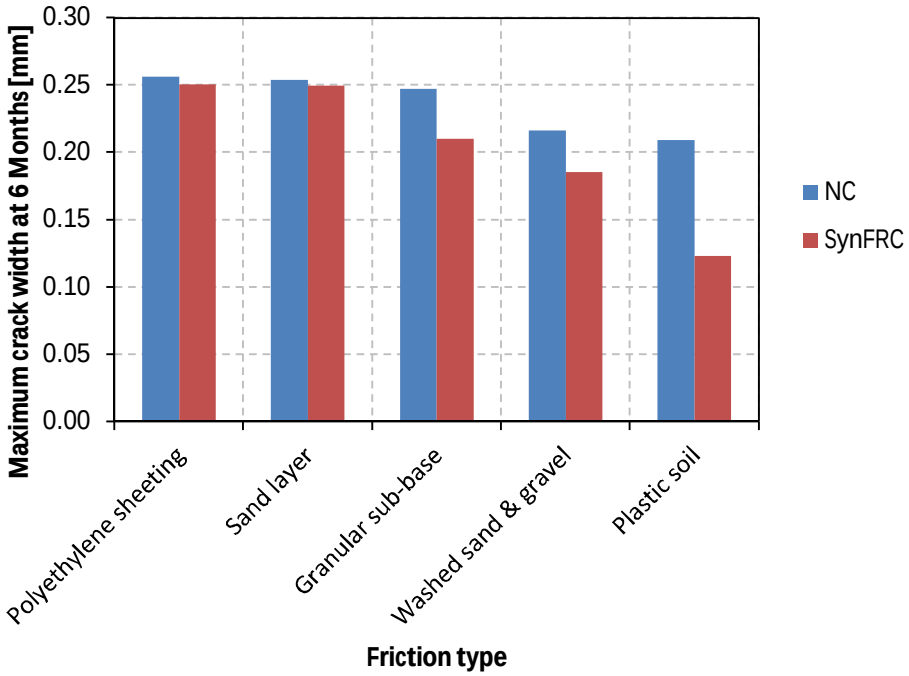

Figure 6.33 Maximum crack widths at a concrete age of 6 months of slabs-on-grade with different friction types for both NC and SynFRC

Figure 6.33 shows that, at a concrete age of 6 months, as the coefficient, α, of friction increased the maximum crack width decreased. This was due to the friction that restrained the concrete from moving horizontally. The difference in maximum crack width between the NC and SynFRC also increased with the increase of the coefficient, α, of friction at early ages. The exact opposite was seen at a concrete age of 30 years, where the difference between the NC and SynFRC was more promising with lower coefficients of friction. At a concrete age of 30 years, the maximum crack widths were much smaller at higher coefficients of friction, see Figure 6.34.

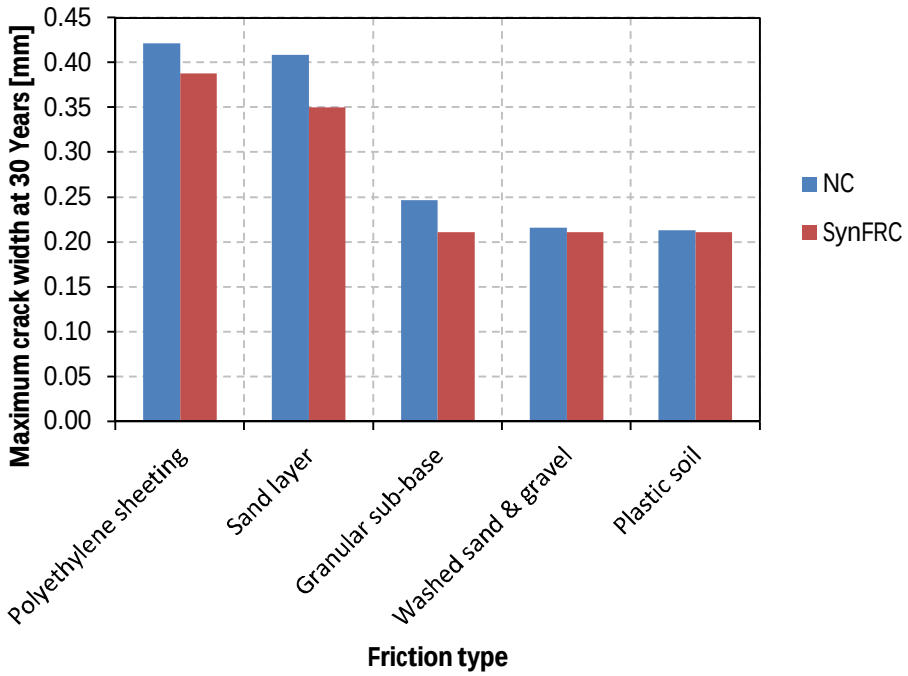

Figure 6.34 Maximum crack widths at a concrete age of 30 years of slabs-on-grade with different friction types for both NC and SynFRC

Figures 6.35 and 6.36 show the maximum crack widths obtained, at the concrete ages of 6 months and 30 years, respectively, for the different elastic slip values, with the DSC analyses performed on slabs-on-grade.

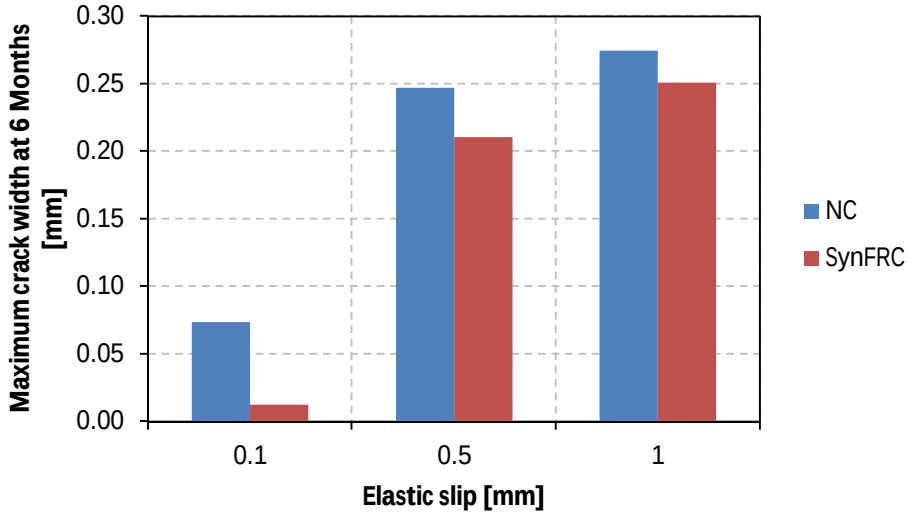

Figure 6.35 Maximum crack widths at a concrete age of 6 months of slabs-on-grade with different elastic slip values for both NC and SynFRC

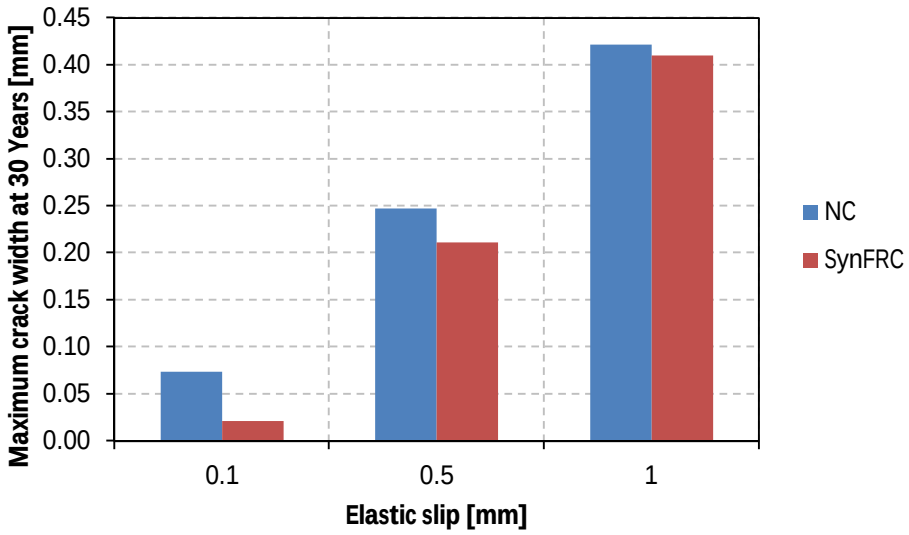

Figure 6.36 Maximum crack widths at a concrete age of 30 years of slabs-on-grade with different elastic slip values for both NC and SynFRC

From Figures 6.35 and 6.36 it is observed that at concrete ages of 6 months and 30 years there was a significant decrease in maximum crack widths for smaller elastic slip values of the friction. The SynFRC performed better with stickier friction (small elastic slip values). It also showed more pronounced improvement in crack widths at the concrete ages of 6 months than at 30 years.

Joint Spacing

Figures 6.37 and 6.38 present the maximum crack widths obtained at the concrete ages of 6 months and 30 years. This was for the different joint spacings, with the DSC analyses performed on slabs-on-grade.

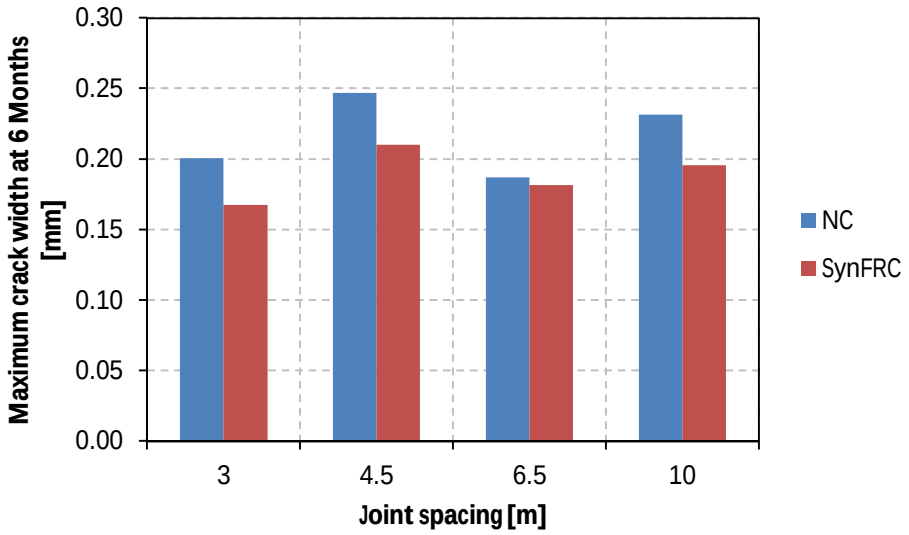

Figure 6.37 Maximum crack widths at a concrete age of 6 months of slabs-on-grade with different joint spacings for both NC and SynFRC

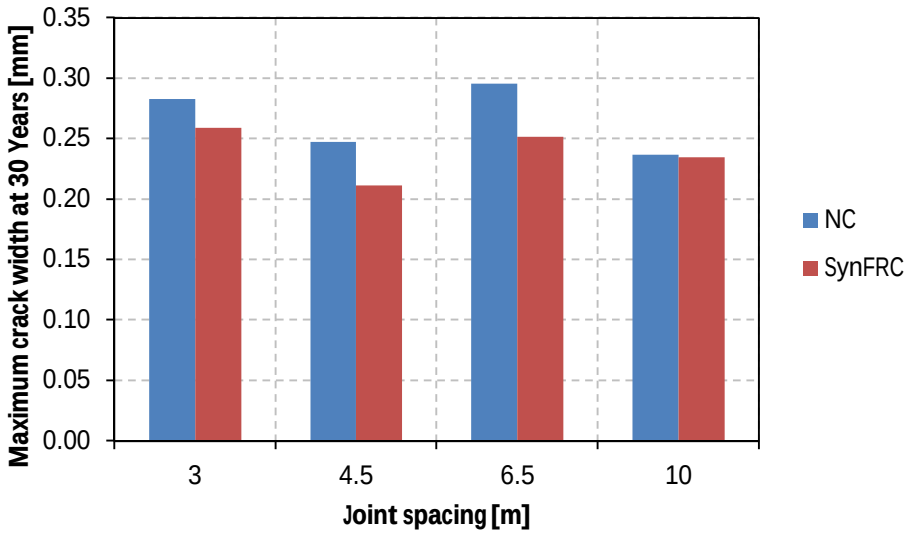

Figure 6.38 Maximum crack widths at a concrete age of 30 years of slabs-on-grade with different joint spacings for both NC and SynFRC

From Figures 6.37 and 3.38 the conclusion can be made that the joint spacing did not have any significant effect on crack widths. The joint spacing determined the number of cracks that were formed between the joints and by adding fibres to the concrete, a decrease in maximum crack widths can be observed.

Slab Thickness

Figures 6.39 and 6.40 present the maximum crack widths obtained, at concrete ages of 6 months and 30 years for the different slab thicknesses, with the DSC analyses performed on slabs-on-grade.

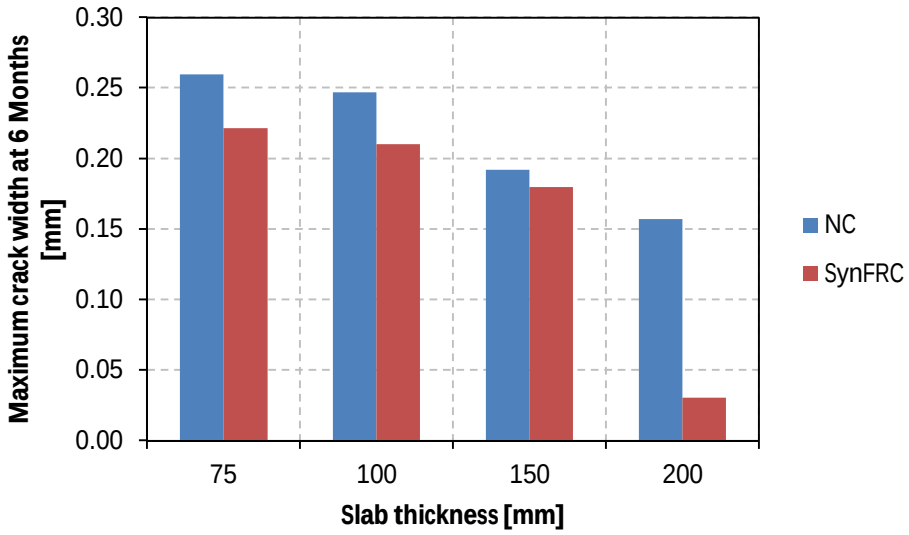

Figure 6.39 Maximum crack widths at a concrete age of 6 months of slabs-on-grade with different slab thicknesses for both NC and SynFRC

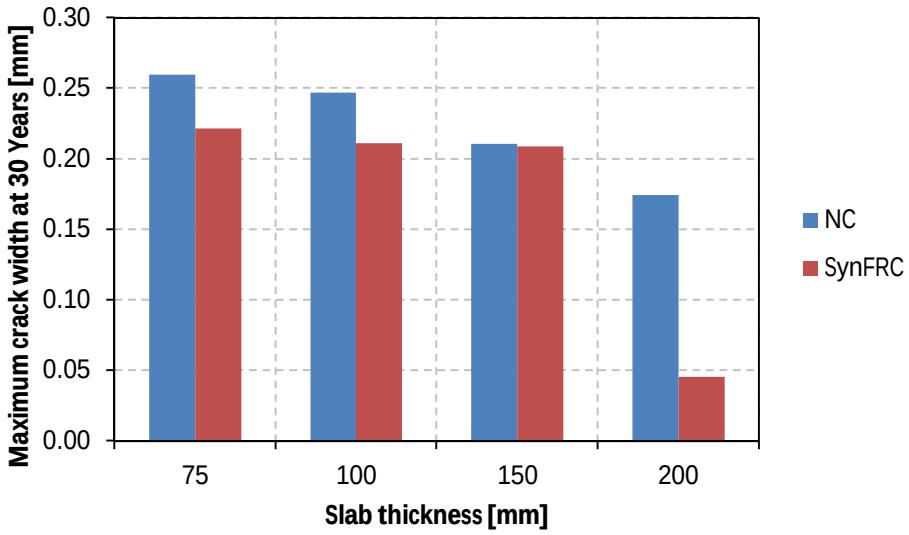

Figure 6.40 Maximum crack widths at a concrete age of 30 years of slabs-on-grade with different slab thicknesses for both NC and SynFRC

Figures 6.39 and 6.40 show the crack widths decreased with increasing slab thickness. This was seen for the NC and SynFRC slabs-on-grade. It is observed that the reduction in maximum crack width by adding fibres to the concrete mix was more pronounced for greater slab thicknesses. This means that it is possible to control DSC with low volumes of synthetic fibres by increasing the slab thickness.

Ambient Relative Humidity

Figures 6.41 and 6.42 show the maximum crack widths obtained at the concrete ages of 6 months and 30 years for the different ambient relative humidities, with the DSC analyses performed on slabs-on-grade.

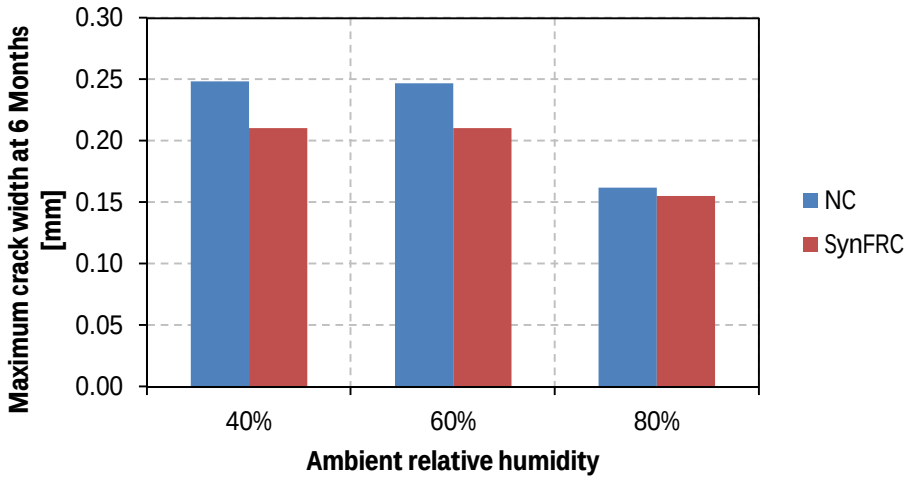

Figure 6.41 Maximum crack widths at a concrete age of 6 months of slabs-on-grade with different ambient relative humidities for both NC and SynFRC

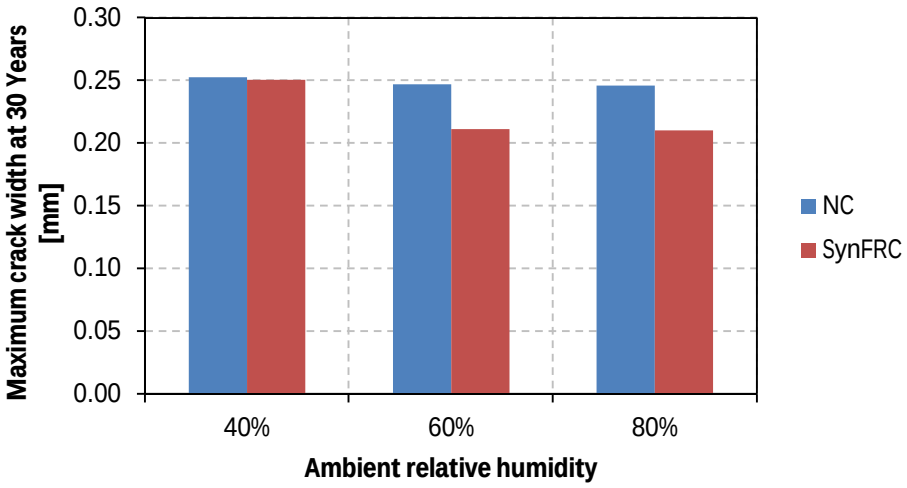

Figure 6.42 Maximum crack widths at a concrete age of 30 years of slabs-on-grade with different ambient relative humidities for both NC and SynFRC

Figure 6.41 shows that at higher ambient relative humidities, smaller crack widths were obtained at the concrete age of 6 months for NC and SynFRC. This was not the case at the concrete age of 30 years. At this age the relative humidity showed no significant difference in maximum crack width, see Figure 6.42.

6.4 Concluding Summary

This chapter covers the finite element analyses that were performed on slabs-on-grade to determine the number of cracks and the maximum crack widths that occurred within these slabs due to drying shrinkage. First the analysis objectives were provided, and then the analysis setup and procedure were discussed. The components, assembly, mesh, material properties, boundary conditions and the different combinations for the analyses were discussed within the procedure section.

After the discussion of the analyses setup and procedure, the results from these analyses were provided and discussed. The results for the different SynFRC- and friction types, joint spacings, slab thicknesses and relative humidities were discussed individually.

The polypropylene fibres tested (discussed in Chapter 5) and the estimated fibre behaviours were analysed. The friction types were also divided into two parts of analyses, looking at the coefficient, α, of friction and the elastic slip value for the friction. The addition of fibres gave the concrete a ductility that allowed the concrete to crack more than NC, but this did not allow the cracks to propagate, therefore the SynFRC is able to control DSC within slabs-on-grade.

The above mentioned response was observed at a lower fibre content of 0.3% and a slab thickness of 200mm. The SynFRC slab had a maximum crack width of 0.03mm at a concrete age of 6 months, which is an 80.9% improvement of the maximum crack width within the NC slab of the same

thickness and age. At a concrete age of 30 years an improvement of 74.3% for the SynFRC slab was observed, with a maximum crack width of 0.045mm for the SynFRC slab. Tests were only conducted on SynFRC specimens with fibre content of up to 0.4% by concrete volume, which is not sufficient to control the DSC in most cases.

The DSC was observed to be controlled in the SynFRC slab model that has $R_{e,3}$ values of 0.51 and higher. This controlled the DSC within a slab with a thickness of 100mm, where the SynFRC slab had a maximum crack width of 0.037mm at the concrete age of 6 months, which is an 85.0% improvement of the maximum crack width within the NC slab of the same thickness and age. At a concrete age of 30 years an improvement of 81.0% for the SynFRC slab was observed, with a maximum crack width of 0.047mm.

There were also improvements observed when adding fibres if the friction is sticky, meaning the maximum friction between the slab and the subgrade were reached with very little movement. Higher friction resulted in smaller maximum crack widths for both the NC and the SynFRC.

Chapter 7 Full Scale Testing

Full scale tests were performed on slabs of normal concrete (NC), wire mesh reinforced concrete (RC) and synthetic fibre reinforced concrete (SynFRC). These tests were performed to design a test method for doing large scale tests for testing DSC on slabs-on-grade. The slabs were subjected to environmental and boundary conditions that should induce cracking on the slab. These conditions included a large coefficient of friction (to increase the presence of a restraint beneath the slab), fixed ends and a slab length of 9.0m without any joints.

7.1 Experimental Framework

Three slabs of 9.0x1.0x0.1m were tested for DSC to determine the cracking behaviour of slabs-on-grade, used for industrial flooring. The test objectives, program, setup and procedure are discussed below as well as the material properties and mix proportions, used for the tests.

7.1.1 Test Objectives

These experimental tests were performed to achieve the following objectives:

Objective 1

Establish whether the test method is sufficient for determining DSC in concrete slabs-on-grade.

Objective 2

Determine the difference in the drying shrinkage strains between the three different slabs and the free drying shrinkage of the beam specimens with the same effective section thickness.

7.1.2 Test Program

Full scale DSC tests were performed on 9.0x1.0x0.1m slabs of NC, RC and SynFRC. The reinforcement used for the RC was a steel wire mesh and the fibres used for the SynFRC are macro polypropylene fibres produced by Geotex. These tests were performed to determine the difference in performance of each slab and its reinforcement system against DSC. The wire mesh used was the ref. 395 according to the SANS 1024:2006 and a fibre content of 0.266% was used for the SynFRC.

Together with these tests the shrinkage-, compressive-, friction- and flexural tests were performed to determine material properties for the FEA performed on these slabs. These tests were discussed in Chapter 5.

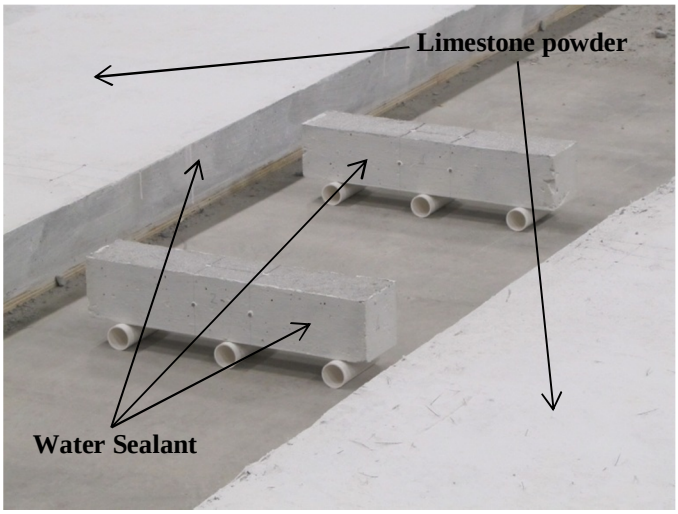

Figure 7.1 Sealant and limestone powder applied to the slabs and beams tested for shrinkage

The slabs were cast and left to set for 24 hours. Thereafter the mould sides were removed and sealed with a water sealer to prevent any evaporation occurring from the sides of the slabs, see Figure 7.1. Therefore evaporation occurred only from the top surface of the slab as is the case for slabs-on-grade. The slabs were not cured since strains were measured from the beginning of the drying of the slabs. The slabs were tested for 90 days to allow the shrinkage strain to reach a strain capable of cracking the concrete slabs.

The concrete used for slabs was supplied by Lafarge Ready mix due to the large volume of concrete required to conduct the tests, see Figure 7.2.

Figure 7.2 Casting procedure used for full scale slab tests

7.1.3 Test Setup and Procedure

The test setup consists of a slab that was cast directly onto a wooden surface which was grooved in the direction of movement and perpendicular to this direction as shown in Figure 7.3. The grooves were cut 13mm apart at a depth of 3mm, which left 10x10mm block patterns on the top surface of the wooden base. The friction results between the concrete slab and this wooden surface were tested and the results are presented in Section 5.2.3.

Figure 7.3 Grooved boards attached to shutter ply boards used for the wooden base beneath the slab-on-grade tests

The grooved boards were fixed on top of 21mm shutter ply boards with the aid of chipboard screws. This was to ensure a stable surface for the concrete slab and therefore restricting the movement of the wooden surface. The ends of the wooden base were fixed to the laboratory floor by clamping the wooden base with the steel angle sections shown in Figure 7.4.

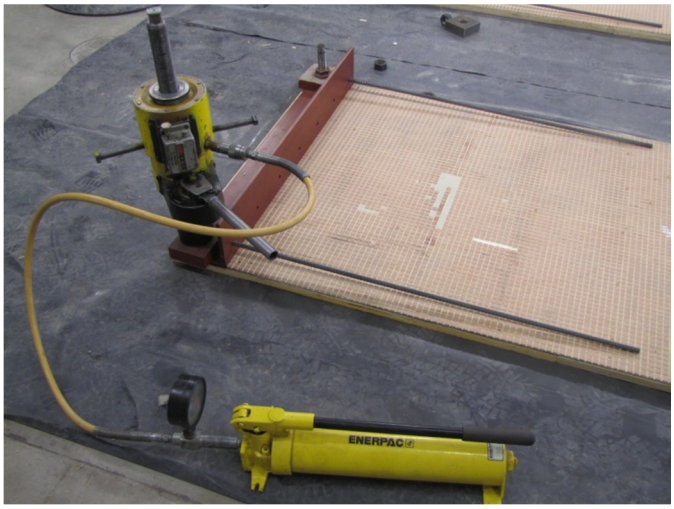

Figure 7.4 Fixing the end connections to the laboratory floor for slab-on-grade tests

These connections consist of 150x150x12mm angles (Figure 7.6), which were connected to the slab with steel reinforcement and to the laboratory floor with post-tensioned treaded bars as shown in Figure 7.5. The reinforcement to fix the slab end to the connection, consisting of seven Y12 bars with nuts welded to the ends of the reinforcing bars to prevent the slab from moving in the horizontal direction, is shown in Figure 7.5. Each of the reinforcement bars was embedded at a length of 1.0m into the slab to allow sufficient bond strength between the concrete slab and these reinforcing bars, see Figure 7.5.

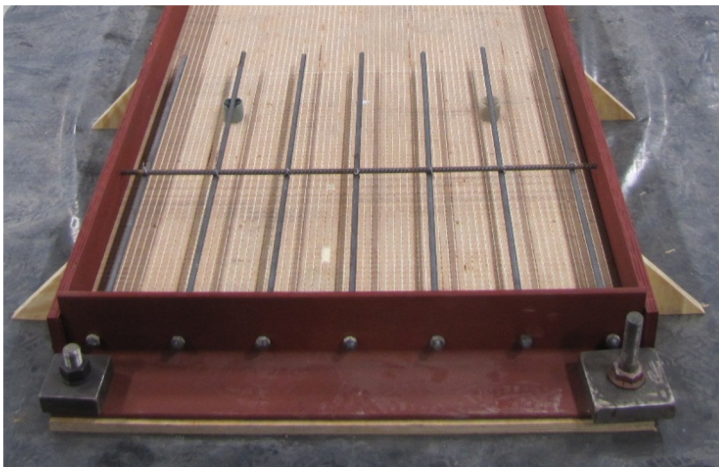

Figure 7.5 The steel angle connection connected to the laboratory floor before the casting of the concrete slab for DSC testing

The reinforcement that connected the slab to the connections and the wire mesh reinforcement were kept at the centre of the slab height, with the aid of spacer blocks, see Figure 7.5. Wooden sides were constructed to complete the mould for the slab. These moulds were connected to the wooden base and were supported by wooden triangles fixed to the sides of the boards as shown in Figure 7.5. The finished moulds for all the slabs cast, are shown in Figure 7.6.

Figure 7.6 Finished moulds for the casting of the slab-on-grade tests

The slabs were cast by using wheelbarrows to move the concrete from the truck to the slabs and then the concrete was vibrated and floated, to ensure an even surface of the top surface of the slabs. One truck supplied the concrete for all three slabs. First the NC and RC slabs were cast and thereafter the polypropylene fibres were added to the concrete in the truck. The truck mixed the concrete for 10 minutes before the SynFRC slab was cast. After the concrete had set, the sides were stripped and sealed with water proof paint. The tops were covered with limestone powder to identify cracks more easily. The finished slabs are shown in Figure 7.7.

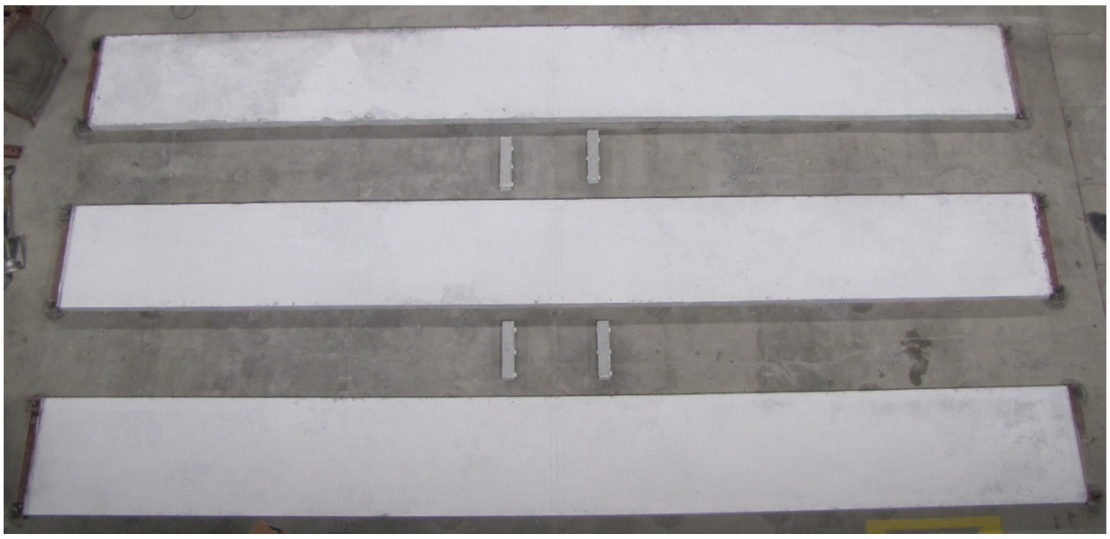

Figure 7.7 Finished concrete slabs-on-grade for testing the effects of DSC

The same markers used for the shrinkage tests, discussed in Chapter 5, were fixed at the centre and over the section where the reinforcement of the end connections ends. These areas were selected since these were the areas where cracking will most likely occur due to the shrinkage. The markers were used to measure the shrinkage strain in these areas in the same manner as the free shrinkage strains were measured as discussed in Section 5.1.3. The markers were also intended to measure the width of cracks that might develop between these markers with the same displacement measurement apparatus shown in Figure 5.10.

Strains were initially measured daily, but at later stages the frequency of measuring decreased as the shrinkage strains developed more slowly. The measurements were taken at the same time as the measurements for the free shrinkage tests, discussed in Chapter 5. With this procedure the shrinkage of each slab was obtained at the ends and the centre of the slab and the cracking behaviour and crack widths of each slab monitored.

The fibre content that was originally required was 3kg/m^3 of concrete which amounts to a percentage of 0.33% per volume. Unfortunately the mixing procedure used for the addition of the fibres caused balling of the fibres, which resulted in a fibre dosage of 0.266% by volume. This value was determined by cleaning and weighing all the fibres that bunched into balls (Figure 7.8) in the mixing

process and by assuming that there was $2m^3$ of concrete left in the truck, since $4m^3$ of concrete were ordered and $2m^3$ were used to cast the first two slabs.

Figure 7.8 Fibres that bunched into balls due to the mixing in the back of the concrete mixing truck

Acid was used to dissolve the concrete from the fibres bunched into balls and then washed with water, shown in Figure 7.9. After the fibres had dried out, they were weighed to determine the fibre content in the slab.

Figure 7.9 Fibres cleaned with acid and washed off with water to determine fibre dosage within the slab

7.1.4 Material Properties

The mix proportions are supplied in the next section. The fibre type used for the SynFRC mix is the Geotex macro polypropylene fibre, which has the same properties as provided in Section 5.1.4.

7.1.5 Mix Proportions

The mix proportions for the concrete mix used in the tests, discussed above, are shown in Table 7.1. This is the same mix used for a number of the flexural, friction, compression and shrinkage tests discussed in Chapter 5.

Table 7.1 Mix proportions for the ready mix concrete used for slab-on-grade tests

Material		[kg/m^3]
Water	Tap	175
Binder	CEM I 52.5	140.7
	Slag	140.7
Stone	19mm Greywacke	740
	13mm Greywacke	306
Sand	Super Sand	360
	Dune Sand	519
Admixture	OMEGA 154	1.5
Fibres dosage [%]	Geotex GRO 50	0.27%

7.2 Experimental Results

The concrete slabs did not show cracks (or cracked, but the cracking was too small to see with the naked eye). This was due to the reinforcement used to connect the slabs to the connections at the end, which were not fixed against the end connection. This occurred in the casting process when the vibrating of the concrete caused the concrete to apply hydrostatic forces to the rebar and push it away from the angle connection as shown in Figure 7.10.

This is not the only reason why the concrete did not show any cracks. The wooden base had a smaller stiffness than the concrete, which allowed the concrete to move a small fraction on the top of the wooden base. The wooden base also curled upwards after casting which could be due to the water that was absorbed into the wood from the concrete during the casting process. This caused the friction to be very small between the wooden base and the laboratory floor. An analysis was performed in Section 7.3 to show this effect. In Figure 7.11 it is shown how the concrete slab moved away from the connections at the end of the slab.

Figure 7.10 Reinforcement connecting the slab to the steel connection at the ends pushed out by concrete

Figure 7.11 The concrete slab moving away from end connection to the laboratory floor

This method did show some promise, though. If the boundary conditions could be satisfied, the slab dimensions could be adjusted and if the frictional restraint at the bottom surface of the slab can be applied by natural compacted aggregate. If the slabs are kept at the same length and the slab thickness and width are decreased then cracking should be more pronounced. A solution for the fixed ends, is to use treaded bars which are fixed to the angles at the end with nuts on both sides. More work should be done on this to confirm whether this method could be used for testing DSC in slabs-on-grade.

The results for the second objective of the tests are shown in Figures 7.12 to 7.14. These figures show the shrinkage strains that were measured for the slabs at both ends and at the centre of the slabs.

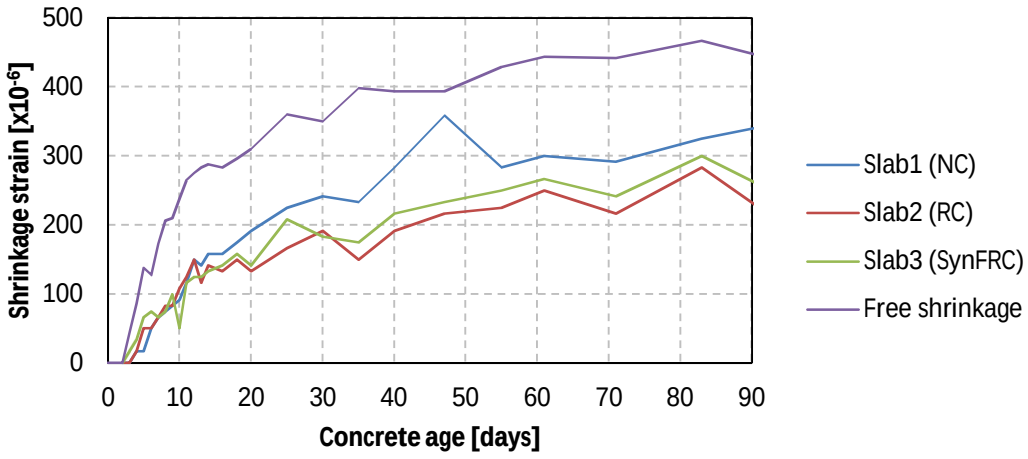

Figure 7.12 Shrinkage strains at the first end of the slabs

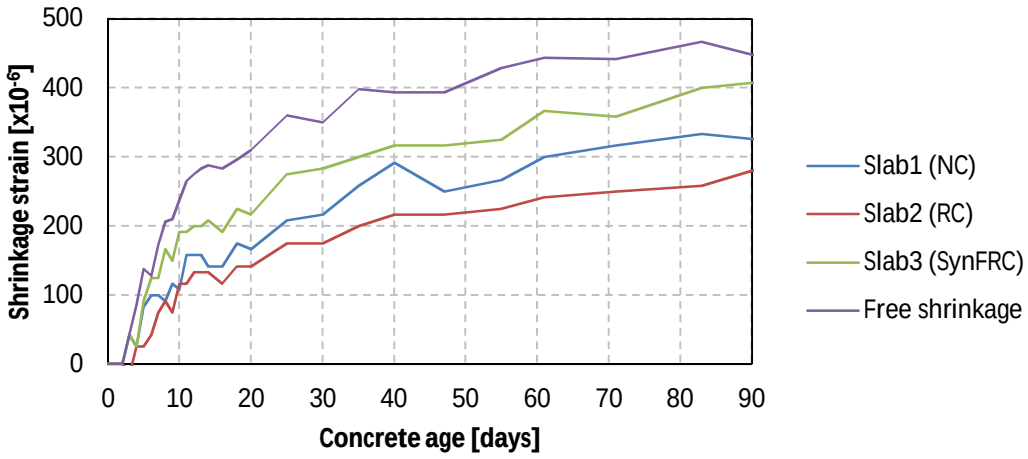

Figure 7.13 Shrinkage strains at the centre of the slabs

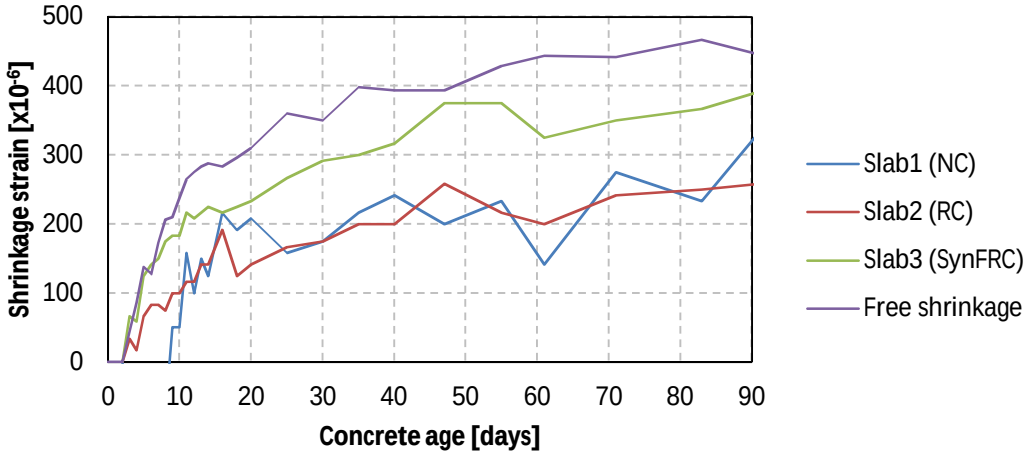

Figure 7.14 Shrinkage strains at the second end of the slabs

The free shrinkage within the beam specimens was more than the shrinkage measured within the slabs. This indicates that there was some friction restraint present, as can be expected. The shrinkage strains of the reinforced concrete were the least in all the results, which indicates steel reinforcement induces an internal restraint.

7.3 FEM of Full Scale Tests

The unexpected behaviour that was observed from the testing of the full scale slabs-on-grade, was analysed to show why the slabs did not show any significant cracking. This was the first part of the analyses performed for the slab tests. Another analysis was performed to estimate the crack widths and cracking behaviour of the NC and SynFRC slabs, if all the boundary conditions were provided to the test specimens. These analyses and the results are provided and discussed in this section.

7.3.1 Analysis Objectives

These FEAs were performed to achieve the following two objectives:

Objective 1

Determine why the slabs tested did not crack.

Objective 2

Determine the cracking behaviour and crack widths that would have been obtained if the boundary conditions were satisfied.

7.3.2 Analysis Procedure

The analysis procedure used to satisfy Objective 1 is discussed in this section. The analysis procedure used to satisfy Objective 2 is the same procedure used for the analyses discussed in Chapter 6.

Components, Assembly, Mesh and Boundary Conditions

The analysis consists of three components; the concrete slab, the wooden base and the laboratory floor. The assembly of these components and the boundary conditions are shown in Figure 7.15. The concrete slab is a rectangular part of 4500x100mm in size (symmetry was used, hence the 4500mm slab length). The wooden base and laboratory floor also has a length of 4500mm with a thickness of only 20mm. The thickness of the laboratory floor was assumed not to be a contributing factor, since it only applies to friction between the wooden base and itself.

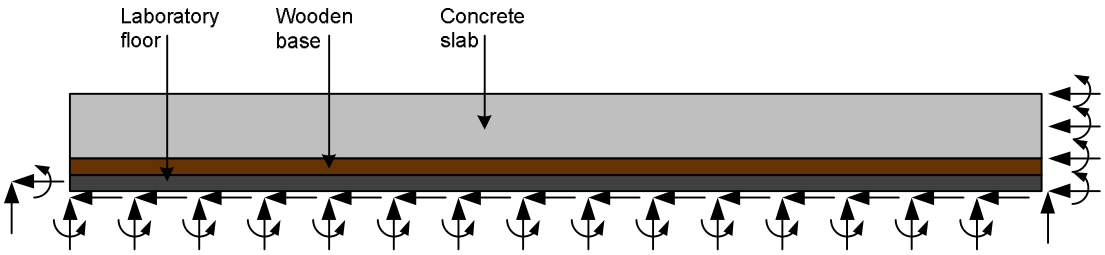

Figure 7.15 The assembly and boundary conditions of the analysis to determine why no cracks formed in the experimental slab specimens

The slab, wooden base and laboratory floor were subjected to symmetry at the centre, hence the horizontal and rotational boundary conditions on the right hand side. The laboratory floor is fixed on the bottom and at the left hand side, hence the boundary conditions in both directions and in rotation. The mesh used for the analysis consists of 10x10mm coupled thermal displacement elements in all three parts. The element size was doubled to decrease the analyses time.

Material Properties

The material properties for the different components of the analysis are shown in Table 7.2. The concrete lab properties are from the compression tests discussed in Chapter 5. The wooden base properties are from the manufacturer and an assumption was made regarding the properties of the laboratory floor.

Table 7.2 Material properties used for analysis to determine why experimental slabs did not crack

Part	Material Property	Value	Unit
Concrete slab	Density	2377	kg/m^3
	Young's Modulus	32	GPa
Wooden base	Density	600	kg/m^3
	Young's Modulus	6	GPa
Laboratory floor	Density	0	kg/m^3
	Young's Modulus	32	GPa

The concrete slab was subjected to a temperature change which was used to apply a shrinkage strain to the slab by changing the expansion coefficient to apply a certain strain (Section 6.2.1). The friction properties used for the different friction interactions are summarised in Table 7.3.

Table 7.3 The friction properties used to analyse why the slab specimens did not crack

Friction Between	Coefficient of Friction	Elastic Slip [mm]
Concrete Slab and Wooden Base	93.5	5
Wooden Base and Laboratory Floor	0.1	2

The analysis model does not take into account the effects of creep relaxation which occurs due to the concrete in tension. This is discussed in more detail in the results section.

7.3.3 Results

The shrinkage strain applied in the analysis was obtained from the shrinkage tests performed on the beam specimens discussed in Chapter 5. A shrinkage strain of 475μm/m was applied to the concrete slab analysis resulting in a stress distribution as shown in Figure 7.16.

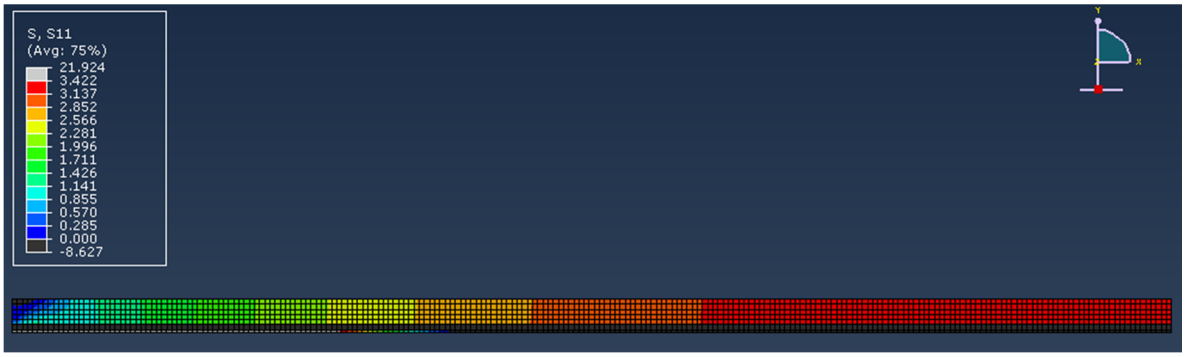

Figure 7.16 Results from analysis where only shrinkage strain was applied

The 475μm/m shrinkage strain resulted in a maximum tensile stress of 3.422MPa within the concrete slab. This resulted in cracks, which were not the case in the actual slabs. Therefore a tensile capacity of 2.7MPa for this specific concrete is obtained from the BS EN 1992-1-1:2004 from Table 3.1. This tensile capacity is smaller than the maximum tensile stress obtained from the analysis. This is because the analysis does not include the effects of creep, but only the effects of shrinkage.

Another analysis was conducted, but with a lower strain, due to the creep strain subtracted from the shrinkage strain. The creep strain is calculated with the prediction method from the SABS 0100-1:2000 by using a creep factor of 4.5. The values used for the input factors to obtain the creep factor are shown in Table 7.4.

Table 7.4 Input factors used to determine the 30 year creep factor

Input Factor	Value	Unit
Relative Humidity	60	%
Age of loading	1	day
Effective section thickness	100	mm

The 30 year creep strain is determined to be 380μm/m and in accordance with the SABS 0100-1:2000 the 3 month creep strain (90 days) is about 50% of the 30 year creep strain. Therefore the 3 month strain within the concrete is:

$$\varepsilon = \varepsilon_{sh} - \varepsilon_{cr} = 475 - 380 \text{ x } 0.5 = 285\mu m/m$$

This strain was then applied to the analysis model, and the results are shown in Figure 7.17.

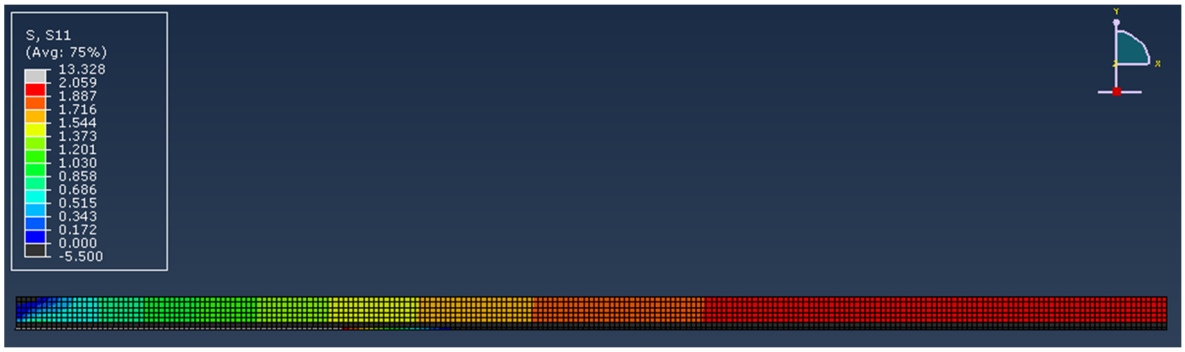

Figure 7.17 Results from analysis where shrinkage strain and creep relaxation are applied

The 285µm/m strain resulted in a maximum tensile stress of 2.059MPa which is smaller than the 2.7MPa obtained from the BS EN 1992-1-1:2004. This means the concrete slab would not crack. This is on account of the effect of creep combined with the effect of the slab, moving away from the connections at the end, and the wooden base not supplying sufficient friction between the slab and the laboratory floor.

The results for the second objective are shown in Figures 7.18 and 7.19.

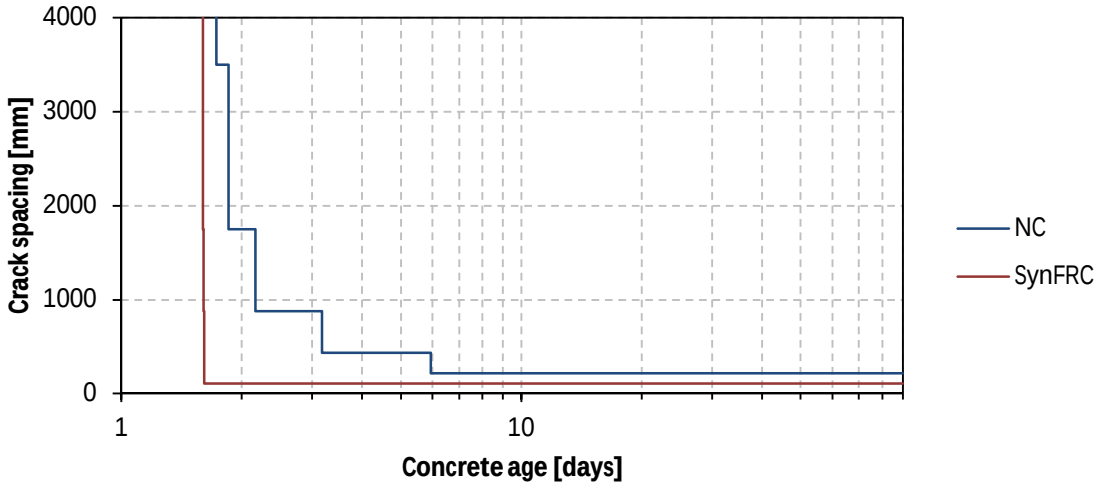

Figure 7.18 Development of crack spacing for the Geotex SynFRC slabs-on-grade if boundary conditions were satisfied in test setup

From Figure 7.18 it is clear that the SynFRC, reaches a crack spacing of 109.4mm earlier than the NC with a spacing of 218.8mm. The SynFRC forms multiple cracks between the end connections at almost exactly the same time while the NC forms cracks gradually as the concrete ages. All the cracking occurred within the first 6 days, after that crack growth took place.

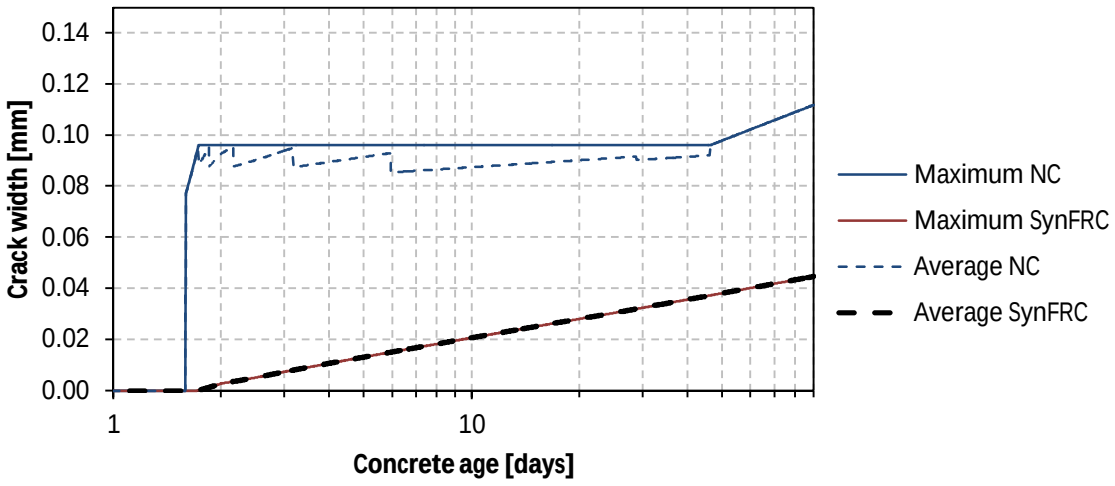

Figure 7.19 Development of the maximum and average crack width within the slabs-on-grade of NC and the Geotex SynFRC if boundary conditions were satisfied in test setup

From Figure 7.19 it is noted that the maximum and average crack width of the NC is much larger than the crack widths of the SynFRC. The multiple cracking that occurs in the SynFRC slab is the reason for the maximum and average crack widths to be equal. The normal concrete reached a maximum crack width of about 0.095mm within the first 2 days and only after 44 days, did the maximum crack width start increasing to 0.11mm which it reached by 90 days. The SynFRC maximum crack width gradually increased after the concrete had cracked and reached a crack width of about 0.043mm at 90 days. The average crack width difference between the NC and the SynFRC is about 0.075mm, between first cracking and 90 days. This is an improvement of about 70% being obtained with the addition of 0.266% fibres by volume of the concrete. This shows a significant improvement of crack widths for the first 90 days of the slab age.

7.4 Concluding Summary

The experimental framework of the full scale tests performed on concrete slabs to simulate the effects of drying shrinkage on slabs-on-grade was discussed. The test objectives, programme, setup and procedure were discussed. The material properties and the mix design, used for the tests were provided. The results from the experimental tests were provided and discussed.

The full scale slabs did not crack, due to boundary conditions not performing as intended. FEAs were also performed on concrete slab models to determine the behaviour and crack widths of the DSC that occur within the concrete slabs, if boundary conditions are satisfied. The prediction of the crack widths showed, within 3 months, an improvement of about 70% with the addition of the synthetic fibres.

Chapter 8 Conclusions and Recommendations

8.1 Conclusions

The objective of this study was to investigate whether it is possible to control drying shrinkage cracking (DSC) within slabs-on-grade by using synthetic fibre reinforced concrete (SynFRC). The conventional method of reinforcement used for this application is a steel mesh. The possibility of using SynFRC instead of steel reinforcement was investigated.

The material parameters were first obtained to determine whether the SynFRC can control DSC. These parameters consist of the compressive strength as well as the flexural- , frictional- and shrinkage behaviour of the SynFRC. The tensile behaviour was obtained by using an inverse analysis. These parameters were then used in the finite element analyses (FEAs). This was carried out in order to determine the difference in cracking behaviour and crack widths of a slab-on-grade between normal concrete (NC) and SynFRC.

Analyses were performed for various sizes of slabs, fibre types and volumes, friction types and ambient relative humidities. The addition of fibres gave the concrete a ductility that allowed the concrete to crack more than NC, but this did not allow the cracks to propagate. Consequently the SynFRC was able to control DSC within slabs-on-grade.

This was noted at a low fibre content of 0.3% and a slab thickness of 200mm. The SynFRC slab had a maximum crack width of 0.03mm at a concrete age of 6 months, which is an 80.9% improvement on the maximum crack width within the NC slab of the same thickness and age. At a concrete age of 30 years an improvement of 74.3% for the SynFRC slab was noted, with a maximum crack width of 0.045mm. Tests were only conducted on SynFRC specimens with fibre content up to 0.4% by concrete volume. The higher fibre content was observed to be insufficient to control the DSC in most scenarios.

The DSC was also controlled in the slab consisting of SynFRC that has $R_{e,3}$ values of 0.51 and higher. This controlled the DSC within a slab with a thickness of 100mm, where the SynFRC slab had a maximum crack width of 0.037mm at the concrete age of 6 months, which is an 85.0% improvement in the maximum crack width within the NC slab of the same thickness and age. At the concrete age of 30 years there was still a crack width improvement of 81.0% for the SynFRC slab, with a maximum crack width of 0.047mm.

There were also improvements in maximum crack widths observed when adding fibres if the friction is sticky, i.e. the maximum friction between the slab and the subgrade were reached with a very small

amount of movement. However, with a higher friction smaller crack widths occur within both the NC and the SynFRC.

8.2 Recommendations

SynFRC can possibly save time and money in the construction of slabs-on-grade. Therefore more research is required investigating the effects of fibres on DSC. A better test setup should also be designed to test DSC within concrete slabs-on-grade.

The following recommendations are made with regards to fibre content:

- Fibre content between 0.5% and 1.5% by concrete volume should be tested to determine at which fibre content the SynFRC starts showing a reduction in crack widths.
- These fibre contents should also be tested for various slab thicknesses and conditions for the slab-on-grade.

The following recommendations are made with regards to testing DSC within slabs-on-grade:

- Ensure a fixed end connection to prevent slabs from moving.
- Use natural subgrades and sub bases to tests realistic friction reactions beneath slabs.
- Use longer slabs and tests for a period of more than six months in the conditions that enhance the drying effects.
- Perform tests on various slab thicknesses.

The following recommendations are made with possible tests that could be conducted on SynFRC for the use in slabs-on-grade:

- Small scale tests can be conducted on notched beams to determine crack growth within the SynFRC. Multiple notches should be used to determine whether multiple cracking occurs.
- Uniaxial tension tests should be conducted on SynFRC specimens to determine more accurate tension behaviours for analyses to model slabs-on-grade.

References

AASHTO, 2000. *AASHTO M145 Classification of Soil and Soil-Aggregate Mixtures for Highway Construction Purposes.* s.l.:AASHTO.

Almusallam, A., 2001. Effect of environmental conditions on the properties of fresh and hardened concrete. *Cement and Concrete Composites,* Volume 23, pp. 353-361.

Al-Nasra, M., 1997. Finite Element Analysis of floor slabs under warping effect. *Engineering Structures,* 19(7), pp. 533-539.

Al-Saleh, S. & Al-Zaid, R., 2006. Effects of drying conditions, admixtures and specimen size on shrinkage strains. *Cement and Concrete Research,* Volume 36, pp. 1985-1991.

ASTM International, 2000. *ASTM D2487 Standard Practice for Classification of Soils for Engineering Purposes (Unified Soil Classification System).* West Conshohocken: ASTM International.

ASTM, 1997. *ASTM C 1018: Standard test method for flexural tougness and first crack strength of fibre-reinforced concrete (using beam with third point loading).* Pennsylvania: ASTM.

Bagherzadeh, R., Sadeghi, A. & Latifi, M., 2001. Utilizing polypropylene fibre to improvephysical and mechanical properties of concrete. *Textile Research Journal,* pp. 1-9.

Banthia, N., Azzabi, M. & Pigeon, M., 1993. Restrainted shrinkage cracking in fibre-reinforced cementitious composites. *Materials and Structures,* Volume 26, pp. 405-413.

Banthia, N. & Gupta, R., 2006. Influence of polypropylene fiber geometry on plastic shrinkage cracking in concrete. *Cement and Concrete Research,* Volume 36, pp. 1263-1267.

Bazant, Z., 1972. Thermodynamics of hindered absorption and its implications for hardened cement paste and concrete. *Cement and Concrete Research,* 2(1), pp. 1-16.

Bazant, Z. & Baweja, S., 2000. *Creep and Shrinkage Prediction Model for Analysis and Design of Concrete Structures: Model B3,* Michigan: American Concrete Istitute.

Bellemare, S., Dao, M. & Suresh, S., 2008. Effects of mechanical properties and surface friction on elasto-plastic sliding contact. *Mechanics of Materials,* Volume 40, pp. 206-219.

Bernard, E., 2000. Behaviour of round steel fibre reinforced concrete panels underpoint loads. *Materials and Structures,* Volume 33, pp. 181-188.

Beushausen, H., 2011. [Art] (Univercity of Cape Town).

Bissonnette, B., Attiogbe, E., Miltenberger, M. & Fortin, C., 2007. Drying Shrinkage, Curling, and Joint Oppening of Slabs-on-Ground. *ACI Materials Journal*, 104(3), pp. 259-267.

Boshoff, W. & Combrinck, R., 2013. Modelling the severity of plastic shrinkage cracking in concrete. *Cement and Concrete Research*, Volume 48, pp. 34-39.

Brandt, A., 2008. Fibre reinforced cement-based (FRC) composites after over 40 years of development in building and civil engineering. *Composite Structures*, Volume 86, pp. 3-9.

British Standards Institution, 2006. *BS EN 14889: Fibres for concrete, Part 2: Polymer fibre-Definition, specification and conformity*. London: BSI.

Choi, S., Park, J. & Jung, W., 2011. *A stydy on the shrinkage Control of Fiber Rienforced Concrete Pavement*. South Korea, Elsevier Ltd. Selection.

Concrete Society Working Group, 2003. *TR 34 Concrete industrial ground floors - A guide to design and construction*, Berkshire: The Concrete Society.

Concrete Society Working Group, 2007. *TR 65 Guidance on the use of Macro-synthetic-fibre-reinforced Concrete*, Camberley: The Concrete Society.

Eguchi, K. & Teranishi, K., 2005. Prediction equation of drying shrinkage of concrete based on composite model. *Cement and Concrete Research*, Volume 35, pp. 483-493.

Esler, M., Tschegg, E. & Stanzl-Tschegg, S., 1996. Fracture behaviour of Polypropylene-Fibre-Reinforced Concrete under Biaxial Loading: An Experimental Investigation. *Composites Sience and Technology*, Volume 56, pp. 933-945.

European Commitee for Standardization, 2004. *BS EN 1992-1-1:2004 Design of Concrete Structures - Part 1-1: General rules and rules for buildings*. Brussels: European Commitee for Standardization.

Feldman, R. & Sereda, P., 1970. A new model for hydrated Portland cement and its practical implications. *Engineering Journal*, 53(9).

FIB Special Activity Group 5, 2010. *FIB Model Code 2010*, s.l.: CEB-FIP.

Gaedicke, C., Roesler, J. & Evangelista Jr., F., 2012. Three-dimensional cohesive crack model prediction of the flexural capacity of concrete slabs on soil. *Engineering Fracture Mechanics*, Volume 94, pp. 1-12.

Gaylard, P., Ballim, Y. & Fatti, L., 2013. A model for the drying shrinkage of South African concretes. *Journal of the South African Institution of Civil Engineering,* 55(1), pp. 45-59.

Gu, X. et al., 2011. Cracking behaviour of cast in situ reinforced concrete slabs with control joints. *Construction and Building Materials,* Volume 25, pp. 1398-1406.

Hannant, D., 1978. *Fibre Cements and Fibre Concretes.* 1st ed. Chichester: John Wiley & Sons.

Hannant, D., 2003. Fibre-reinforced concrete. *Advanced Concrete Technology,* pp. 6/1-6/17.

Heere, R. & Morgan, D., 2003. Specification of shotcrete toughness. *Shotcrete,* 5(4).

Hughes, T., Ashgari, A., Abbas, N. & Barr, B., 1990. Fracture behaviour of concrete and FRC in tension. *Engineering Fracture Mechanics,* 35(1/2/3), pp. 181-185.

Igarashi, S., Bentur, A. & Kovler, K., 2000. Autogenous shrinkage and induced restraining stresses in high-strength concretes. *Cement and Concrete Research,* Volume 30, pp. 1701-1707.

Illston, J. & Domone, P., 2001. *Construction materials: their nature and behaviour.* 3rd ed. New York: Spon Press.

Ishai, O., 1965. *The time-dependent deformational behaviour of cement paste, mortar and concrete.* London, Cement and Concrete Association.

Jerga, J., 2004. Physico-mechanical properties of carbonated concrete. *Construction and Building Materials,* Volume 18, pp. 645-652.

Johnston, C., 2001. *Fibre-Reinforced Cement and Concretes.* New York: Taylor & Francis.

Labib, W. & Eden, N., 2004. An Investigation into the use of Fibres in Concrete Industrial Ground-Floor Slabs.

Lee, S., 2001. Behavior of Concrete Slab under Frictional Drag. *KSCE Journal of Civil Engineering,* 5(2), pp. 141-145.

Maitra, S., Reddy, K. & Ramachandra, L., 2009. Experimental Evaluation of Interface Friction and Study of Its Influence on Concrete Pavement Response. *JOURNAL OF TRANSPORTATION ENGINEERING © ASCE,* 135(8), pp. 563-571.

Manolis, G., Gareis, P., Tsonos, A. & Neal, J., 1997. Dynamic Properties of Polypropylene Fiber-Reinforced Concrete Slabs. *Cement and Concrete Composites,* Volume 19, pp. 341-349.

Marais, L. & Perrie, B., 1993. *Concrete industrial floors on the ground.* Midrand: Portland Cement Istitute.

Maritz, J., 2012. *An Investigation into the Use of Low Volume - Fibre Reinforced Concrete for Controlling Plastic Shrinkage Cracking,* Stellenbosch: University of Stellenbosch.

Oh, B. H., Park, D. G., Kim, J. C. & Choi, Y. C., 2004. Experimental and theoretical investigation on the postcracking inelastic behavior of synthetic fiber reinforced concrete beams. *Cement and Concrete Research,* Volume 35, pp. 384-392.

Oslejs, J., 2008. New Frontiers for Steel Fiber-Reinforced Concrete. *Concrete International,* pp. 45-50.

Owens, G., 2009. *Fulton's concrete technology.* 9th ed. Midrand: Intrepid Printers.

Ozcan, D. et al., 2009. Experimental and finite element analysis on the steel fiber-reinforced concrete (SFRC) beams ultimate behavior. *Construction and Building Materials,* Volume 23, pp. 1064-1077.

Pan, Z., Li, B. & Lu, Z., 2013. Re-evaluation of CEB-FIP 90 prediction models for creep and shrinkage with experimental database. *Construction and Building Materials,* Volume 38, pp. 1022-1030.

Pelisser, F., Santos Neto, A. d. S., La Rovere, H. & de Andrade Pinto, R., 2010. Effect of the addition of synthetic fibers to concrete thin slabs on plastic shrinkage cracking. *Construction and Building Materials,* Volume 24, pp. 2171-2176.

Pickett, G., 1956. Effect of aggregate on shrinkage of concrete and hypothesis concerning shrinkage. *Journal of American Concrete Institute.*

Powers, T., 1965. *Mechanisms of shrinkage and reversible creep of hardened cement paste.* London, Cement and Concrete Association.

Raoufi, K., Pour-Ghaz, M., Poursaee, A. & Weiss, J., 2011. Restrained Shrinkage Cracking in Concrete Elements: Role of Substrate Bond on Crack Development. *JOURNAL OF MATERIALS IN CIVIL ENGINEERING © ASCE,* pp. 895-902.

Ratcliffe, R., 2006. Fibre reinforcement - steel versus macro (structural) synthetic. *Concrete in Australia,* pp. 42-46.

Richardson, A., 2005. *Bond characteristics of structural fibres in concrete with regard to post-crack strength and durable design,* Newcastle: Univercity of Newcastle.

RILEM, 2001. RILEM TC 162-TDF: Test and design methods for steel fibre reinforced concrete - Uni-axial test for steel fibre reinforced concrete. *Materials and Structures,* 34(235), pp. 3-6.

RILEM, 2002. RILEM TC 162-TDF: Test and design methods for steel fibre reinforced concrete - Design of reinforced concrete using the sigma-epsilon method: principles and applications. *Materials and Structures,* 35(249), pp. 262-278.

Roesler, J. et al., 2006. Effect of Synthetic Fibers on Structural Behavior of Concrete Slabs-on-Ground. *ACI Materials Journal,* pp. 3-10.

Saetta, A., Schrefler, B. & Vitaliani, R., 1993. The carbonation of concreteand the mechanism of moisture, heat and carbon dioxide flow through porous materials. *Cement and Concrete Research,* Volume 23, pp. 761-772.

Shoya, M., 1979. Drying shrinkage and moisture loss of superplasticiser admixed concrete of low water/cement ratio. *Transactions of the Japan Concrete Institute,* 2(5).

Sorelli, L., Meda, A. & Plizzari, G., 2006. Steel Fiber Concrete Slabs on Ground: A Structural Matter. *ACI Structural Journal,* pp. 551-558.

Soroka, I., 1979. *Portland Cement Paste and Concrete.* London: Macmillan.

Soroushian, P., Elyamany, H., Tlili, A. & Ostowari, K., 1998. Mixed-mode Fracture Properties of Concrete Reinforced with Low Volume Fractions of Steel and Polypropylene Fibers. *Cement and Concrete Composites,* Volume 20, pp. 67-78.

South African Bureau of Standards, 2000. *SANS 10100-1:2000 The structural use of concrete Part 1: Design.* Pretoria: South African Bureau of Standards.

South African National Standards, 2006. *SANS 1024:2006 Welded steel fabric for reinforcement of concrete.* Pretoria: Standards South Africa.

Tazawa, E., Miyazawa, S. & Kasai, T., 1995. Chemical Shrinkage and Autogenous Shrinkage of Hydrating Cement Paste. *Cement and Concrete Research,* 25(2), pp. 288-292.

Troxell, G., Rapheal, J. & Davis, R., 1958. Long-time creep and shrinkage tests of plain and reinforced concrete. *Proceedings of the American Society's Testing of Materials.*

Wang, Y., Li, V. & Backer, S., 1988. Modelling of fibre pull-out from a cement matrix. *The International Journal of CementCompisites and Lightweight Concrete,* 10(3), pp. 143-149.

Wire Reinforcement Institute, 2003. *Formulas for Success: Innovative Ways to Reinforce Slabs-On-Grade.* [Online]
Available at: www.wirereinforcementinstitute.org

Wittman, F., 1968. Surface tension, shrinkage and strength of hardened cement paste. *Material Structures,* 1(6).

Wongtanakitcharoen, T., 2005. *Effects of randomly distributed fibres on plastic shrinkage cracking of cement composites,* Michigan: The Univercity of Michigan.

Younsi, A., Turcry, P., Ait-Mokhtar, A. & Staquet, S., 2013. Accelerated carbonation of concrete with high content of mineral additions: Effect of interactions between hydration and drying. *Cement and Concrete Research,* Volume 43, pp. 25-33.

Ytterberg, R., 1993. *Control of shrinkage and curling in slabs on grade,* s.l.: The Aberdeen Group.

Zhang, J., Gong, C., Guo, Z. & Zhang, M., 2009. Engineered cementitious composite with characteristic of low drying shrinkage. *Cement and Concrete Research,* Volume 39, pp. 303-312.

Zhang, J. & Stang, H., 1998. Applications of Stress Crack Width Relationship in Predicting the Flexural Behaviour of Fibre-Reinforced Concrete. *Cement and Concrete Research,* 28(3), pp. 439-452.

Zheng, Z. & Feldman, D., 1995. Synthetic Fibre-Reinforced Concrete. *Prog. Polym. Sci.,* Volume 20, pp. 185-210.

Zollo, R., 1996. Fiber-reinforced Concrete: an Overview after 30 Years of Development. *Cement and Concrete Compisites,* Volume 19, pp. 107-122.

Appendix A: Flexural Results

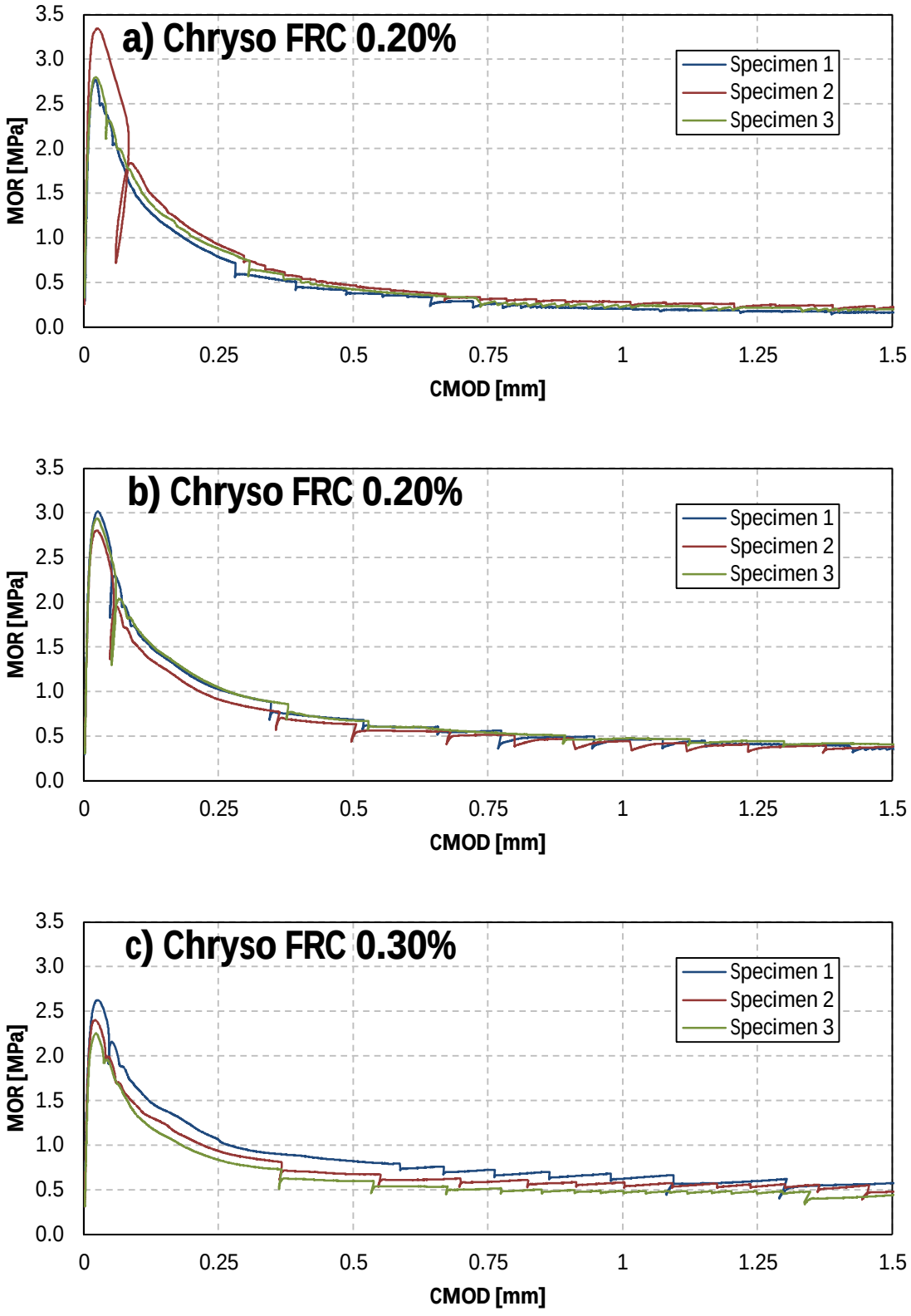

Figure A. 1 Flexural results of all specimens for micro polypropylene FRC using Chryso fibres

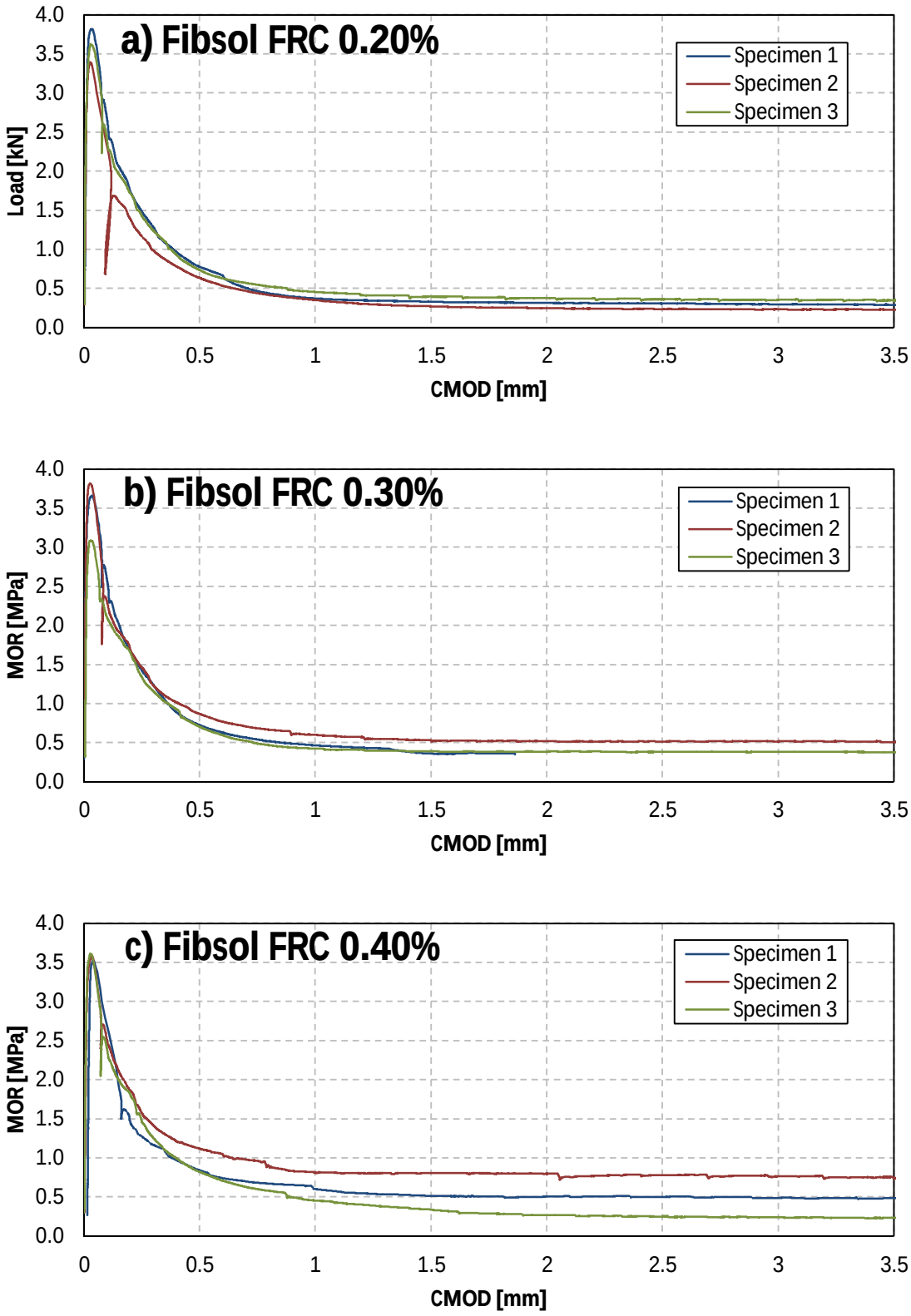

Figure A. 2 Flexural results of all specimens for macro polypropylene FRC using Fibsol fibres

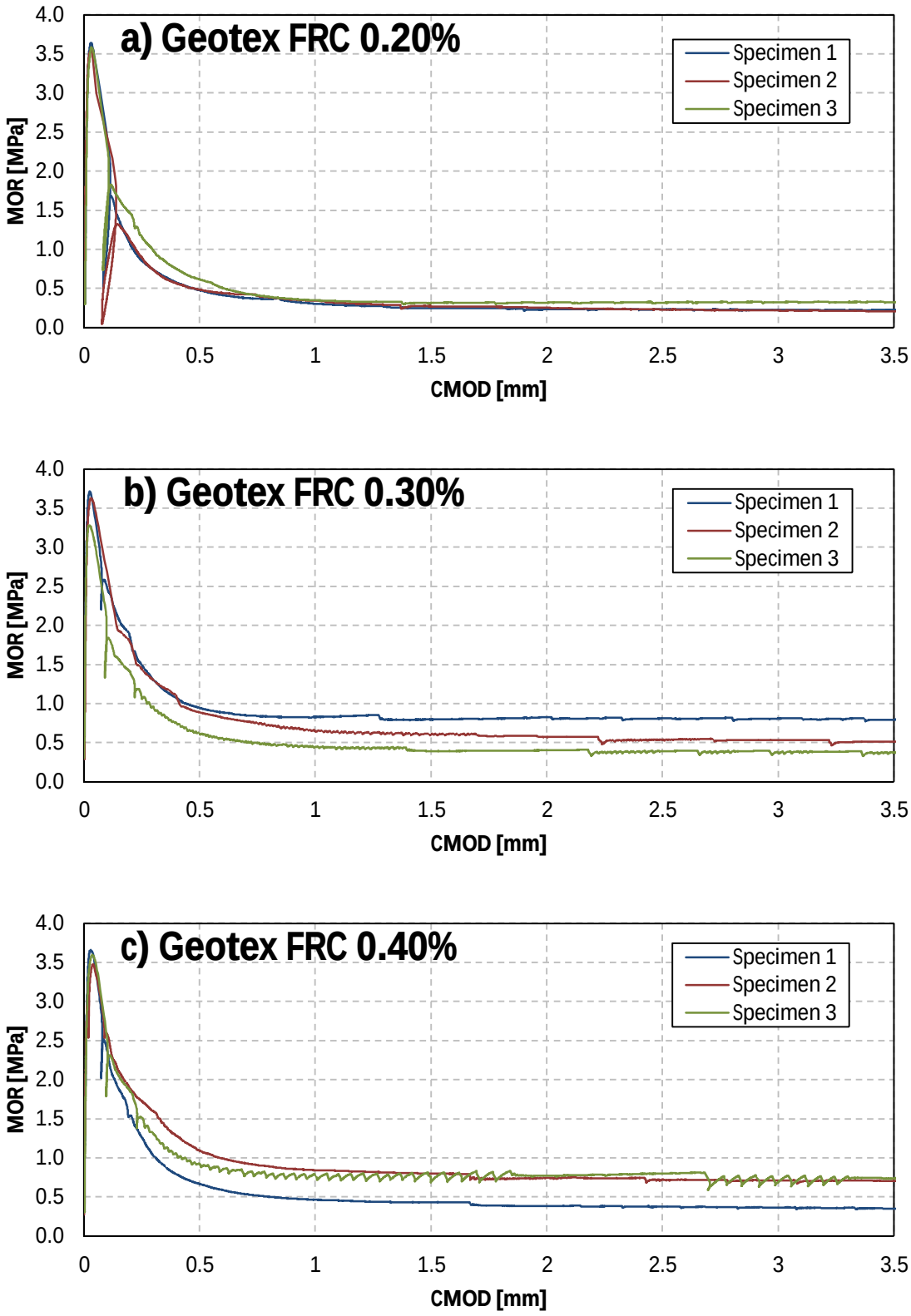

Figure A. 3 Flexural results of all specimens for macro polypropylene FRC using Geotex fibres

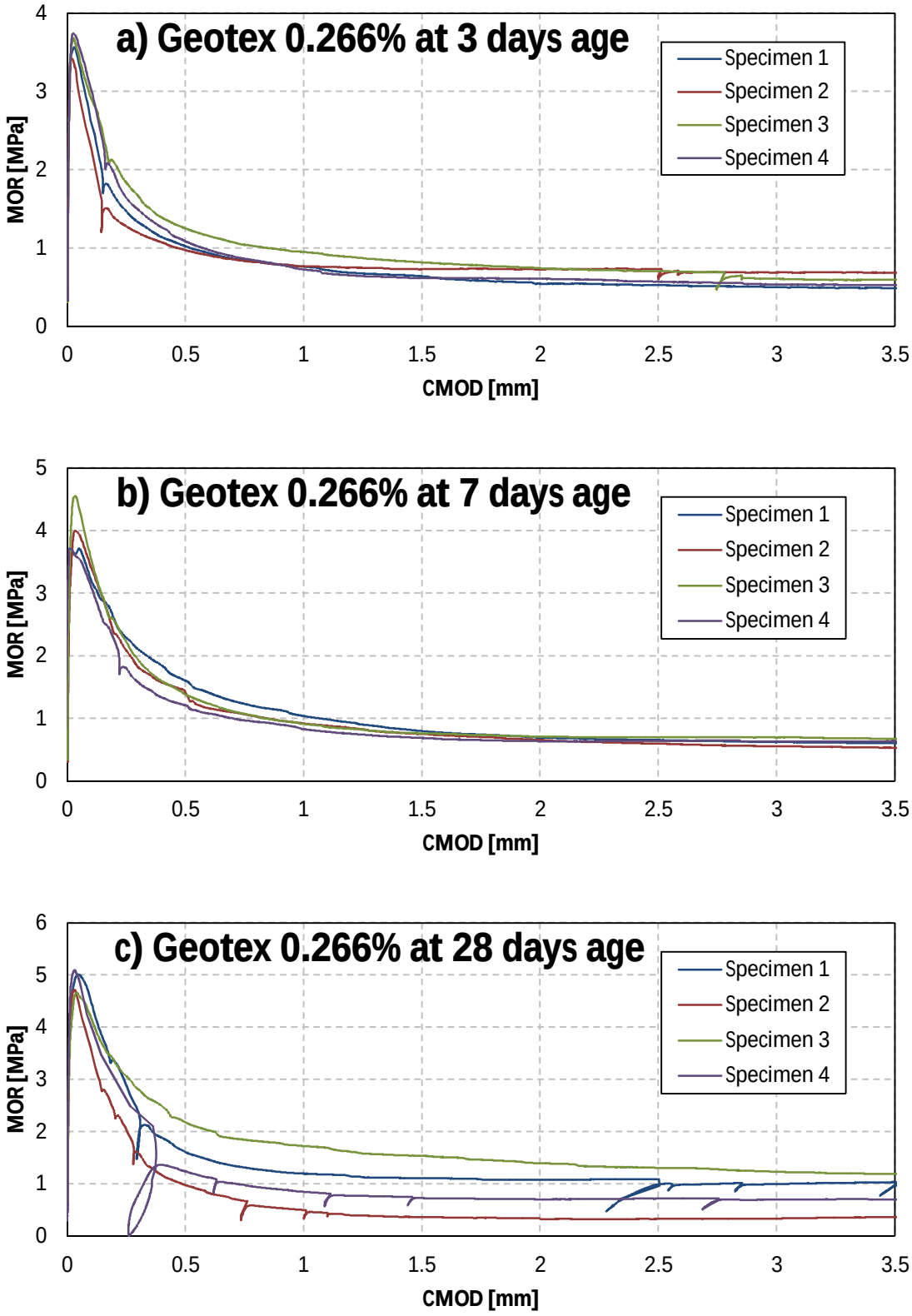

Figure A. 4 Flexural development results of all specimens tested with the Geotex macro polypropylene FRC

Appendix B: Friction Results

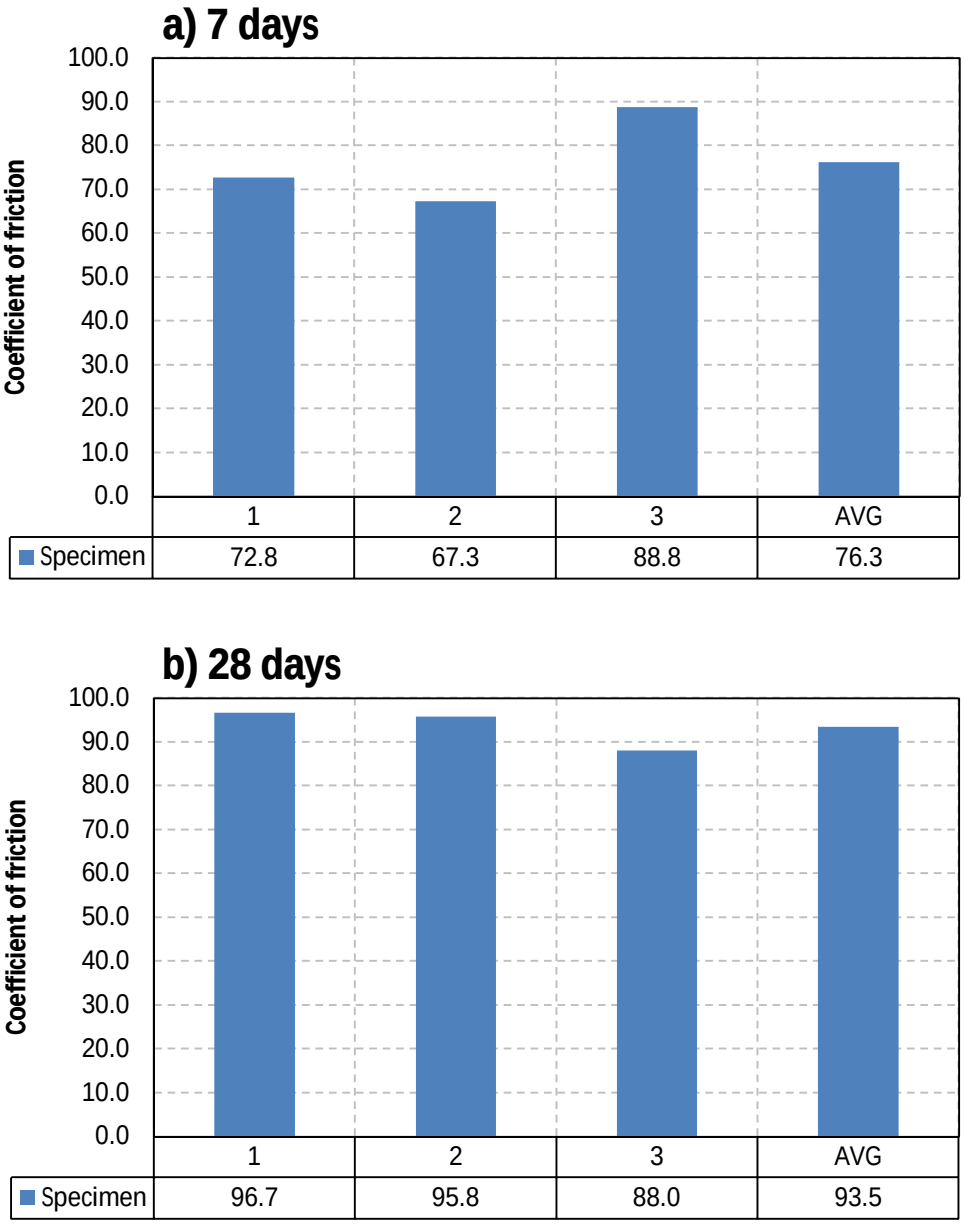

Figure B. 1 Coefficients of friction for cube specimens tested for friction development with age

Appendix C: Shrinkage Results

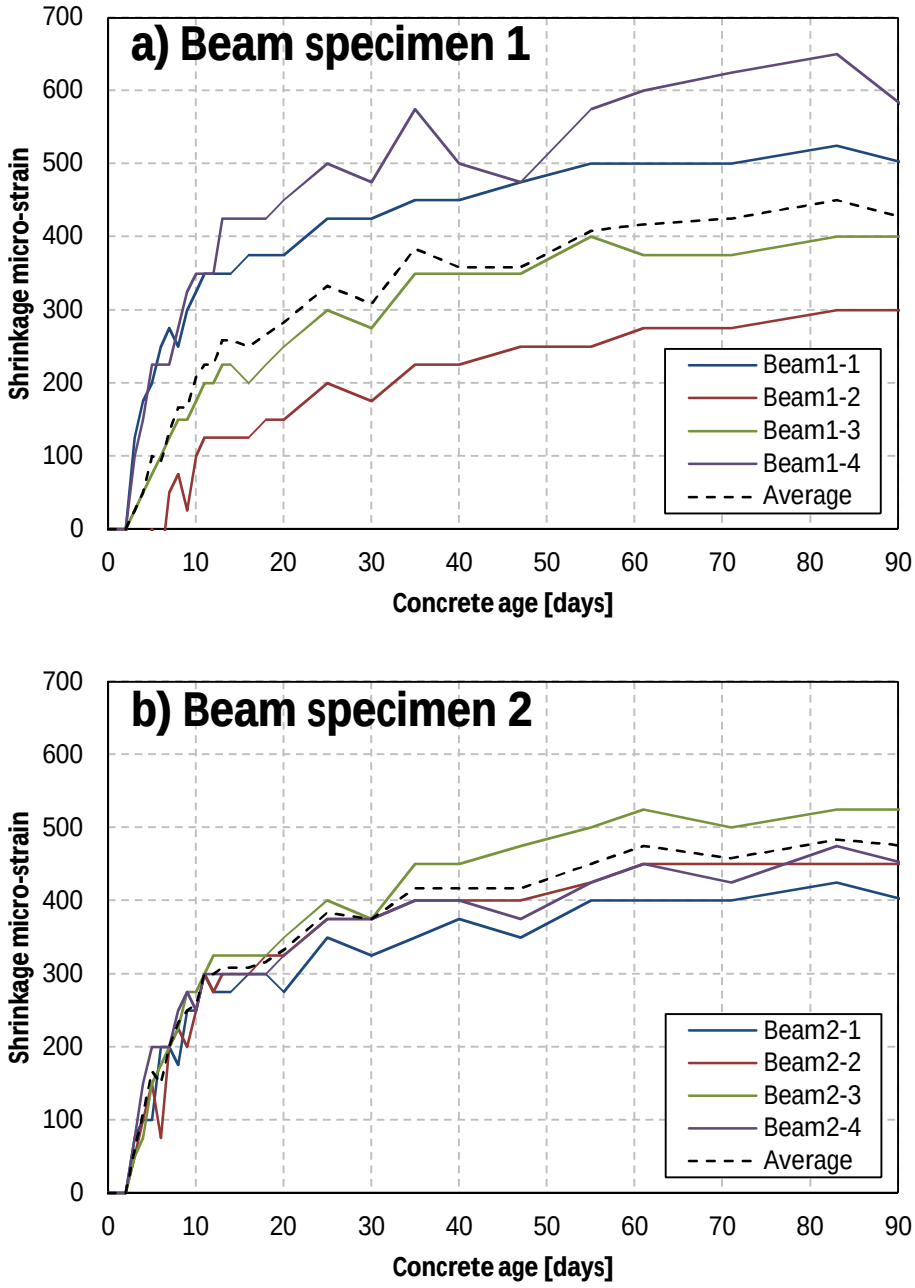

Figure C. 1 Free shrinkage results from beam specimens (1&2)

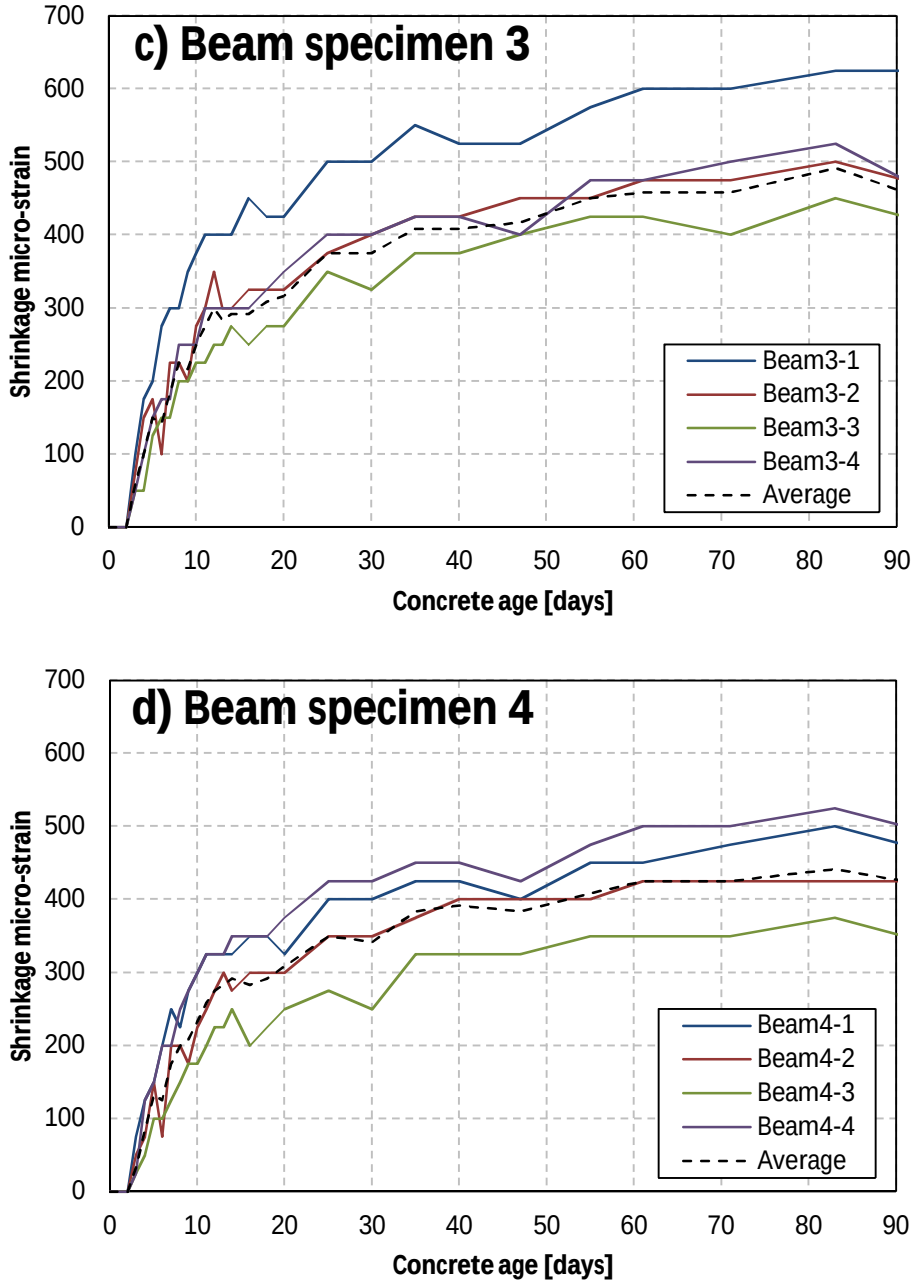

Figure C. 2 Free shrinkage results from beam specimens (3&4)

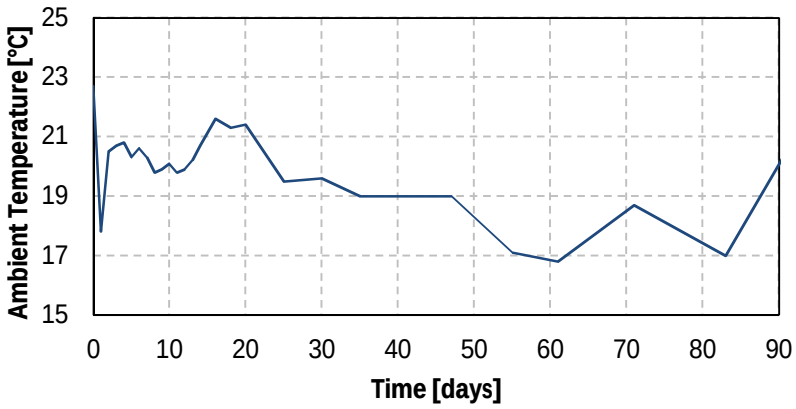

Figure C. 3 Ambient Temperature measured when strain measurements were recorded

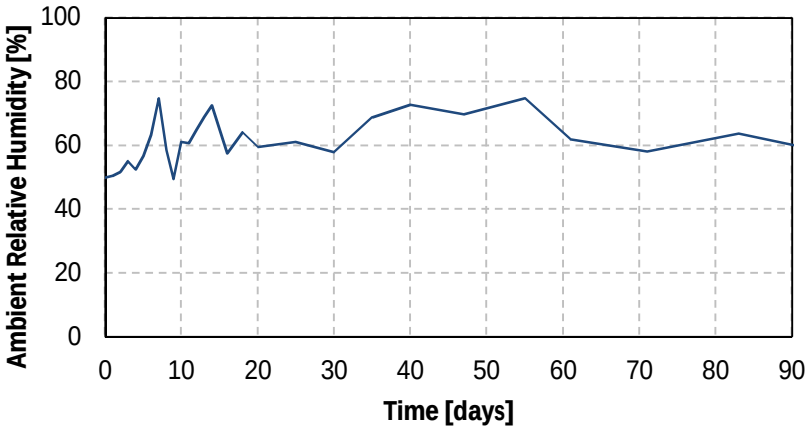

Figure C. 4 Ambient relative humidity measured when strain measurements were recorded

Appendix D: Inverse Analysis Results

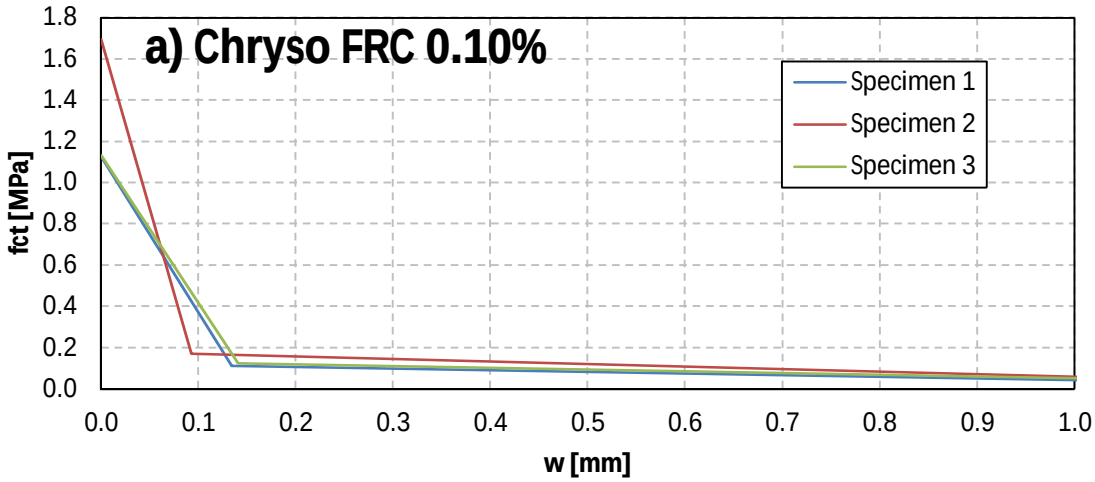

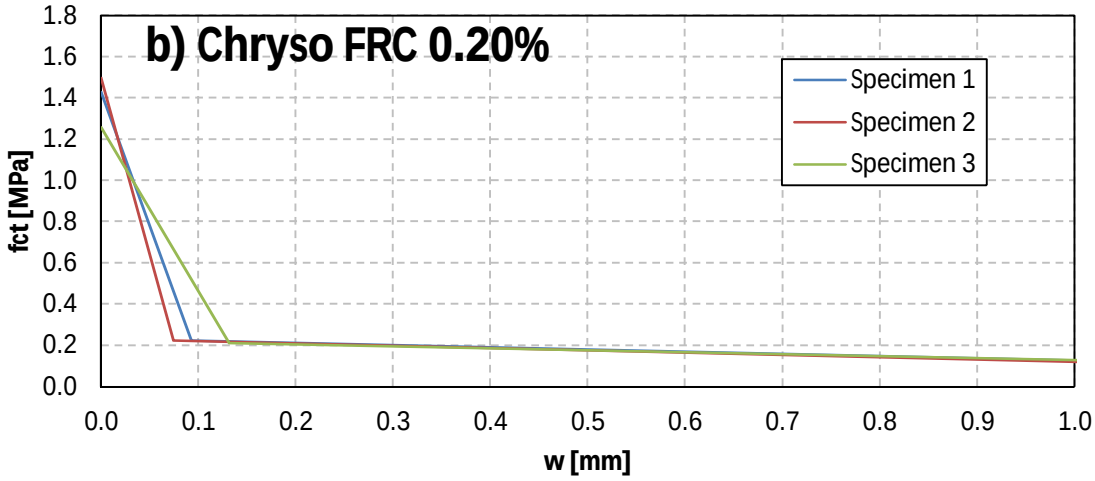

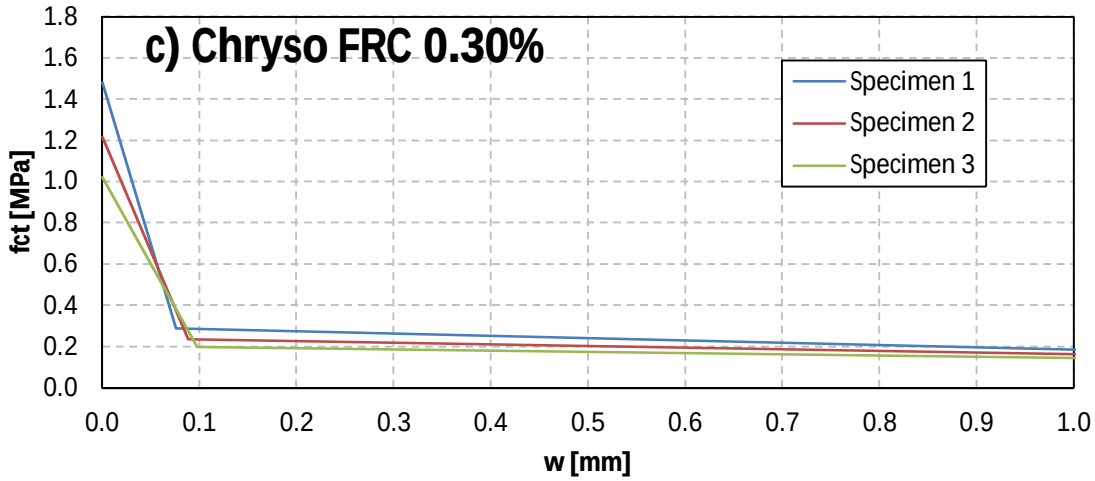

Figure D. 1 Indirect tensile results of all specimens for macro polypropylene FRC using Chryso fibres

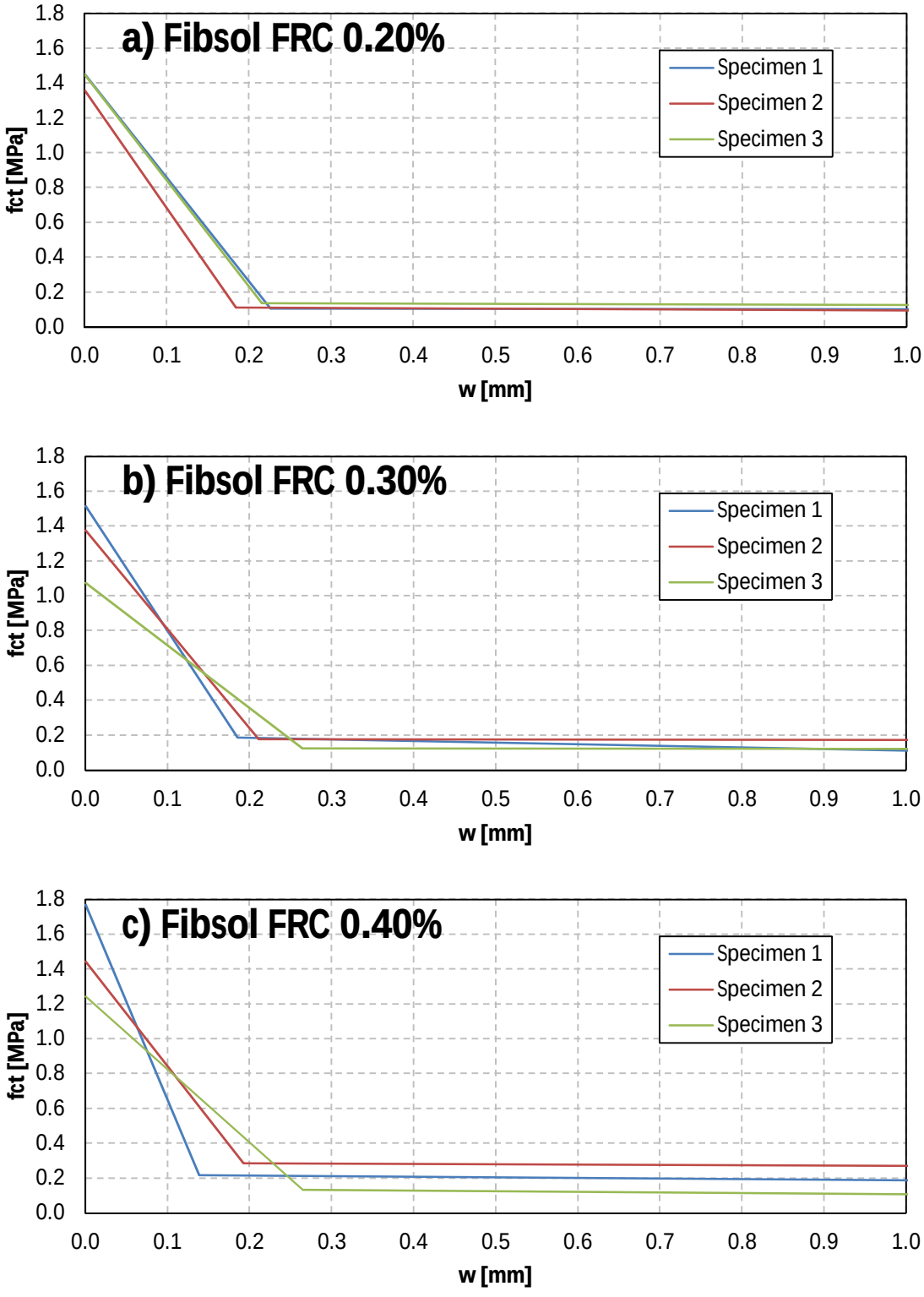

Figure D. 2 Indirect tensile results of all specimens for macro polypropylene FRC using Fibsol fibres

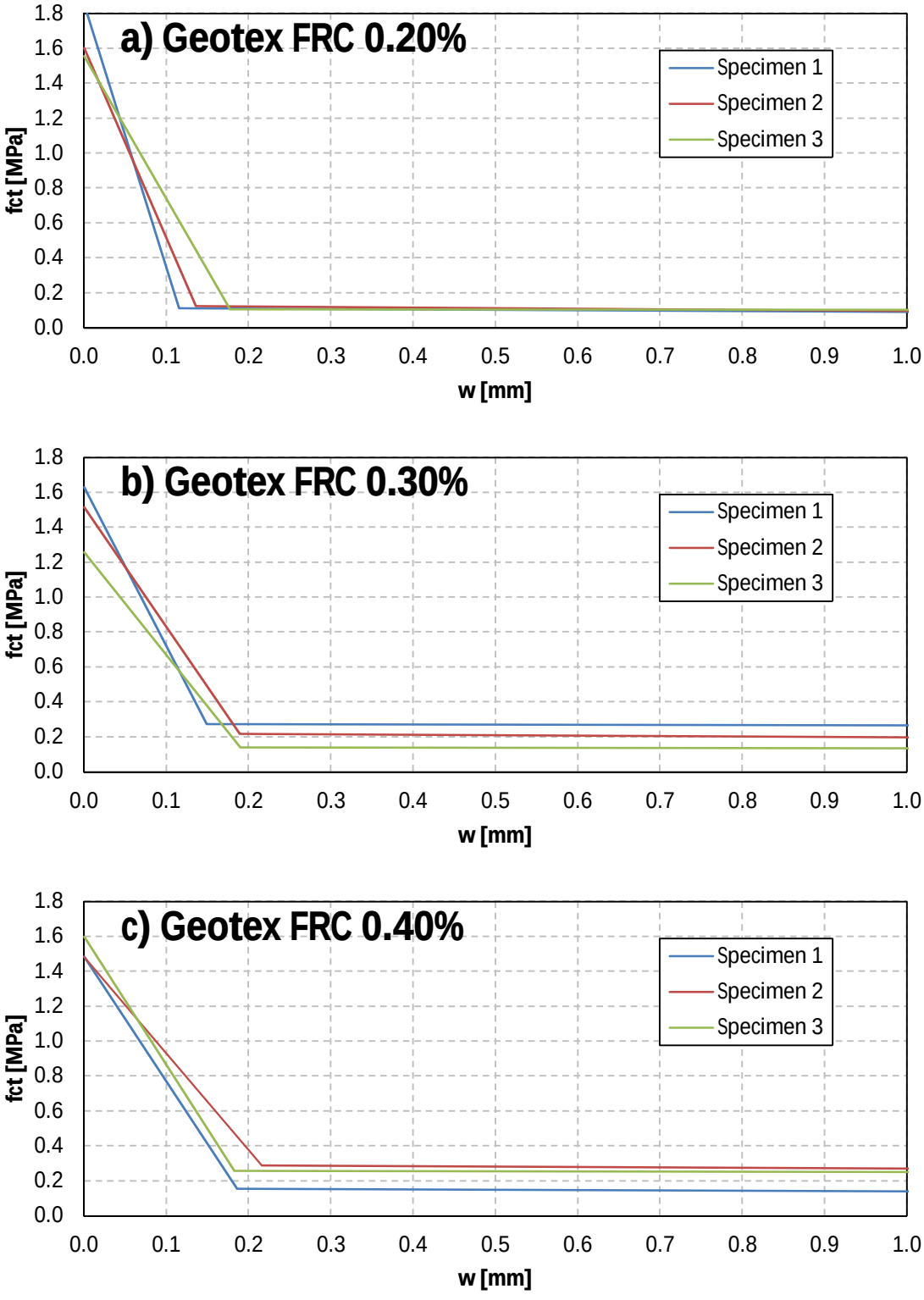

Figure D. 3 Indirect tensile results of all specimens for macro polypropylene FRC using Geotex fibres

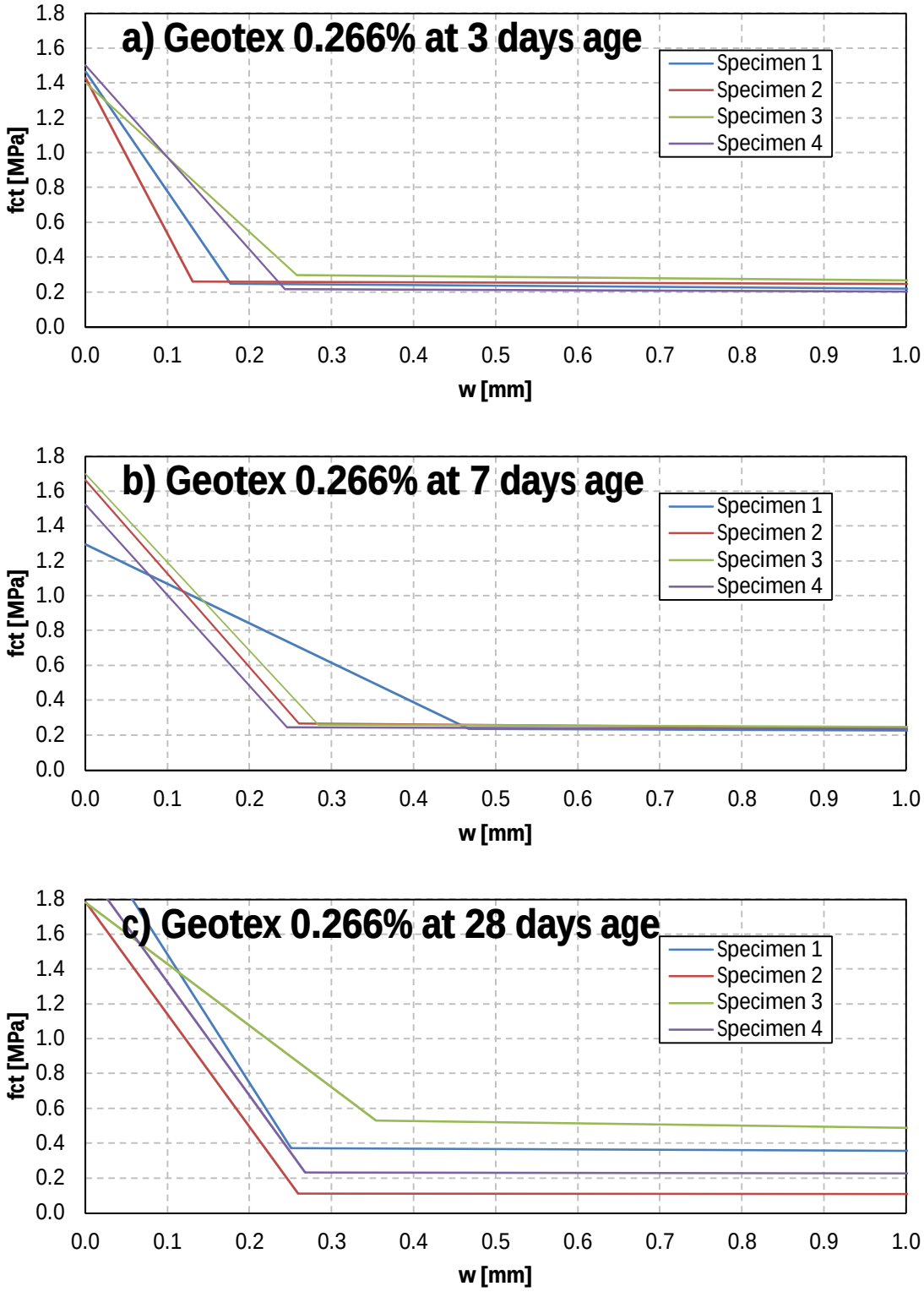

Figure D. 4 Indirect tension development results of all specimens tested with the Geotex macro polypropylene FRC

Appendix E: Analysis of Crack Width Results

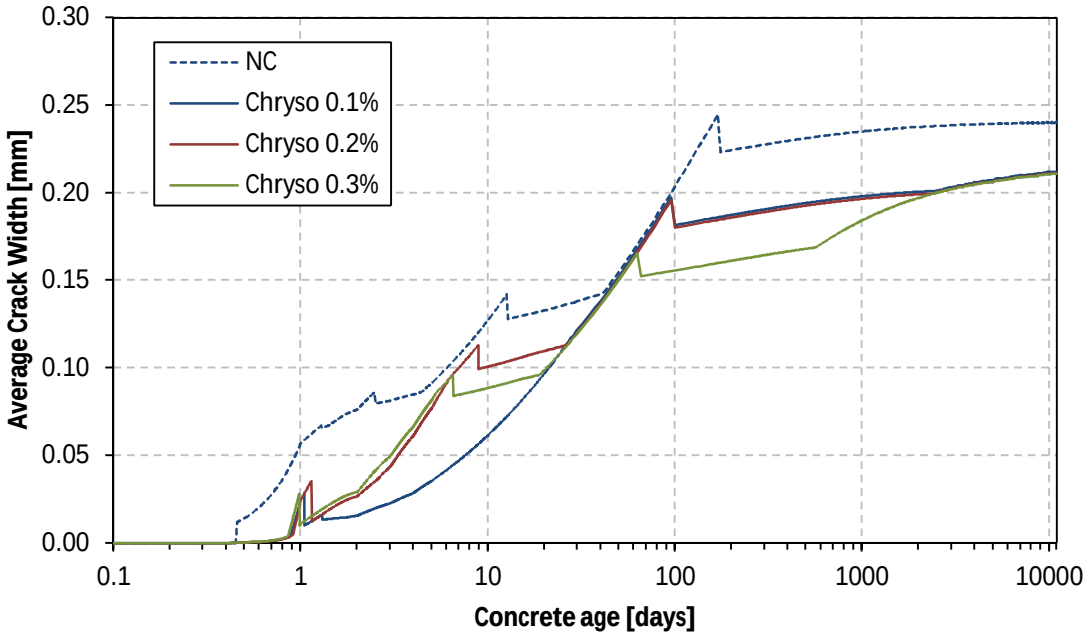

Figure E. 1 Development of the average crack width within the slab-on-grade of the Chryso SynFRC

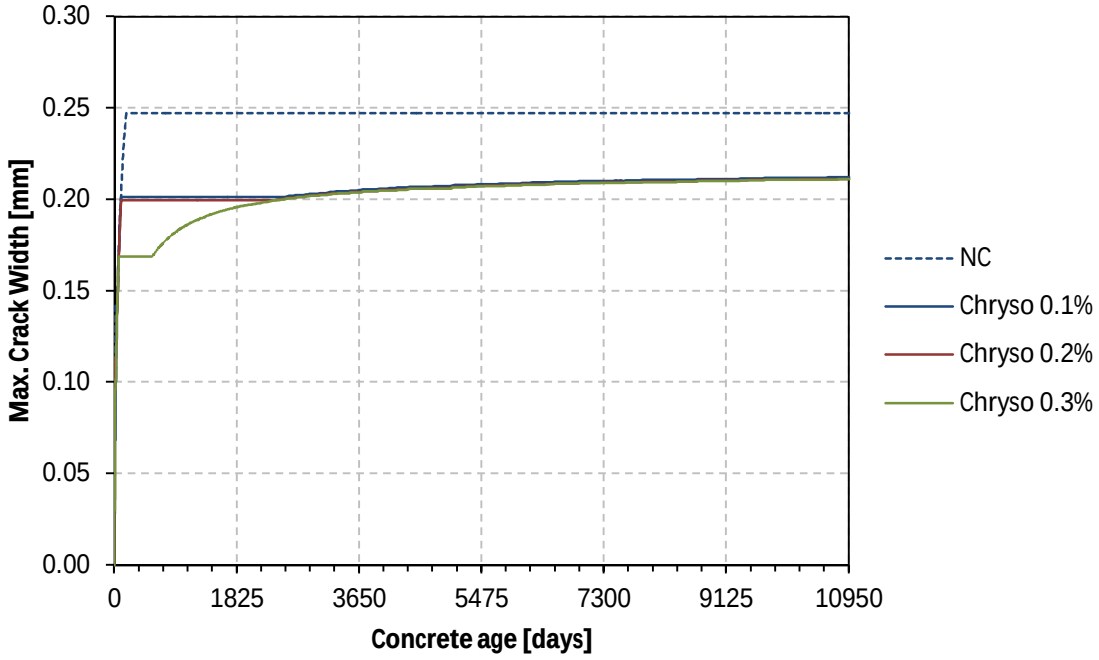

Figure E. 2 Development of the maximum crack width within the slab-on-grade of the Chryso SynFRC (on a normal axis)

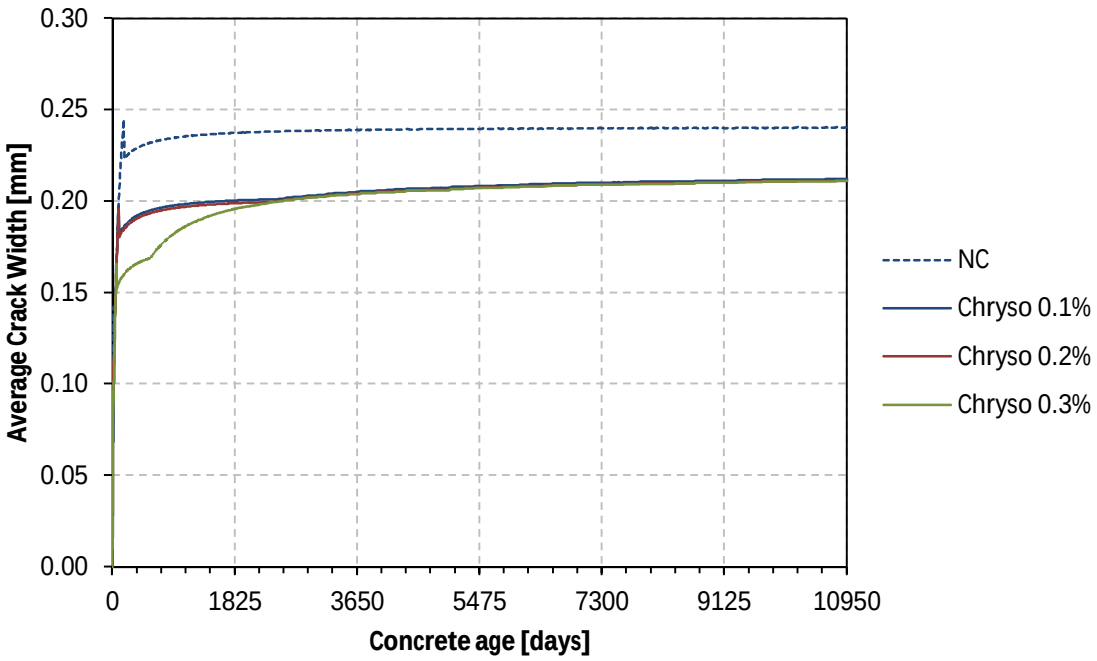

Figure E. 3 Development of the average crack width within the slab-on-grade of the Chryso SynFRC (on a normal axis)

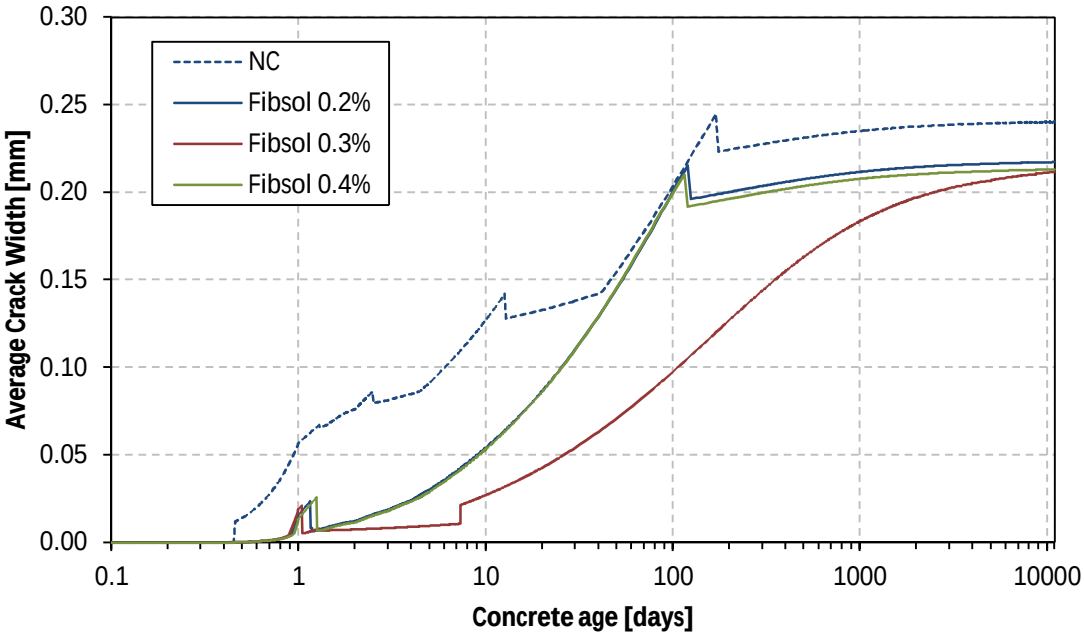

Figure E. 4 Development of the average crack width within the slab-on-grade of the Fibsol SynFRC

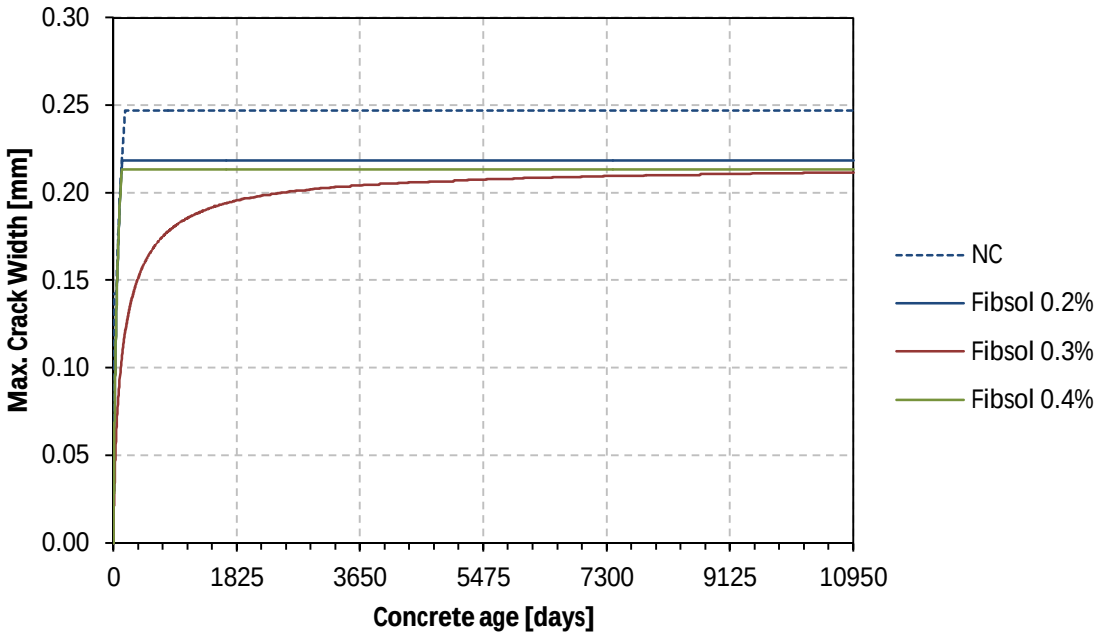

Figure E. 5 Development of the maximum crack width within the slab-on-grade of the Fibsol SynFRC (on a normal axis)

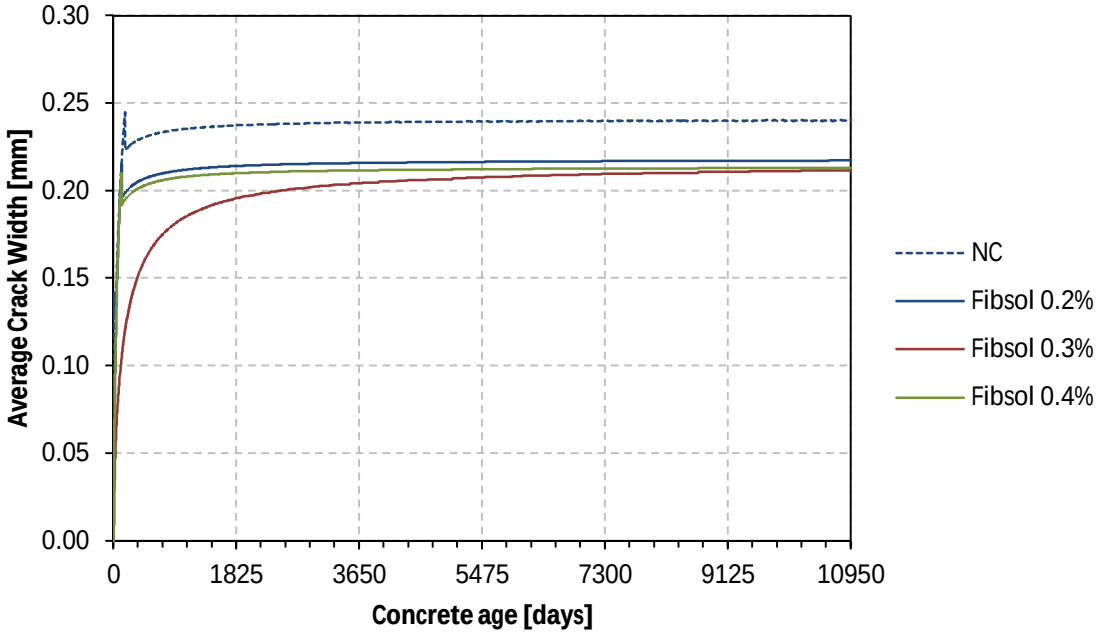

Figure E. 6 Development of the average crack width within the slab-on-grade of the Fibsol SynFRC (on a normal axis)

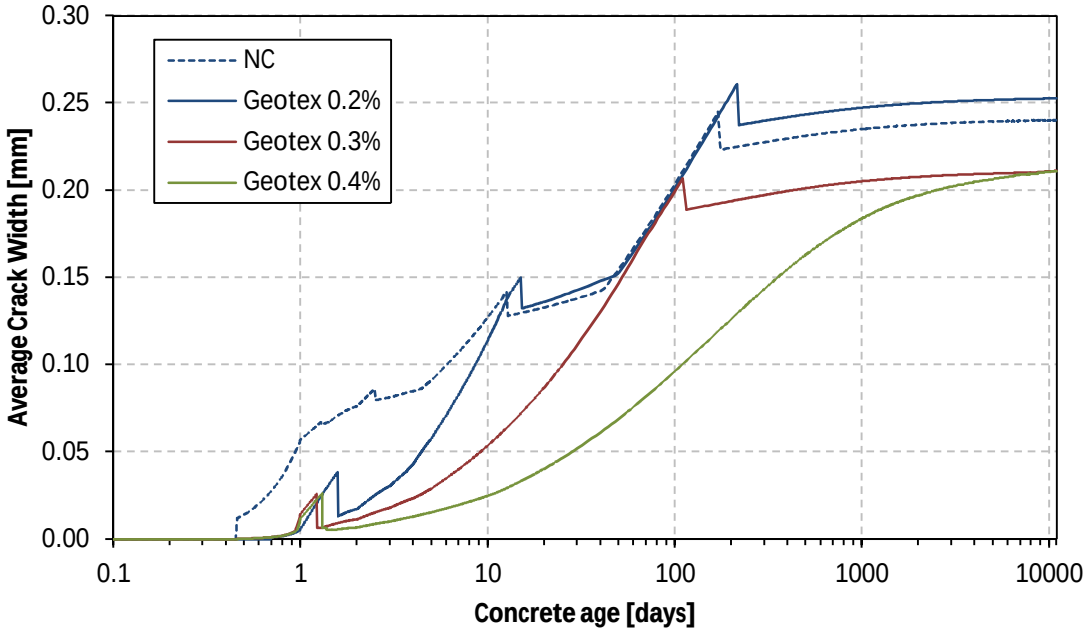

Figure E. 7 Development of the average crack width within the slab-on-grade of the Geotex SynFRC

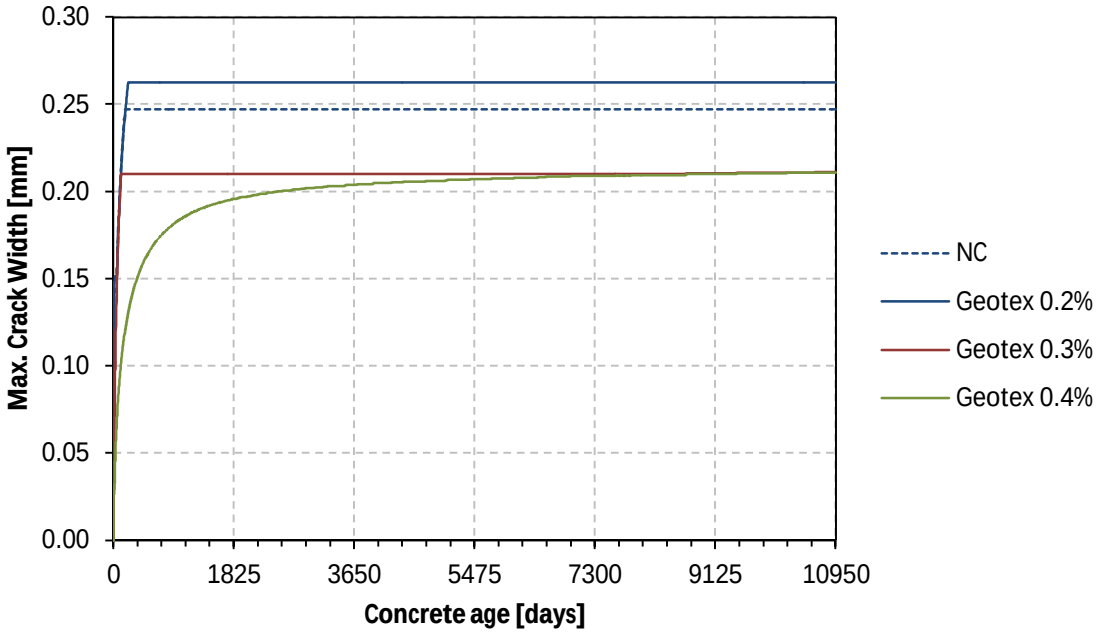

Figure E. 8 Development of the maximum crack width within the slab-on-grade of the Geotex SynFRC (on a normal axis)

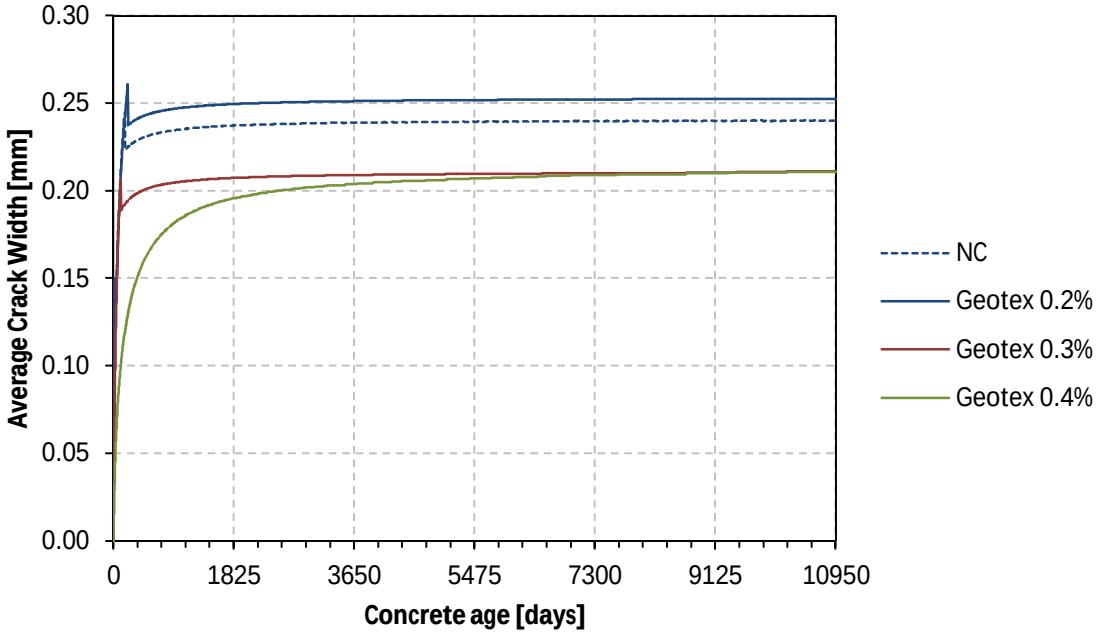

Figure E. 9 Development of the average crack width within the slab-on-grade of the Geotex SynFRC (on a normal axis)

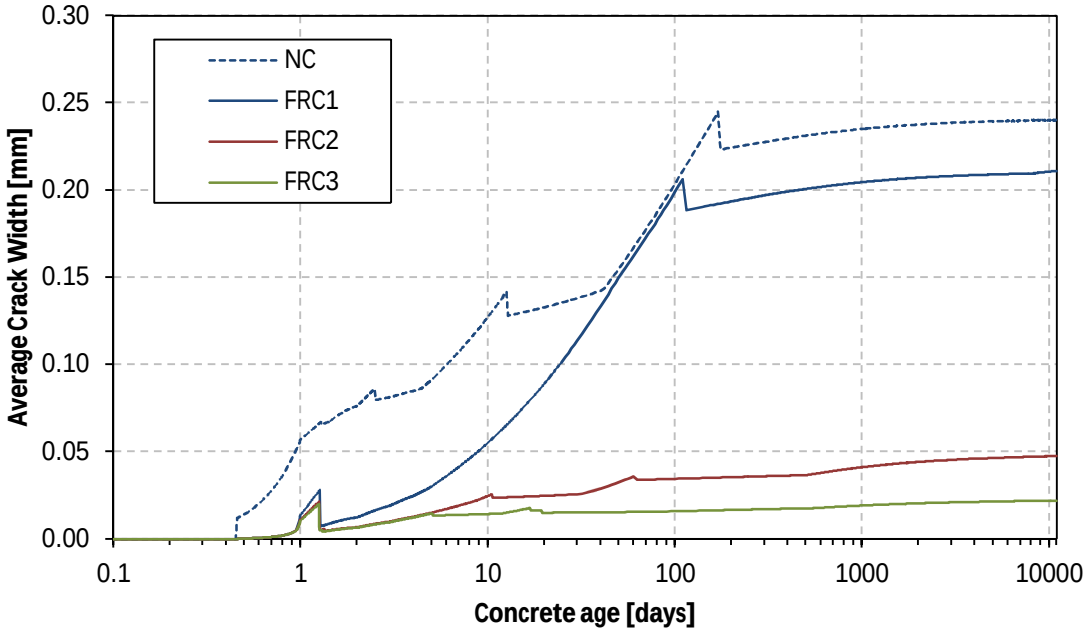

Figure E. 10 Development of the average crack width within the slab-on-grade of the estimated SynFRC

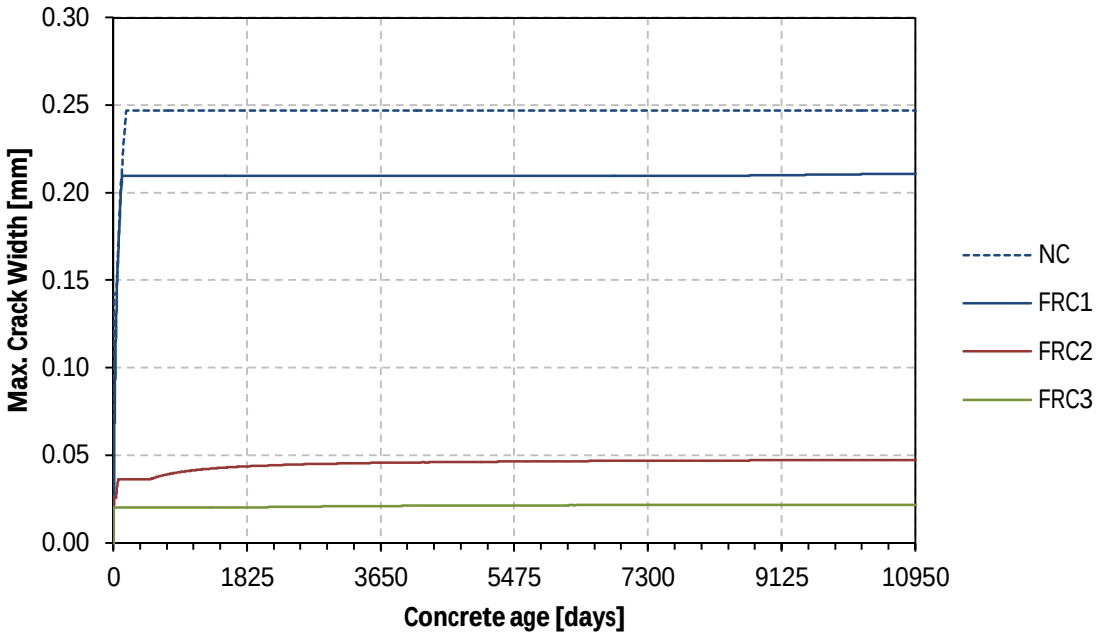

Figure E. 11 Development of the maximum crack width within the slab-on-grade of the estimated SynFRC (on a normal axis)

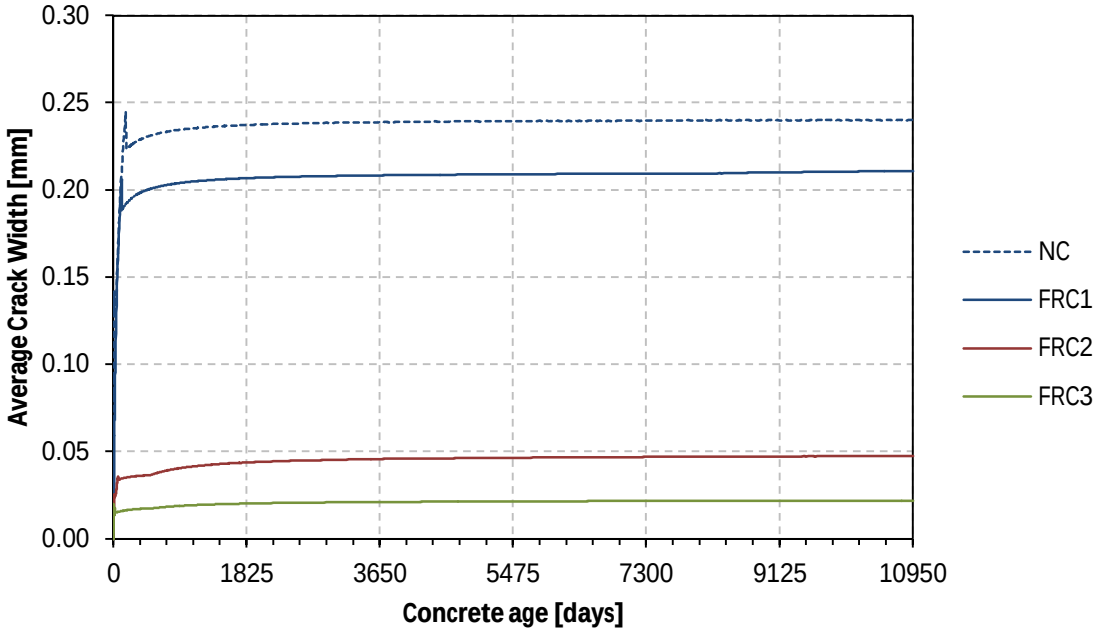

Figure E. 12 Development of the average crack width within the slab-on-grade of the estimated SynFRC (on a normal axis)

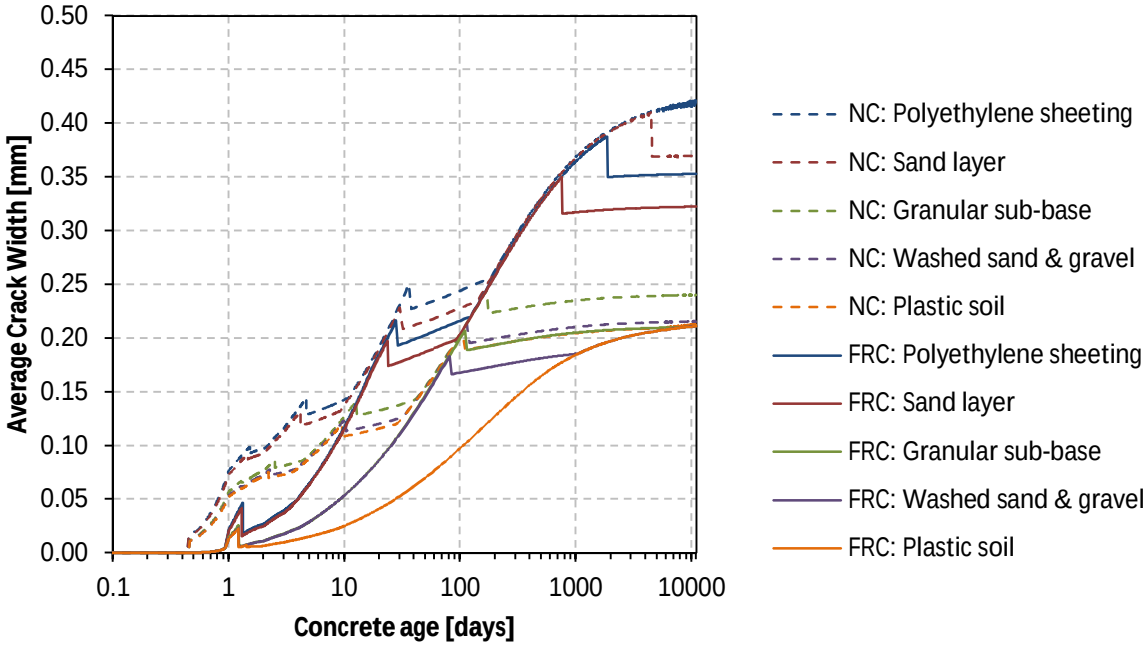

Figure E. 13 Development of the average crack width within the slab-on-grade for different coefficients of friction

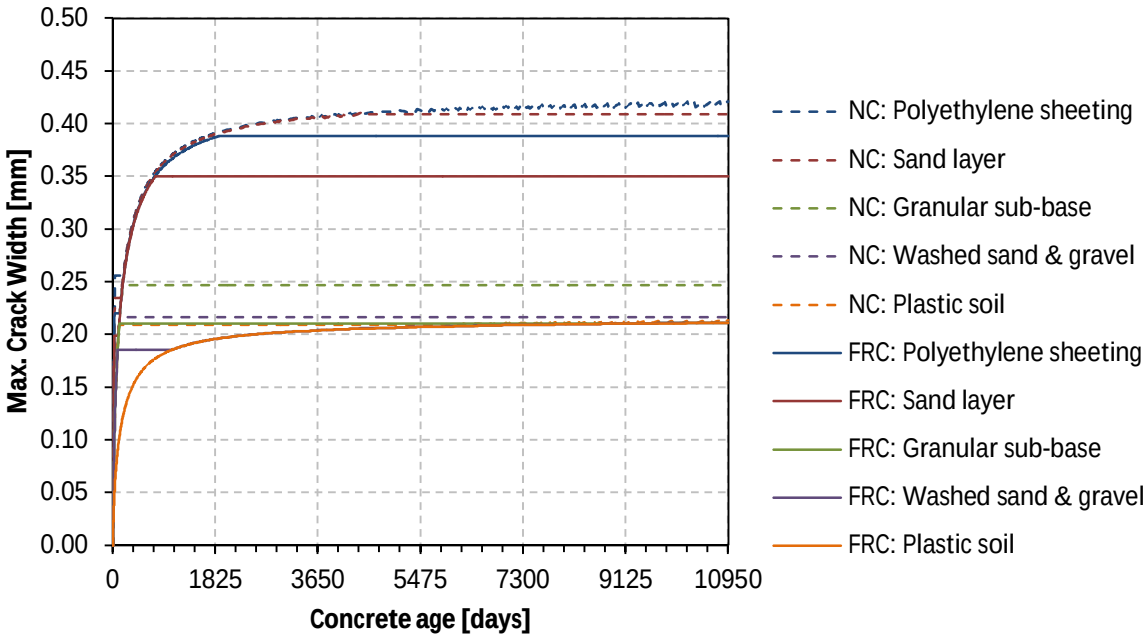

Figure E. 14 Development of the maximum crack width within the slab-on-grade for different coefficients of friction (on a normal axis)

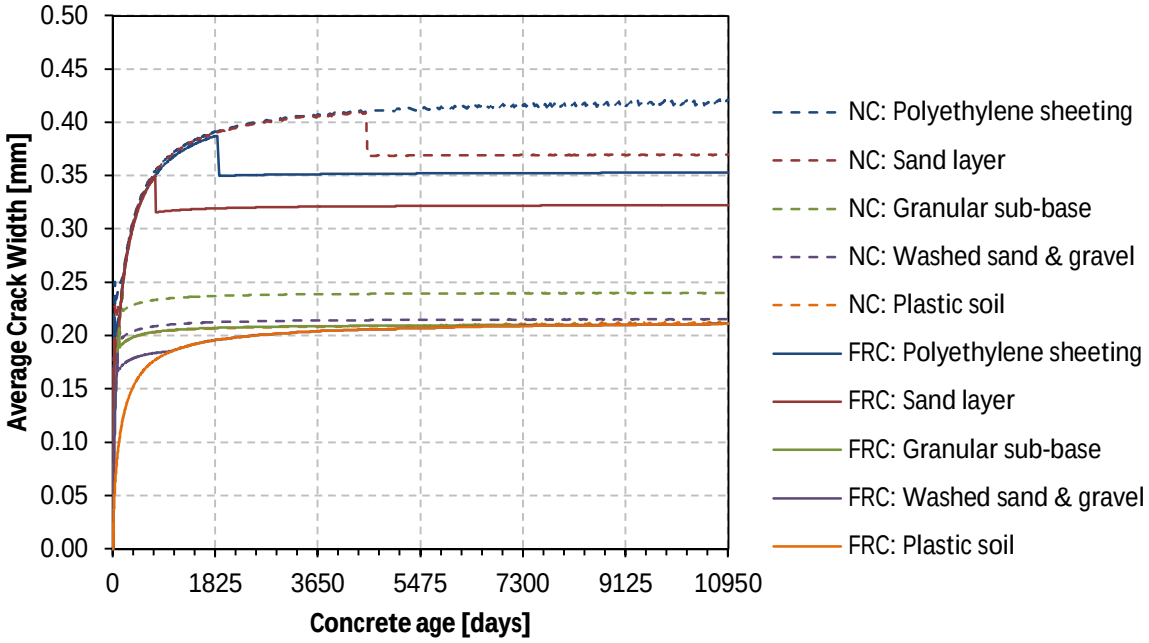

Figure E. 15 Development of the average crack width within the slab-on-grade for different coefficients of friction (on a normal axis)

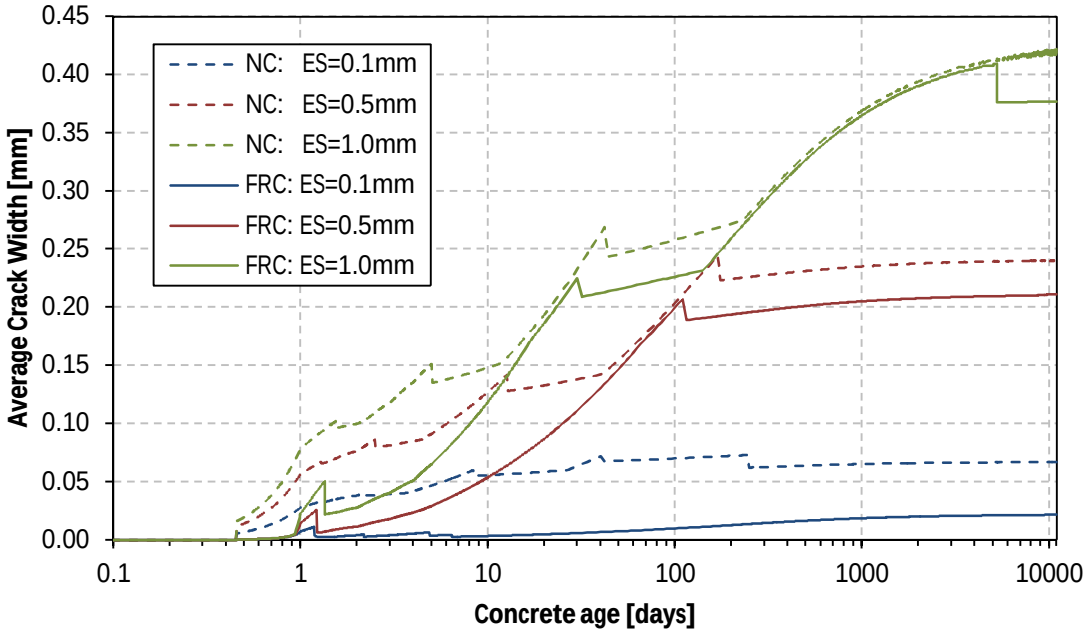

Figure E. 16 Development of the average crack width within the slab-on-grade for different elastic slip values

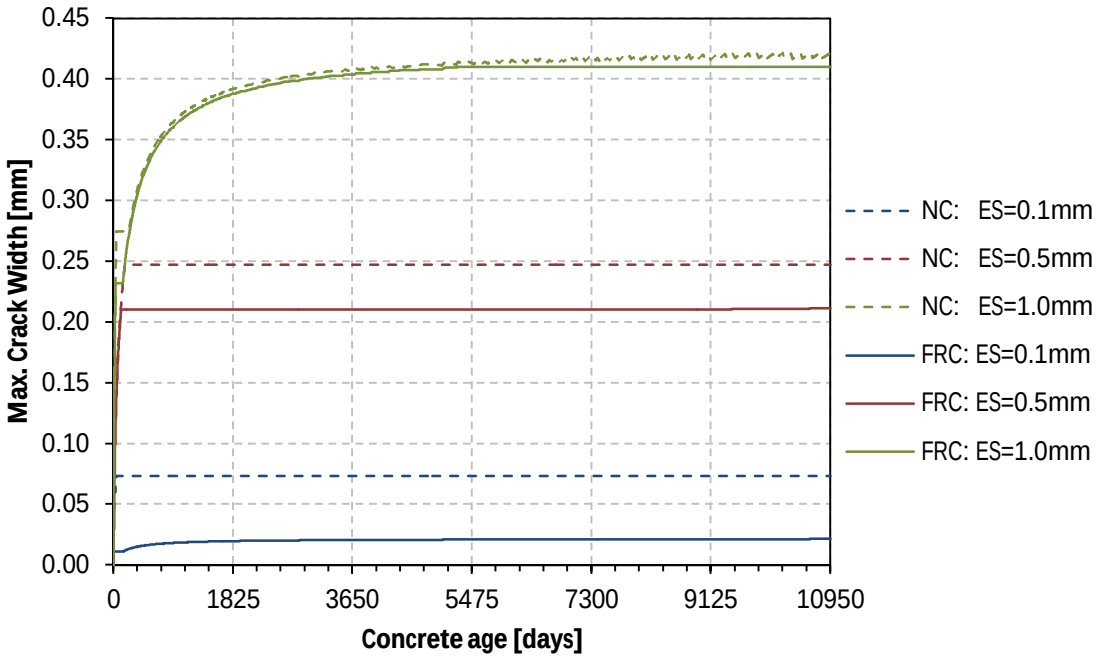

Figure E. 17 Development of the maximum crack width within the slab-on-grade for different elastic slip values (on a normal axis)

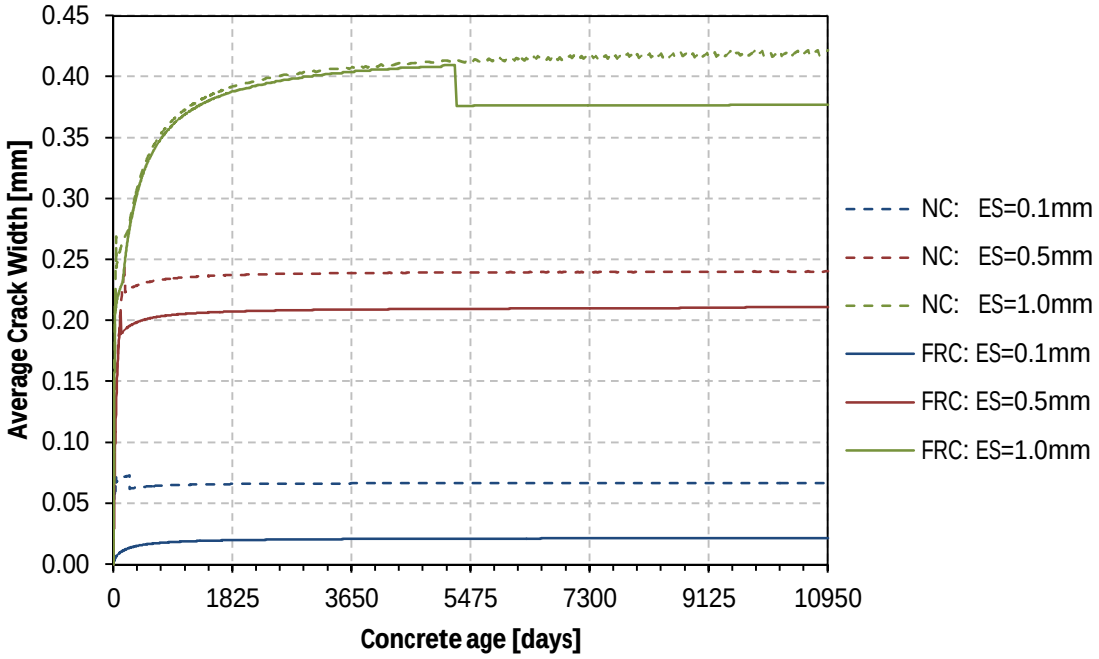

Figure E. 18 Development of the average crack width within the slab-on-grade for different elastic slip values (on a normal axis)

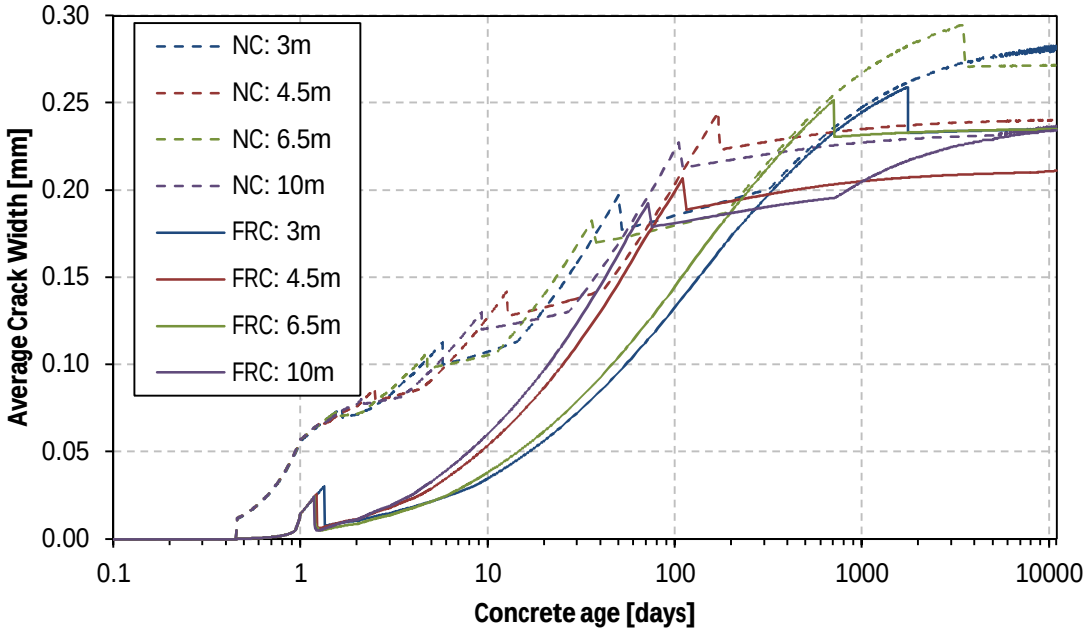

Figure E. 19 Development of the average crack width within the slab-on-grade for different joint spacings

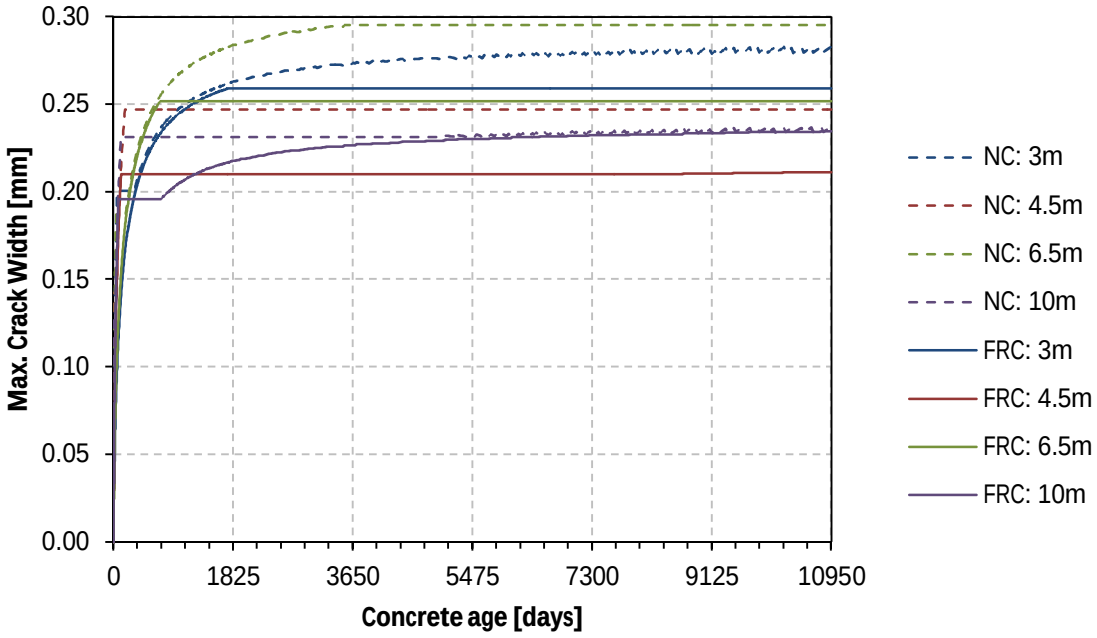

Figure E. 20 Development of the maximum crack width within the slab-on-grade for different joint spacings (on a normal axis)

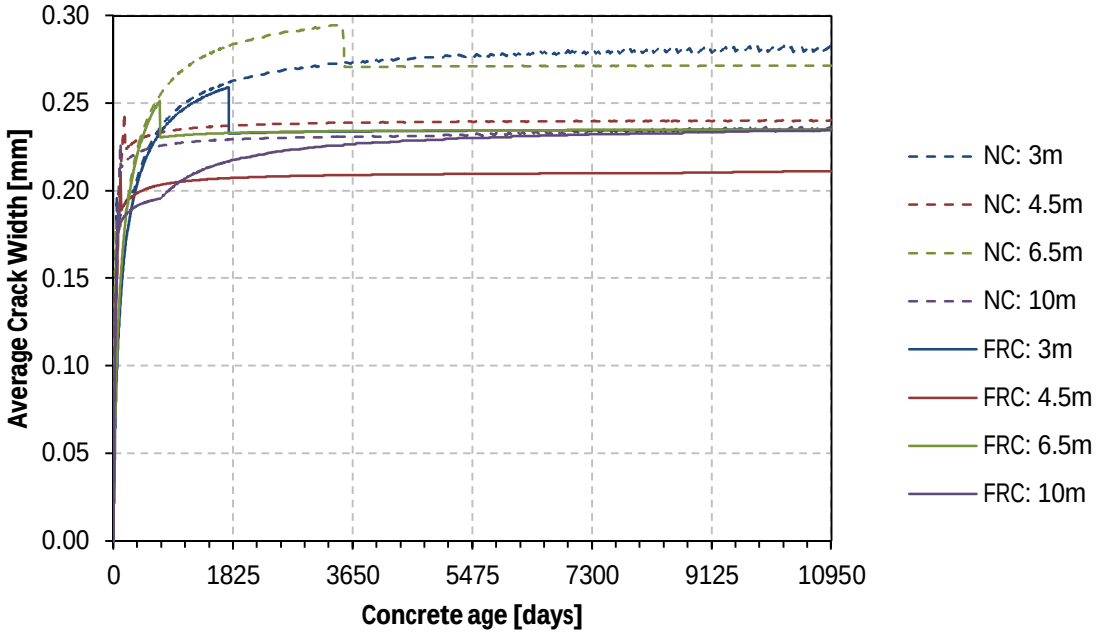

Figure E. 21 Development of the average crack width within the slab-on-grade for different joint spacings (on a normal axis)

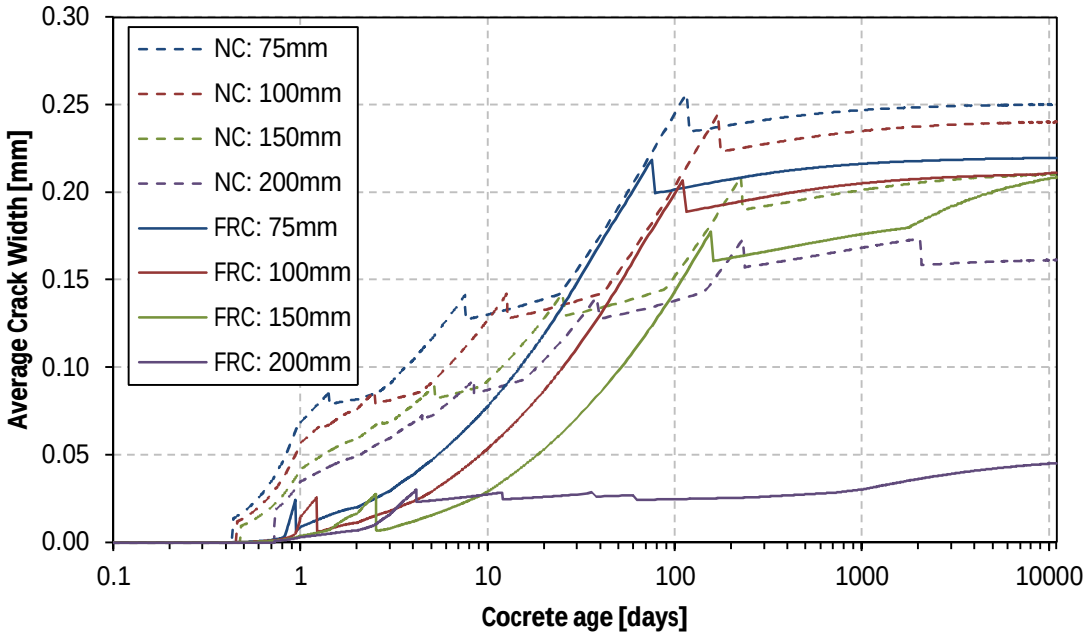

Figure E. 22 Development of the average crack width within the slab-on-grade for different slab thicknesses

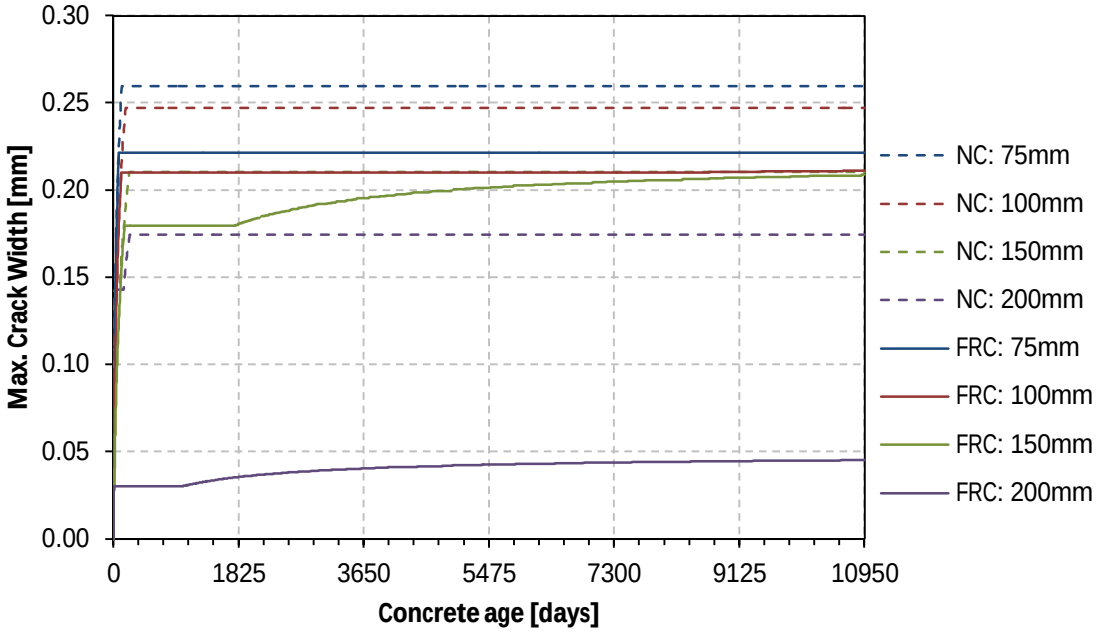

Figure E. 23 Development of the maximum crack width within the slab-on-grade for different slab thicknesses (on a normal axis)

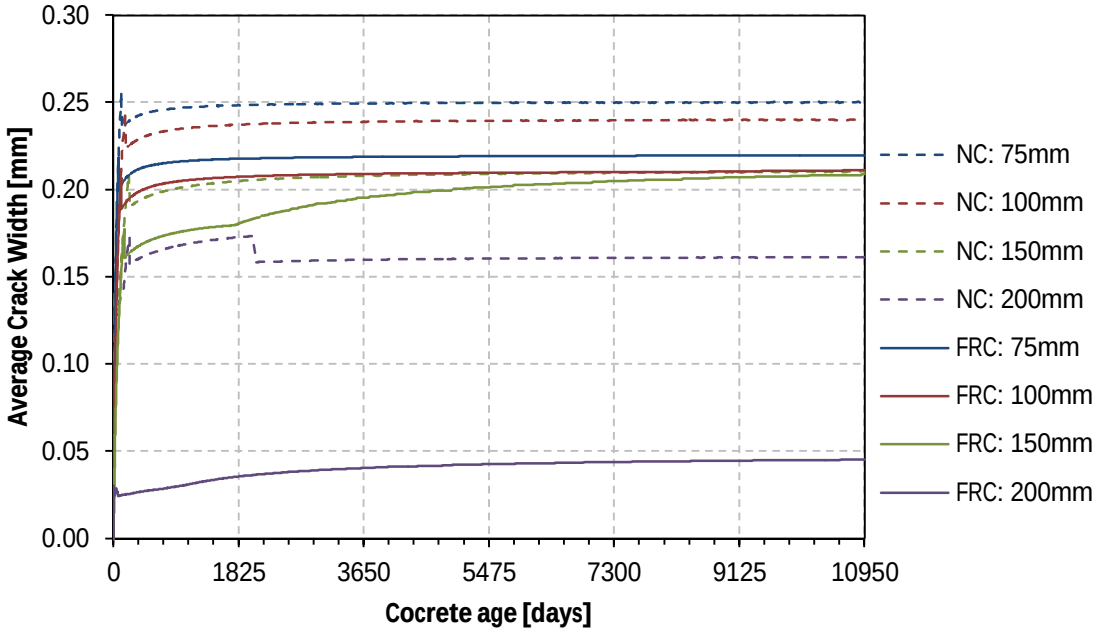

Figure E. 24 Development of the average crack width within the slab-on-grade for different slab thicknesses (on a normal axis)

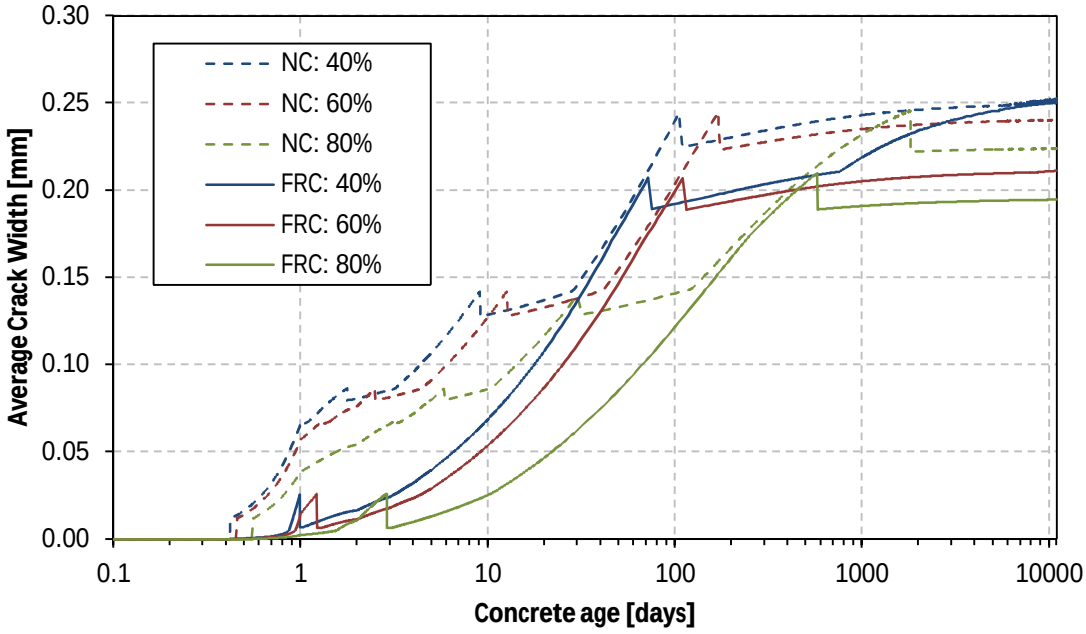

Figure E. 25 Development of the average crack width within the slab-on-grade for different relative humidities

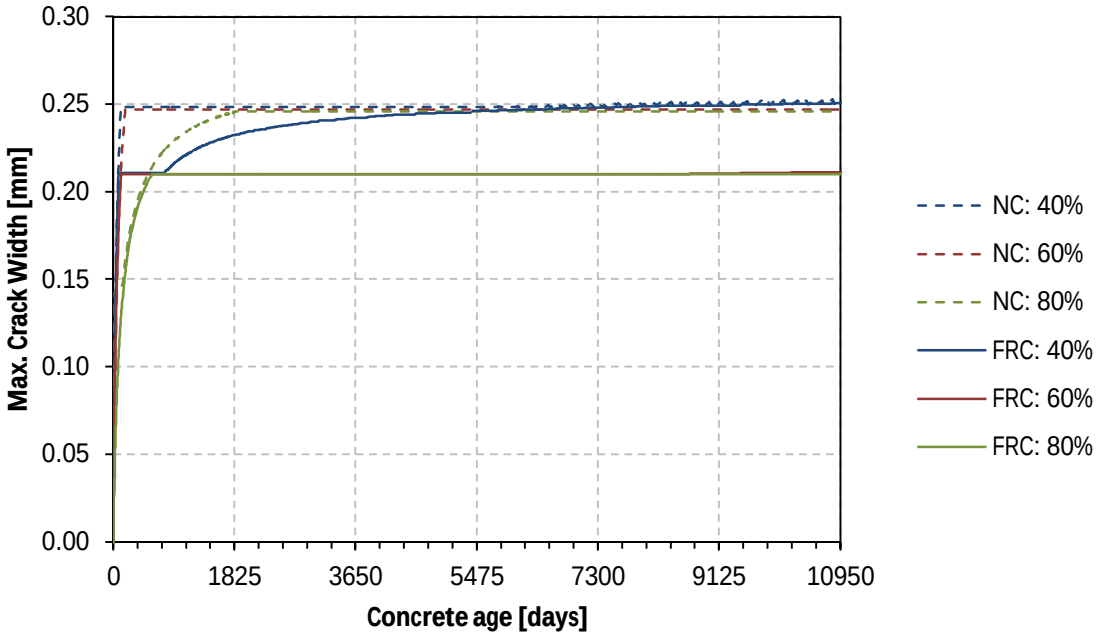

Figure E. 26 Development of the maximum crack width within the slab-on-grade for different relative humidities (on a normal axis)

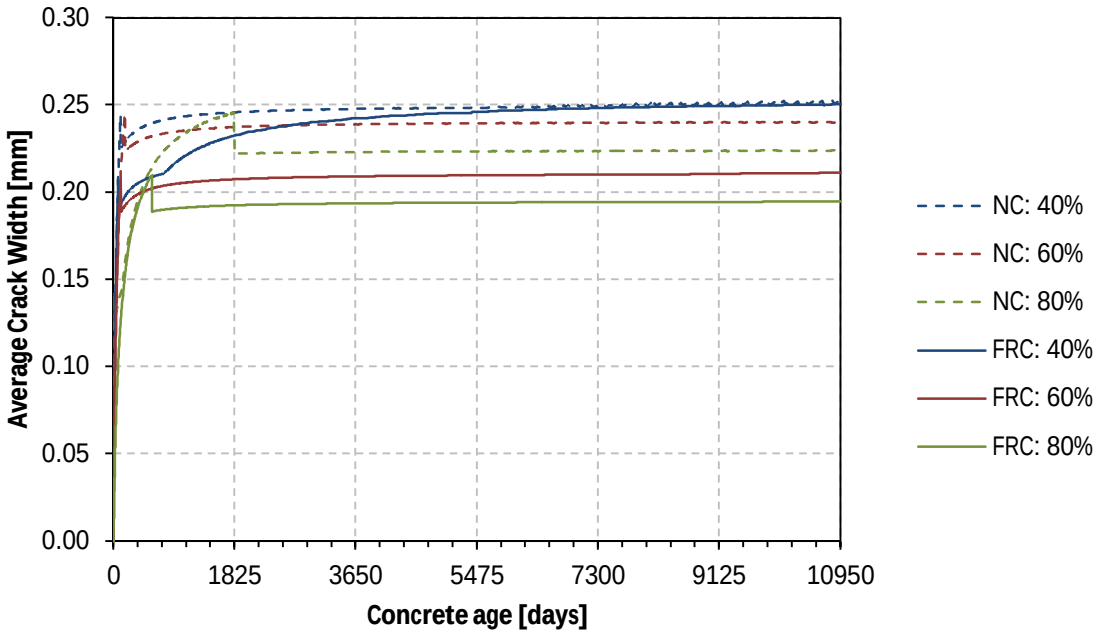

Figure E. 27 Development of the average crack width within the slab-on-grade for different relative humidities (on a normal axis)